博士論文

Critical Phenomena of the Ising Model with Non-Integer Effective Dimensions - a Monte Carlo Study

(非整数有効次元をもつイジング模型の臨界現象

- モンテカルロ法による研究)

堀田 俊樹

Abstract

We have studied the critical phenomena of the Ising model with long-range interaction and the Ising model with spatially correlated random field, both of which are expected to change the effective dimension of the system continuously. The investigation was conducted from the numerical viewpoint by using the Markov chain Monte Carlo method. Second order phase transitions can be classified into the universality classes and the dimensionality of the Ising model changes the universality class: the one-dimensional Ising model has no long-range order at finite temperatures (lower critical dimension), four or higher dimensional model has the mean-field universality (upper critical dimension), two-dimensional Ising model belongs to different universality from either of them, and so on. Although both of the Ising models with long-range interaction and the Ising model with spatially correlated random field are believed to change their critical behavior from its real spatial dimension into different effective dimensions, their detailed behavior has not been known well because of the notorious difficulties in analysis. In this work, we have obtained the detailed behavior of these models by introducing and developing the various methods. To investigate the Ising model with long-range interaction, we introduced the Fukui-Todo method, which drastically reduces the computational cost from $O(N^2)$ to $O(N)$, where N is the number of spins, and developed the generalized Ewald summation, the improved estimator, and the combined Binder ratio technique, which improves the convergence of the estimation. These techniques lead to the successful estimation of the boundary of the universality classes. We also investigated the Ising model with correlated random field by introducing the method for correlated random number generation and the various techniques for the precise analysis. Although the present numerical investigations suggested that the correlated random field causes a shift of effective dimensionality, they also revealed the difficulty for stronger random-field correlations because of the huge finite-size effects.

Acknowledgements

Prof. Synge Todo was the main adviser of this thesis and my researches. I greatly appreciate his fully supports and contributions to my researches. The discussions with him always provide me keen insights and abundant knowledge of statistical physics and computational technique. As a research member of the Todo group, Dr. T. Okubo, Dr. H. Suwa, and Dr. T. Shirai helped my researches with highly suggestive discussions. Dr. R. Igarashi and Dr. T. Sakashita, the former research member of Todo group, also helped my researches and had managed Todo group's PC clusters. The former and present students of the Todo group, Dr. Y. Motoyama, Dr. S. Yasuda, K. Yanagisawa, Y. Sakagawa, D. Adachi, K. Shimagaki, F. Ishikawa, T. Yamamoto, M. Suzuki, and K. Nakanishi shared time to discuss various topics, physics, mathematics, computation, programming, and so on.

Regarding the present study, I am obliged and shared time for discussions with many people. I would like to appreciate the insightful and fruitful discussions with Prof. K. Hukushima, Prof. N. Kawashima, Prof. Y. Yamaji, Dr. H. Ishizuka, Dr. T. Ohgoe, Dr. S. Morita. I also shared the discussions and conversations with M. Okada, T. Kirii, T. Suzuki, H. Sugihara, K. Takai.

The part of the simulations in the present thesis had been done by using the facility of the Supercomputer Center, Institute for Solid State Physics, the University of Tokyo. The simulation code has been developed based on the ALPS/looper library [1,2]. I also acknowledge the support from Graduate School of Engineering, the University of Tokyo Doctoral Student Special Incentives Program (SEUT-RA).

Finally, let me show the thanks to my family, Seiichi, Yukie, Kotomi, and Kento.

A Part of the present thesis has been published in the following journal article:

Paper

- Toshiki Horita, Hidemaro Suwa, and Synge Todo,
  "Upper and Lower Critical Decay Exponents of Ising Ferromagnets with Long-range Interactions,"
  Phys. Rev. E **95**, 012143 (2017).

Contents

Chapter 1

Introduction

Classification of critical phenomena has been one of the most important and central issues in the statistical physics for many-body problems for a long time, and has been studied extensively analytically, experimentally, as well as numerically [3]. Critical phenomena can be classified into "universality classes" according to their critical exponents (or critical indices). In general, the critical exponents depend on only a few basic properties of the system, such as the dimensionality, symmetry of the order parameter, and so on. However, the existence of long-range interaction (LRI) and/or randomness sometimes changes the behavior of the system completely [4]. Many materials exhibit nontrivial phenomena in which the long-range nature of the interactions, such as the dipole-dipole interaction and the Ruderman-Kittel-Kasuya-Yoshida (RKKY) interaction, plays an essential role. The randomness also causes various nontrivial behavior such as the spin-glass transition and extremely slow dynamics, and so on [5]. As for the phase transitions, they can alter the critical exponents and thus the universality class. Interestingly, this change of universality can be interpreted as the change of the effective dimension of the system as discussed below.

In the Ising model with long-range interaction, all possible pairs of spins interact with each other. The simplest and most fundamental long-range interaction is the algebraically decaying interaction characterized by the exponent, $d+\sigma$, where d is the dimension of the lattice and we call σ the decay exponent in the present work. For sufficiently small σ, the finite-temperature phase transition is expected to belong to the mean-field universality class. Especially, in the limit of $d+\sigma \to 0$, the system becomes equivalent to the fully connected Ising model. On the other hand, when σ is sufficiently large, the nearest-neighbor interaction dominates and the transition belongs to the short-range universality class. In the intermediate regime, between the mean-field and the short-range limits, the critical exponents that characterize the universality class vary continuously as σ changes. For the d-dimensional system with the long-range interaction, this continuous change of the critical exponents between short-range and mean-field universalities can be interpreted as a continuous change of the effective dimension between d and the upper critical dimension of the corresponding short-range model [6]. Thus, one can say that the

long-range interaction effectively increases the dimension of the system.

Similarly, the presence of randomness can also change the effective dimension of the system. The random-field Ising model (RFIM) is one of the representative random systems, which has randomly distributed external field [7]. In contrast to the long-range interaction, however, the random field is considered to decrease the effective dimension. Especially, near the upper critical dimension, it is predicted that the critical behavior of the d-dimensional RFIM is the same as the pure system in $d-2$ dimensions. This phenomena is called "dimensional reduction" [8–10]. Spatial correlation between random fields can also alter the critical behavior. For the spatial correlation that decreases algebraically with exponent $d-\rho$ as the distance between spins increases, the renormalization group study predicts that the upper critical dimension D_{U} and the lower critical dimension D_{L} become as $D_{\mathrm{U}} = d_{\mathrm{U}} + \rho$ and $D_{\mathrm{L}} = d_{\mathrm{L}} + \rho$, respectively, where $d_{\mathrm{U}} = 6$ and $d_{\mathrm{L}} = 2$ are the upper and lower critical dimensions of the Ising model with uncorrelated random field [3, 7]. In other words, the correlation in random field makes the effective dimension lower.

An interesting point is that the shift of effective dimension is controlled by the continuous parameter, σ or ρ. By interpreting these continuous parameters as the shift of dimensionality, we are able to obtain the critical behavior between integral dimensions, i.e., non-integer effective dimension like a fractal. Thus, in spite of the simpleness of the Hamiltonian, both of the long-range interacting Ising model and the RFIM are famous for rich behavior and are also notorious for the difficulty in analysis.

In the present thesis, we investigate the long-range interacting Ising model and the RFIM with algebraically decaying random-field correlation by means of the large-scale Monte Carlo simulations and clarify the universality regime boundaries and the decay-exponent dependence of the universality class.

In the Ising model with long-range interaction, each spin has $(N-1)$ interactions, where N is a number of spins. Therefore, simulation of Ising model with long-range interaction needs to consider $O(N^2)$ interactions and thus computation cost becomes large quickly as the system size increases. Moreover, the long-range interaction causes extremely large finite-size corrections in critical exponents and critical amplitudes especially near the boundary between the mean-field and the intermediate regimes, and that between the intermediate and the short-range regimes. To overcome the difficulties that make conventional analysis ineffective, we utilize several important techniques: the $O(N)$ Fukui-Todo cluster algorithm [11], the (self-)combined Binder ratio, the generalized Ewald summation, and a generalization of the improved estimator for higher-order moments of magnetization.

Systems with randomness, such as the present RFIM, are also known by their difficulties in analytical calculations as well as in numerical simulations. Several previous studies of the Ising model with correlated random field are conducted in the analytical way. The renormalization group analysis [4, 12, 13] and the droplet argument [13] for the random systems are believed

to be valid near the upper and lower critical dimensions, respectively, and both are considered to fail to predict correct critical behavior at least quantitatively in the intermediate dimensions. Therefore, the precise numerical simulation is quite important to check the validity of analytic predictions. Main difficulties of the Monte Carlo simulation of RFIM are the requirement of average over large number of random samples and extreme slow convergence of the Markov chain to the equilibrium (c.f. the infinite disorder fixed point [5]). Thus, we use the state-of-the-art massively parallel supercomputer systems to simulate larger systems for longer Monte Carlo steps and take an average over several random samples. To conduct Monte Carlo simulation with the correlated random field, another essential technique, generation of correlated random number is needed. We generate random fields with arbitrary correlation matrix and with Gaussian marginal distribution by using diagonalization. Since the computation cost of diagonalization proportional to $O(N^3)$, correlated random-field generation step becomes a bottleneck for sufficient large system. We overcome this difficulty by introducing the parallel eigensolver that works efficiently on the massively parallel supercomputer. We perform Monte Carlo simulations for three and four dimensional RFIMs and precisely investigate the change of critical properties and effective dimension, especially the competition between the randomness and correlation of random field, and discuss the validity of the previous analytic predictions.

The present thesis is organized as follows: Chapters 2 and 3 are the introduction and review parts of the phase transition phenomena and the Monte Carlo algorithms, respectively. New numerical methods introduced in this work and their results are summarized in Chap. 4 and 5 for the Ising model with LRI and the spatially correlated RFIM, respectively. Finally, Chap. 6 summarizes the entire thesis.

Chapter 2

Critical Phenomena and Effective Dimensions

2.1 Phase transition phenomena

A "phase" is a state of matter in which the macroscopic physical properties of the substance are uniform on a macroscopic length scale [3]. Ice, water, and vapor are familiar examples of a phase of macroscopic numbers of H_2O molecules. H_2O molecules change its macroscopic behavior for each varied parameters such as the temperature and pressure. A "phase transition" is a phenomenon in which a drastic change between thermodynamic phases, like a transition from ice to water or from water to vapor. At the phase transition point, singular behaviors appear in physical quantities. Phase transitions are roughly divided by the degree of singularity in physical quantities. When the first-order derivative of the free energy F shows a discontinuity, the transition is of first order. On the other hand, the transition is called continuous if the second- or higher-order derivatives of the free energy shows a discontinuity or a divergence. It is also common to name phase transitions by the order of the derivative that first shows a discontinuity or divergence, e.g. it is called second order if it is the second-order derivative of the free energy that first displays the discontinuity or divergence.

A material may show both first- and second-order transitions depending on the conditions. Consider the phase diagram of a magnetic material placed in an external magnetic field h. If the temperature T is lower than critical temperature T_c, the magnetization m jumps discontinuously along with the direction of external magnetic field h, thus a first order transition. For negative h, the spins in the magnetic material align with that negative direction on the macroscopic scale. They suddenly change the directions as the external field becomes positive. When the temperature T is higher than T_c, the magnetization changes smoothly at $h = 0$ without any singularities. On the other hand, if we keep the external magnetic field infinitesimally small, $h = 0+$, and lower the temperature across T_c, then the spontaneous magnetization changes continuously from 0 to a positive value, thus defining a second-order transition.

2.1.1 Critical exponents

The degree of singularity or divergence of physical quantities near the critical point is described by critical exponents. Experiments show that physical quantities generally have power-law singularities as functions of the difference between the control parameters (such as the temperature) and their critical values. The critical exponents of simple magnetic materials are defined as follows.

$$\chi \propto |t|^{-\gamma} \tag{2.1}$$
$$C \propto |t|^{-\alpha} \tag{2.2}$$
$$m \propto |t|^{\beta} \tag{2.3}$$
$$m \propto |h|^{1/\delta} \qquad (T = T_{\mathrm{c}}) \tag{2.4}$$
$$G(r) \propto r^{-\tau} e^{-r/\xi} \qquad (T \neq T_{\mathrm{c}}) \tag{2.5}$$
$$G(r) \propto r^{-d+2-\eta} \qquad (T = T_{\mathrm{c}}) \tag{2.6}$$
$$\xi \propto |t|^{-\nu}, \tag{2.7}$$

where $t = (T - T_{\mathrm{c}})/T_{\mathrm{c}}$ is the dimensionless temperature difference from the critical temperature T_{c}, h is the external field, $\chi = \lim_{h\to 0} \frac{\partial^2}{\partial h^2}(-k_B T \ln Z)$ is the magnetic susceptibility, C is the specific heat, $m = |\sum_i^N S_i|/N$ is the magnetization, $G(r) = \langle S_i S_{i+r}\rangle - \langle S_i\rangle\langle S_{i+r}\rangle$ is the correlation function, and ξ is the correlation length.

The critical exponents are very basic quantities to characterize critical phenomena. An important goal of the theory of critical phenomena is to develop a systematic method of calculating the values of critical exponents. Most importantly, there are simple relations between exponents, scaling relations, and thus each exponents are not independent of each other. Scaling relations allow determining an exponent from the value of other exponents. A review of the scaling relations and the way to estimate critical exponents from numerical data are described in Sec. 2.1.2.

2.1.2 Scaling relations

Scaling relations are conducted by the scaling law, which is formulated by the exponents y_t and y_h of eigenvalues of the linearized renormalization group transformation. The free energy is transformed by a renormalization group transformation,

$$f(g_t, g_h, g_3, \cdots) = b^{-d} f(g_t', g_h', g_3', \cdots) + w(g_t, g_h, g_3, \cdots), \tag{2.8}$$

where g_t and g_h are proportional to the deviation of temperature and external field from the critical value t and h, respectively. The second term in the right-hand side of Eq. (2.8) expresses non-singular behavior. Although w does not play a critical role in the determination of the critical behavior, taking into account the non-singular term is very important to conduct a

precise analysis from small-size lattices or a model with strong finite-size effect. Especially, our main targets, the system with LRI and correlated random-field are known as its strong finite-size effect and high costs in numerical simulation, and thus overcoming the finite-size effect is one of the main challenges in our current work.

To investigate critical behavior, we can drop the non-singular term, irrelevant fields $g_3, g_4, \cdots$, and the proportionality constant between g_t and t and between g_h and h. After n steps of renormalization, we have

$$f(t,h) = b^{-nd} f(b^{ny_t} t, b^{ny_h} h). \tag{2.9}$$

For $t \neq 0$, we may choose the number n such that the first argument of the right-hand side reduces to unity, $b^{ny_t} t = 1$. Then, by inserting $b^n = t^{-1/y_t}$ in the right-hand side of Eq. (2.9), we find a very important relation known as the "scaling law,"

$$f(t,h) = t^{d/y_t} f(1, ht^{-y_h/y_t}) = t^{d/y_t} \Psi(ht^{-y_h/y_t}). \tag{2.10}$$

Although the free energy originally has two independent variables, in the most right-hand side of Eq. (2.10), the scaling function Ψ depends on these variables only through the combination ht^{-y_h/y_t}.

The scaling relations are deduced by a comparison between the scaling law and the critical exponents. For instance, since the specific heat is the second-order derivative of the free energy with respect to the temperature, we obtain

$$C(t,0) \propto \frac{\partial^2 f(t,0)}{\partial t^2} \propto t^{d/y_t - 2}. \tag{2.11}$$

From Eqs. (2.2) and (2.11), we conclude $\alpha = 2 - d/y_t$. The magnetization m and the magnetic susceptibility χ at $h = 0$ are described as

$$m(t,0) \propto \left.\frac{\partial f(t,h)}{\partial h}\right|_{h=0} \propto t^{(d-y_h)/y_t} \tag{2.12}$$

$$\chi \propto \left.\frac{\partial^2 f(t,h)}{\partial h^2}\right|_{h=0} \propto t^{(d-2y_h)/y_t}, \tag{2.13}$$

respectively. Thus we obtain $\beta = (d - y_h)/y_t$ and $\gamma = (2y_h - d)/y_t$. The critical exponent δ is deducted by setting $t = 0$ in Eq. (2.9) and differentiating with respect to h as

$$m(0,h) \propto \frac{\partial f(0,h)}{\partial h} = b^{-nd-ny_h} f_2(0, b^{ny_h} h), \tag{2.14}$$

where f_2 is the partial derivative of f with respect to the second argument. If we choose n to become $b^{ny_t} h = 1$, the h-dependence of the right-hand side becomes $h^{(d-y_h)/y_h}$, and thus

$\delta = y_h/(d - y_h)$. Those results are summarized as

$$\alpha = 2 - \frac{d}{y_t}, \tag{2.15}$$

$$\beta = \frac{d - y_h}{y_t}, \tag{2.16}$$

$$\gamma = \frac{2y_h - d}{y_t}, \tag{2.17}$$

$$\delta = \frac{y_h}{d - y_h}. \tag{2.18}$$

Remember that there are usually only two relevant scaling fields. Accordingly, there are only two relevant exponents y_t and y_h, which implies that the four critical exponents α, β, γ, and δ are not mutually independent. A knowledge on two of them is sufficient to deduce the rests. By eliminating y_t and y_h from the scaling relations, we obtain

$$\alpha + 2\beta + \gamma = 2 \tag{2.19}$$

$$\gamma = \beta(\delta - 1). \tag{2.20}$$

Additional scaling relations, *hyperscaling relations*, are obtained by considering the critical behavior of the correlation function $G(\vec{r}, t) = \langle S(0)S(\vec{r})\rangle - \langle S(0)\rangle\langle S(\vec{r})\rangle$. Assume that $h = 0$ and $G(\vec{r}, t)$ is independent of the direction of $\vec{r}$, and then $G(\vec{r}) = G(r)$, where $r = |\vec{r}|$. According to the transformation rule of the spin variable S, $G(r, t)$ acquires the factor $c(b)^2$ after a single step of a renormalization group operation since the correlation function is the average of the product of two spin variables,

$$G(r, t) = c^2(b)G(b^{-1}r, b^{y_t}t). \tag{2.21}$$

On the other hand, the scaling law of the magnetization m is obtained by differentiating Eq. (2.9), for $n = 1$ and $h = 0$ as

$$m(t, 0) = b^{-d+y_h}m(b^{y_t}t, 0). \tag{2.22}$$

By comparing Eq. (2.22) and a renormalization group operation similar to Eq. (2.21),

$$m(t, 0) = c(b)m(b^{y_t}t, 0), \tag{2.23}$$

we obtain

$$c(b) = b^{-d+y_h}. \tag{2.24}$$

By rewriting Eq. (2.22) as

$$m(b^{y_t}t, 0) = b^{d-y_h}m(t, 0), \tag{2.25}$$

the scaling dimension of the spin variable is determined as $d - y_h$. Therefore, Eq. (2.21) with n times renormalization group becomes

$$G(r, t) = b^{n(-2d+2y_h)}G(b^{-n}r, b^{ny_t}t). \tag{2.26}$$

For $t \neq 0$, we can choose n such as $b^{ny_t}t = 1$, and then the scaling law of the correlation function is derived as

$$G(r,t) = b^{2(d-y_h)/y_t}\Phi(rt^{1/y_t}) \ \ (T \neq T_c). \tag{2.27}$$

The correlation function should decay exponentially as $e^{-r/\xi}$ at small but finite t and sufficient large r. Since the correlation length ξ diverges as $t^{-\nu}$, the exponent r/ξ should be proportional to rt^{ν}. Eq. (2.27) indicates that r appears as a product with a power of t, rt^{1/y_t}. Since rt^{1/y_t} and $r/\xi \propto rt^{\nu}$ should represent the same function, $\nu = 1/y_t$ is concluded.

By setting $t = 0$ and $b^n = r$ in Eq. (2.26), we obtain

$$G(r,0) \sim r^{-2d+2y_h} \ \ (T = T_c). \tag{2.28}$$

The critical exponent η, defined by $G(r,0) \sim r^{-d+2-\eta}$, is then determined as $\eta = d - 2y_h + 2$. To summarize,

$$\nu = \frac{1}{y_t} \tag{2.29}$$

$$\eta = d - 2y_h + 2. \tag{2.30}$$

Eq. (2.15) to Eq. (2.18) are also able to be rewritten as

$$\alpha = 2 - d\nu, \tag{2.31}$$

$$\beta = \frac{\nu(d-2+\eta)}{2}, \tag{2.32}$$

$$\gamma = \nu(2-\eta), \tag{2.33}$$

$$\delta = \frac{d+2-\eta}{d-2+\eta}, \tag{2.34}$$

respectively. These equations are known as the "hyperscaling relations."

2.1.3 Finite-size scaling

Scaling laws are also useful to estimate critical values from numerical data. The finite-size scaling technique provides us to estimate critical values from numerical data for finite-size lattices. We show how to extract critical exponents from numerical data for the magnetic susceptibility. Suppose that we perform the process of renormalization group for a system on a hypercubic lattice with linear size L. Theoretically, the critical phenomena, the singular behavior of the physical quantities, occur only when the system size is infinite. The parameters of the system should be tuned for the system to be at the critical point, i.e. $t = h = 0$. System size L is also needed to be tuned at an infinite value so that the critical behavior of the system appeared, $L \to \infty$. This condition is able to be rewritten as $1/L \to 0$, which implies L^{-1} must be tuned to 0 in addition to t and h to keep the system at the critical point. We thus include L^{-1} in the relevant argument of the free energy and write

$$f(t,h,L^{-1}) = b^{-d}f(b^{y_t}t, b^{y_h}h, bL^{-1}). \tag{2.35}$$

It is seen that L^{-1} is a relevant variable with exponent $y_L = 1$. Magnetic susceptibility is described by differentiating Eq. (2.35) by h. At $h = 0$,

$$\chi(t, 0, L^{-1}) = b^{2y_h - d} f_2(b^{y_t} t, 0, bL^{-1}), \tag{2.36}$$

where f_2 is the second-order partial derivative of $f(t, h, L^{-1})$ with respect to the second argument. By choosing $b = L$, we obtain the following equation with the scaling function $\tilde{\Psi}(\cdot)$, analytic for finite L,

$$\chi(t, 0, L^{-1}) = L^{2-\eta} \tilde{\Psi}(tL^{-1/\nu}), \tag{2.37}$$

where we have used $2y_h - d = 2 - \eta = \gamma/\nu$ and $y_t = 1/\nu$.

The analysis of numerical data proceeds as follows. Plot the data by changing t for various L with abscissa $tL^{1/\nu}$ and ordinate $L^{\eta-2}\chi$, with presumed values of T_c, η, and ν. If these presumed values are appropriate, these plots fall on the same curve. As in the case of experimental or numerical data, one adjusts the critical values T_c, η, and ν by trial and error to find the best possible single curve. In this work, to find the appropriate critical values, we have used the Bayesian scaling analysis [14, 15] which estimates the appropriate critical values automatically by the Bayesian statistical technique from numerical data.

2.2 Ising model with long-range interaction

A system with LRI can exhibit substantially different physics from the corresponding system only with short-range interaction [16–18]. Many materials show non-trivial phenomena to which long-range nature of the interactions, such as the dipole-dipole interaction [19] and the Ruderman-Kittel-Kasuya-Yoshida (RKKY) interaction [20], plays an essential role. The competition between the short-range and the LRIs has also been studied in the cold-atom systems [21].

One of the simplest and the most fundamental playgrounds for LRI is the Ising model with the algebraically decaying interaction:

$$\mathcal{H} = -\sum_{i<j}^{N} J_{ij} S_i S_j, \tag{2.38}$$

where S_i ($= \pm 1$) is the Ising spin on the i-th site, J_{ij} is the coupling constant between two spins (S_i and S_j), and N is the total number of spins. The summation in Eq. (2.38) runs over all spin pairs. The algebraically decaying ferromagnetic LRI is expressed as

$$J_{ij} = \frac{1}{|\vec{r}_i - \vec{r}_j|^{d+\sigma}}, \tag{2.39}$$

where d is the dimension of the system, and $\vec{r}_i$ is the coordinate of the i-th site on the square lattice. The decay exponent, σ, in Eq. (2.39) should be positive to ensure the extensiveness of the energy, i.e., finite energy density in the thermodynamic limit. Otherwise, one has to introduce

an appropriate system-size-dependent normalization factor. The system with the algebraically decaying LRI shows richer critical phenomena than those with only nearest-neighbor interaction. For sufficiently small σ, the finite-temperature phase transition is expected to belong to the mean-field universality class: in the limit of $d+\sigma \to 0$, the system becomes the fully connected model, or the Husimi-Temperley model [22, 23]. On the other hand, when σ is sufficiently large, the nearest neighbor interaction dominates and the transition belongs to the short-range universality class. In the "intermediate regime" between the mean-field and the short-range limits, the critical exponents that characterize the universality class vary continuously [17, 18]. For the d-dimensional system with LRI, this continuous change of the critical exponents between the short-range and the mean-field universalities can be interpreted as the continuous change of the effective dimension between d and the upper critical dimension of the corresponding short range model. Although a number of theoretical and numerical studies [6, 17, 18, 24–30] have been conducted in order to interpret the intermediate regime as non-integral dimensions, precise identification between the decay exponent, σ, and the effective dimension has not been well established so far, in spite of the simple form of the Hamiltonian (2.38).

The Ising model with LRI (2.39) has two limits, the fully connected Ising model [$(d+\sigma) \to 0$] and the Ising model only with short-range interaction ($\sigma \to \infty$). The critical property of the phase transition in these limits is well established. The coupling constants of the former model are given by

$$J_{ij} = \frac{1}{N}. \tag{2.40}$$

On the other hand, those of the latter are

$$J_{ij} = \begin{cases} 1 & \text{if } i \text{ and } j \text{ are nearest neighbor,} \\ 0 & \text{otherwise.} \end{cases} \tag{2.41}$$

In Table 2.1, the critical exponents of these models are summarized. Note that the critical exponents of the fully connected (mean-field) model depend on its dimension because its physical quantities scale with the total number of sites $N = L^d$ instead of system length L. The well known values $\nu = 1/2$ and $\eta = 0$ for the mean-field model are those at the upper critical dimension, i.e., $d = 4$.

A number of theoretical and numerical studies have been conducted mainly based on the renormalization group argument and the Monte Carlo simulations. For the O(n) model with LRI, Fisher *et al.* [17] performed the renormalization group analysis. The O(n) model is a generalization of the Ising model ($n = 1$). They found three different regimes, depending on the value of the exponent σ as listed in Table 2.2. In the intermediate regime, the critical exponent of the correlation function, η, varies linearly to σ. The results of their renormalization group analysis have a flaw that η at $\sigma = 2$, on the boundary between the intermediate regime and the short range regime, is not determined uniquely. The exponent η becomes zero if one approaches

Table 2.1: Critical exponents of the d-dimensional fully connected Ising model and the two-dimensional short-range Ising model [3].

	fully connected	short-range
α	0 (discontinuous)	0 (log)
β	$1/2$	$1/8$
γ	1	$7/4$
δ	3	15
ν	$2/d$	1
η	$2-d/2$	$1/4$

Table 2.2: Renormalization-group prediction for the critical exponent η by Fisher *et al.* [17].

	σ	η
mean field regime	$\sigma < d/2$	1
intermediate regime	$d/2 < \sigma < 2$	$2-\sigma$
short range regime	$2 < \sigma$	$\eta_{\rm sr}$

to $\sigma = 2$ from the side of the intermediate regime, while the finite value ($\eta_{\rm sr} = 1/4$) in the short range regime; thus, η changes discontinuously at $\sigma = 2$.

The boundary between the intermediate and the short-range regimes was more carefully considered by Sak [18] taking into account the higher-order terms in the renormalization group calculations. In Ref. 18, it was concluded that the boundary is $\sigma = 2 - \eta_{\rm sr}$ instead of $\sigma = 2$ as listed in Table 2.3. Then, the exponent η becomes a continuous function of σ. Its derivative, nevertheless, is discontinuous at $\sigma = 2 - \eta_{\rm sr}$ (and also at $\sigma = 1$).

Several theoretical studies have reported different conclusions. Most of them are based on the renormalization group approach and the ϵ-expansion of the Landau-Ginzburg effective Hamiltonian, where the propagator contains the p^σ term in addition to the ordinary p^2 term. For example, van Enter [24] pointed out that the long-range perturbation is relevant for $2-\eta_{\rm sr} \leq \sigma \leq 2$ in contradiction to the result obtained by Sak [18].

In the meantime, the first numerical study of the Ising model with the LRI was reported by

Table 2.3: Renormalization-group prediction for the critical exponent η by Sak [18].

	σ	η
mean field regime	$\sigma < d/2$	1
intermediate regime	$d/2 < \sigma < 2 - \eta_{\rm sr}$	$2-\sigma$
short range regime	$2 - \eta_{\rm sr} < \sigma$	$\eta_{\rm sr}$

Luijten and Blöte [25]. By means of the cluster-algorithm Monte Carlo method, they calculated the exponent η for $d = 2$ as a function of σ, concluding that $\eta = 2 - \sigma$ up to $2 - \sigma = \eta_{\rm sr}$ and $\eta = \eta_{\rm sr} = 1/4$ for larger σ. This result seems consistent with the renormalization group prediction by Sak [18]. Its error bar, however, is too large to exclude the possibility proposed by van Enter [24]. Recently, Picco [26] showed the more precise Monte Carlo data than before and concluded that the exponent η varies smoothly, connecting the intermediate regime and the short range regime, which disagrees with the previous renormalization group analysis. Blanchard *et al.* [27] then supported the numerical result by means of the renormalization-group analysis with the double expansion. Nonetheless, another Monte Carlo calculation by Angelini *et al.* [6] and renormalization group study by Defenu *et al.* [30] agree with the result by Sak [18]. The discrepancy between the previous researches has been an enigma for years.

2.3 Random field Ising model

In general, real materials contain some impurities or randomness. Although the idealized pure effective model is widely used to conduct the theoretical analysis of the behavior of materials for simplicity, to take into account the influence of randomness is occasionally important since even the infinitesimal small randomness possibly changes the quantitative/qualitative behavior of the system, as described below. Phase transitions continue to exist as long as randomness is not too strong, but the critical behavior may get modified and becomes different from the pure model.

A Hamiltonian describing phase transitions and critical phenomena usually consists of interaction and field terms. These are competing relevant terms, in the sense of renormalization group, that determine the values of the exponents y_t and y_h, respectively. The random field Ising model (RFIM), one of the targets of the current work, is a model with randomness in the field term,

$$\mathcal{H} = -J \sum_{\langle i,j \rangle} S_i S_j - \sum_i h_i S_i. \tag{2.42}$$

The external field at each site is assumed to take a random value according to a probability distribution function. Adopting a model distribution function of random fields $\{h_i\}$ is a customary since in most cases it is virtually impossible to identify the values of randomness h_i at each site i from experiments. Typically, the following Gaussian distribution and the binary distribution are occasionally use:

$$P(h_i) = \frac{1}{\sqrt{2\pi} h_{\rm R}} \exp\left(-\frac{h_i^2}{2h_{\rm R}^2}\right) \tag{2.43}$$

$$P(h_i) = \frac{1}{2}\delta(h_i - h_{\rm R}) + \frac{1}{2}\delta(h_i + h_{\rm R}). \tag{2.44}$$

In this work, we will assume the Gaussian marginal distribution (2.43). Difference of the critical behavior between Gaussian and binary distributions is an unsolved interesting problem but we

avoid discussing here. In the mean-field region, the binary distribution is believed to have tricritical point and shows first-order phase transition above the tricritical point, although the Gaussian distribution has no tricritical point and the second-order transition continues to zero temperature [31]. In many cases, an independent and identically distributed (i.i.d.) random field distribution for each site is assumed in theoretical or numerical studies. In this work, we introduce some correlation between random fields and thus they are no longer independent with each other. The correlation changes the critical behavior toward lower dimensional one [4, 13], i.e., the critical dimensions of correlated random-field Ising model become higher than uncorrelated one, as discussed in Sec. 2.3.3.

2.3.1 Critical dimension of the uncorrelated random-field Ising model

So far, the critical phenomena of the Ising model with the independently distributed random field is widely studied with various aspects and approaches. Even the simplest random field model, there are various unsolved problems, the difference between the Gaussian and binary distributions, the structure of the phase diagram, the critical exponents between upper and lower critical dimensions, and so on. An Ising model with relatively weak Gaussian random field, below the critical random-field intensity $h_{\mathrm{R}} < h_{\mathrm{Rc}}$, is believed to exhibit a second-order phase transition and we will assume this region following discussion if there is no mention. Qualitatively, a common sense is that the random fields work as a scattering noise of spin clusters and disturb to make an ordered phase, and thus critical dimensions become higher than the pure case.

Lower critical dimension

The lower critical dimension of the random-field Ising model is known to be $d_{\mathrm{lRF}} = 2$, which is first shown by Imry and Ma [7]. In all dimensions $d \leq d_{\mathrm{lRF}} = 2$, the ferromagnetic ground-state becomes unstable with respect to the formation of ill-oriented domains.

Suppose that a cluster of spins of linear size R surrounded by spins with the same direction. If this cluster is reversed, the energy cost from the domain wall, E_{dom}, is proportional to the domain wall surface area:

$$E_{\mathrm{dom}}(R) \sim JR^{d-1}. \tag{2.45}$$

On the other hand, random fields inside the cluster also increase/decrease the energy and compete to flip a cluster. The average of the random field contribution is clearly zero, but the variance is non-zero and thus there is non-zero contribution by a certain random field configuration in general. According to the central limit theorem, the mean square random field energy E_{RF}^2 inside a region of volume R^d is expressed as

$$E_{\mathrm{RF}}^2 \sim h_{\mathrm{R}}^2 R^d. \tag{2.46}$$

The energy E_{RF} may be positive or negative with equal probability. It is always possible however to find a region $E_{\mathrm{RF}} > 0$ which compete with the contribution from the domain wall. The total energy to reverse the domain of the size R is therefore

$$E(R) \sim JR^{d-1} - h_{\mathrm{R}}R^{d/2}. \tag{2.47}$$

For sufficient large R, $E(R)$ is positive for $d > 2$ but negative for $d < 2$. Thus the inversion of spins due to random fields happen at many locations for $d < 2$ and the ferromagnetic state becomes unstable. When $d > 2$, the increase of the interaction energy is the dominant term and the ferromagnetic state is stable against spin inversion by random fields. The case exact $d = 2$ is also shown by Binder [32] as an unstable long-range order.

Upper critical dimension

The upper critical dimension of the random-field Ising model is able to be estimated as $d_{\mathrm{uRF}} = 6$ [3]. It is necessary to take the configuration average of the free energy $-T[\log Z]$, which is apparently a difficult task because the dependence of $\log Z$ on random fields $\{h_i\}$ is quite complicated. To obtain the logarithm of the partition function of the random system, the replica method [3] is widely used. Remember here that each h_i appears in the exponent as $\exp(\beta \sum_i h_i S_i)$ in the partition function Z. The same is true for Z^n, where n is a natural number. We then use the identify

$$[\log Z] = \lim_{n \to 0} \frac{[Z^n] - 1}{n}. \tag{2.48}$$

This allows us to first calculate the configuration average of Z^n and then take the limit $n \to 0$, where Z^n means to prepare n replicas with identical random field configuration. The operation of the limit $n \to 0$ for a natural number n requires the validity of such an analytical continuation. Nevertheless, it turns out that most of the results obtained in this way for random systems have been proved or conjectured to be true. The validity of the replica method is widely believed and used.

Let us consider the behavior of the system in the Fourier space by taking the configurational average using the replica method. It is needed to check the wave number dependence of the Gaussian effective Hamiltonian, which is simply $\tilde{G}(q)^{-1}$, where $\tilde{G}(q)$ is the Forier transformation of the correlation function $G(r)$. The n-time replicated partition function is expressed as

$$\begin{aligned} Z^n &= \int \left(\prod_{\vec{r}} \prod_{\alpha=1}^{n} \mathrm{d}\phi^\alpha(\vec{r}) \right) \exp\left(-\sum_{\alpha=1}^{n} \left(kt \int \mathrm{d}\vec{r}\, (\phi^\alpha(\vec{r}))^2 \right.\right. \\ &\quad \left.\left. + b \int \mathrm{d}\vec{r}\, (\nabla\phi^\alpha(\vec{r}))^2 + \int \mathrm{d}\vec{r}\phi^\alpha(\vec{r}) h(\vec{r}) \right) \right). \end{aligned} \tag{2.49}$$

Where ϕ is the continuous order parameter,kt is the temperature difference from the critical point, b is the constant known as stiffness, and α is the replica index. We average Z^n over

the distribution of random fields following the prescription of the replica method. Using the Gaussian distribution (2.43) for each $h(\vec{r})$, the random-field part of the above equation is squared,

$$\begin{aligned} Z^n &= \int \left(\prod_{\vec{r}} \prod_{\alpha=1}^{n} \mathrm{d}\phi^\alpha(\vec{r}) \right) \exp\left(-\sum_{\alpha=1}^{n} \left(kt \int \mathrm{d}\vec{r}\, (\phi^\alpha(\vec{r}))^2 \right.\right. \\ &\quad \left.\left. + b \int \mathrm{d}\vec{r}\, (\nabla\phi^\alpha(\vec{r}))^2 \right) + \frac{h_{\mathrm{R}}^2}{2} \int \mathrm{d}\vec{r} \sum_{\alpha,\beta=1}^{n} \phi^\alpha(\vec{r})\phi^\beta(\vec{r}) \right). \end{aligned} \tag{2.50}$$

The representation in the wave number q by Fourier transformation is

$$\begin{aligned} Z^n &= \int \left(\prod_{\vec{q}} \prod_{\alpha=1}^{n} \mathrm{d}\tilde{\phi}^\alpha(\vec{q}) \right) \exp\left(-\sum_{\alpha=1}^{n} \left(kt \int \mathrm{d}\vec{q}\, \tilde{\phi}^\alpha(\vec{q})\tilde{\phi}^\alpha(-\vec{q}) \right.\right. \\ &\quad \left.\left. + \int \mathrm{d}\vec{q}\, bq^2 \tilde{\phi}^\alpha(\vec{q})\tilde{\phi}^\alpha(-\vec{q}) \right) + \frac{h_{\mathrm{R}}^2}{2} \int \mathrm{d}\vec{q} \sum_{\alpha,\beta=1}^{n} \tilde{\phi}^\alpha(\vec{q})\tilde{\phi}^\beta(-\vec{q}) \right). \end{aligned} \tag{2.51}$$

The exponent on the right-hand side is the effective free energy $-F$.

In order to confirm $\tilde{G}(q)$ at $t = 0$, we have to study the coefficient of $\tilde{\phi}(\vec{q})\tilde{\phi}(-\vec{q})$, which is now an $n \times n$ matrix with index $\{\alpha\}$ for each $\vec{q}$. Let us write the matrix $\tilde{G}(\vec{q})^{-1}$ at the critical point $t = 0$,

$$\tilde{G}(\vec{q})^{-1} = bq^2 - \frac{h_{\mathrm{R}}^2}{2} E, \tag{2.52}$$

where the first term on the right-hand side is the $n \times n$ unit matrix multiplied by bq^2 and the second term is the matrix E with all elements unity multiplied by $-h_{\mathrm{R}}^2/2$. The diagonal element of the inverse of the above matrix, $\tilde{G}^{\alpha\alpha}(\vec{q})$, gives the Fourier transformation of the correlation function $G^{\alpha\alpha}(\vec{r}) = \langle \phi^\alpha(\vec{r})\phi^\alpha(\vec{0}) \rangle$. If we notice the relation $E^2 = nE$, it is straightforward to see that the inverse matrix is written as

$$\begin{aligned} \tilde{G}(\vec{q}) &= \left(bq^2 - \frac{h_{\mathrm{R}}^2}{2} E \right)^{-1} \\ &= (bq^2)^{-1} \left(1 + \sum_{j=1}^{\infty} \left(\frac{h_{\mathrm{R}}^2}{2bq^2} \right)^j n^{j-1} E \right) \\ &= \frac{1}{bq^2} + \frac{h_{\mathrm{R}}^2 E}{bq^2(2bq^2 - nh_{\mathrm{R}}^2)}. \end{aligned} \tag{2.53}$$

The mean-field approximation is valid only when fluctuations around the average of physical quantities are negligible. To measure the fluctuations. We accumulate fluctuations of magnetization $h_{\mathrm{R}m}^2$ up to the length scale of the correlation length ξ,

$$h_{\mathrm{R}m}^2 = \int_0^\xi \langle (S_r - \langle S_r \rangle)(S_0 - \langle S_0 \rangle) \rangle \, \mathrm{d}\vec{r} = \int_0^\xi (\langle S_r S_0 \rangle - \langle S_r \rangle \langle S_0 \rangle) \mathrm{d}\vec{r}. \tag{2.54}$$

The integrand in this equation is the two-point correlation function $G(r)$. $G(r)$ takes some finite value for r smaller than the correlation length ξ and rapidly decreases for $r > \xi$. We, therefore,

approximate $G(r)$ by its value at the correlation length $G(\xi)$ and multiply the correlated volume as

$$h_{\mathrm{R}m}^2 \approx G(\xi)\xi^d. \tag{2.55}$$

Thus, $G(r)\xi^d \ll m^2\xi^d$ is the condition of the mean-field approximation, so that

$$G(\xi) \ll m^2. \tag{2.56}$$

The Fourier transformation of Eq. (2.53) is expressed as $G(\xi) \propto \xi^{4-d}$, since the leading term of Eq. (2.53) is q^{-4} in the limit $n \to 0$ and $q \to 0$. This equation and the critical behavior (2.56) lead the condition:

$$(d-4)\nu > 2\beta. \tag{2.57}$$

By using the mean-field critical exponents, it is concluded that the mean-field behavior is valid for $d > 6$, and the upper critical dimension of the random-field Ising model is $d_{uRF} = 6$.

2.3.2 Scaling relations of random system

Dimensional reduction

Critical behavior of the random-field Ising model between upper and lower critical dimensions is one of the representative unsolved problems of random systems. A perturbation theory known as "dimensional reduction" [7–9, 33] predicts that the universality class of the $d = d_{\mathrm{uRF}} - \epsilon$ dimensional random-field Ising model corresponds to $D = d_{\mathrm{uSR}} - \epsilon$ dimensional pure model, where $d_{\mathrm{uSR}} = 4$ is the upper critical dimension of the pure Ising model. The dimensional reduction prediction is known to lose its validity and breakdown with larger $\epsilon = d_{\mathrm{uRF}} - d$, i.e., in lower dimensions. The dimensional reduction mentions the critical behavior of the d dimensional random-field Ising model correspond to $d-2$ dimensional pure Ising model. If we conjecture the lower critical dimension of the random-field Ising model d_{lRF} by dimensional reduction, $d_{\mathrm{lRF}} = 2 + d_{\mathrm{l}} = 2 + 1 = 3$, where $d_{\mathrm{l}} = 1$ is the lower critical dimension of the pure Ising model. This estimation does not correspond to the simple and intuitive result shown in Sec. 2.3.1, $d_{\mathrm{lRF}} = 2 \neq 3$, and thus dimensional reduction does not provide a valid estimation in lower dimensions.

We have discussed in Sec. 2.3.1 that the Ising model in a short-range correlated random field has an ordered phase and phase transition at finite temperature in more than two dimensions, but not the order of the transition. The mean field approximation predicts a second order transition for a Gaussian distribution of the random field, but for a bimodal distribution the transition becomes first order if h_{R} is larger than tricritical point [31]. Although there is still a matter of controversy and is so far no proof for a continuous transition in finite dimensions, we will assume in the following the transition is indeed continuous, which seems to be at least true for a Gaussian random field distribution [34].

Modified hyperscaling relation

Critical phenomena of the random-field Ising model also believed to be described by the scaling relations, but its formulations do not correspond to that of the pure system. Generally, the hyperscaling relation of the random-field Ising model is believed to be replaced by the following "modified hyperscaling relation" [5, 35]:

$$\nu(d-\theta) = 2\beta + \gamma = 2 - \alpha, \tag{2.58}$$

where θ is an additional critical exponent, so-called "violation of hyperscaling exponent". The exponent θ can be interpreted as a quantity that relates the d dimensional random system with the

$$D = d - \theta \tag{2.59}$$

dimensional pure system since we can obtain the standard hyperscaling relation from Eq. (2.58) by replacing $d-\theta$ as D, that implies that θ decreases the effective dimension D from d to $d-\theta$. The dimensional reduction prediction claims $\theta = 2$. The exponent θ is described by the singular part of the free energy caused by random field in a correlation volume Δf_{RF} as following,

$$\Delta f_{\mathrm{RF}} \propto \xi^{\theta}. \tag{2.60}$$

Having $\theta > 0$ implies that hyperscaling relation must be modified.

The following inequality is exactly proven by Schwartz and Soffer [36],

$$\theta \geq \frac{\gamma}{\nu} = 2 - \eta, \tag{2.61}$$

and this inequality is believed to be asymptotic to an equality [37–39]

$$\theta = \frac{\gamma}{\nu} = 2 - \eta. \tag{2.62}$$

The relations described above are deduced as follows [34]. Near the criticality, the singular part of the free energy can be attributed to correlated regions of spins(clusters) of linear size ξ. For the pure system, singular part of the free energy F is described as $F = -(k_B T \ln 2)N/\xi^d$ since each cluster with one Ising degree of freedom can be taken as independently from its neighbors and singular part of F is described by the entropic part of N/ξ^d independent clusters. Hence, singular part of the free energy density of pure system $f_{\mathrm{sing}}(t,h)$ is described as

$$f_{\mathrm{sing}}(t,0) \propto \xi^{-d} \propto |t|^{d\nu}, \tag{2.63}$$

where Eq. (2.7) was used. On the other hand, for an Ising model with quenched random-field, singular part of the free energy is caused by the contribution of the Zeeman energy rather than entropy. Consider the system with clusters of linear dimension ξ, such that each cluster may be considered as independent of its neighbors. Each cluster is acted by random fields h_{R}.

In a region of volume ξ^d, expectation value of the sum of the random fields is described as $[\sum_i^{\xi^d} h_i] \propto \pm h_{\rm R}\xi^{d/2}$ by the central limit theorem, and thus excess random field per spin is

$$\Delta_h \propto h_{\rm R}\xi^{-d/2}. \tag{2.64}$$

This implies that a finite magnetization per spin is

$$\langle m\rangle \propto \chi\Delta_h \propto \pm r\chi\xi^{-d/2}. \tag{2.65}$$

The Zeeman contribution to the free energy thus becomes

$$f_{\rm sing}(t,0) \propto \langle m\rangle\,\Delta_h \propto h_{\rm R}^2\chi\xi^d \propto |t|^{d\nu-\gamma}. \tag{2.66}$$

This dominates the entropy contribution near the critical point since $|t|^{d\nu-\gamma} > |t|^{d\nu}$ for $t \ll 1$. Eq. (2.10) is rewritten as

$$f(t,0) \propto |t|^{2-\alpha} \tag{2.67}$$

and by comparing with Eq. (2.66), the relation

$$2-\alpha = \nu(d-\gamma/\nu) \tag{2.68}$$

is obtained rather than the relation of pure system $2-\alpha = \nu d$. By the way, the critical behavior of the free energy of pure system is expressed as follows by using the hyperscaling relation,

$$f_{\rm pure} \propto |t|^{2-\alpha} \propto |t|^{d\nu} \propto \xi^{-d}. \tag{2.69}$$

On the other hand, the free energy of random system is expressed by Eq. (2.68) as

$$f_{\rm RF} \propto |t|^{2-\alpha} \propto |t|^{\nu(d-\gamma/\nu)} \propto \xi^{-(d-\gamma/\nu)}. \tag{2.70}$$

If we separate the singular behavior of $f_{\rm RF}$ into $f_{\rm pure}\times\Delta f_{\rm RF}$ and compare with Eq. (2.60),

$$f_{\rm RF} \propto \xi^{-d}\xi^{\gamma/\nu} \propto f_{\rm pure}\Delta f_{\rm RF} = \xi^{-d}\xi^{\theta}, \tag{2.71}$$

and thus we have obtained the relation $\theta = \gamma/\nu$ and Eq. (2.68) becomes the modified hyperscaling relation (2.58).

The dynamical behavior of the random-field Ising model also differs from the pure system. Instead of the power law critical slowing down $\tau \propto \xi^z$ with the "dynamic critical exponent" z [40], "thermally activated critical slowing down" [5, 35]

$$\ln\tau \propto \xi^{\theta} \tag{2.72}$$

appears.

Connected and disconnected physical quantities and their critical behavior

To estimate the statistical physical quantities of a random system, we have to take into account two types of fluctuations, thermal fluctuation and random fluctuation. An naive generalization from the pure case is called the "connected" physical quantity, where the expectation value of the thermally fluctuated physical quantities for each quenched random field replica are first estimated, and then the random average of the average values is taken. On the other hand, to estimate the fluctuation of the physical quantities by randomness, we have to analyze the behavior of the thermally averaged order parameter, which is called the "disconnected" physical quantity. The connected and disconnected correlation functions (and their critical behavior) are expressed as follows:

$$G_{\rm con}(r) = [\langle S(0)S(r)\rangle - \langle S(0)\rangle \langle S(r)\rangle] \propto r^{-d+2-\eta} \tag{2.73}$$

$$G_{\rm dis}(r) = [\langle S(0)\rangle \langle S(r)\rangle] - [\langle S(0)\rangle][\langle S(r)\rangle] \propto r^{-d+4-\bar{\eta}}, \tag{2.74}$$

where $\langle\cdot\rangle$ is the thermal average and $[\cdot]$ is the random average. We introduced another critical exponent $\bar{\eta}$ in the last equation. The magnetic susceptibility of random system are also able to be defined as follows:

$$\chi_{\rm con} = L^d \left[\langle m^2\rangle - \langle|m|\rangle^2\right] \propto |t|^{-\gamma} \tag{2.75}$$

$$\chi_{\rm dis} = L^d(\left[\langle|m|\rangle^2\right] - [\langle|m|\rangle]^2) \propto |t|^{-\bar{\gamma}}. \tag{2.76}$$

The new exponent $\bar{\eta}$ is related with $\bar{\gamma}$ as follows

$$\bar{\eta} = 4 - \frac{\bar{\gamma}}{\nu}, \tag{2.77}$$

as the relation between η and γ. The exact relation between the disconnected and connected critical exponents, $\bar{\eta}$ and η, is obtained as follows [36]:

$$\bar{\eta} \leq 2\eta. \tag{2.78}$$

This inequality has been asserted to be equality [37, 39]

$$\bar{\eta} = 2\eta, \tag{2.79}$$

which also implies

$$\bar{\gamma} = 2\gamma. \tag{2.80}$$

The violation of hyperscaling exponent θ can be expressed as [5, 35, 41]

$$\theta = 2 - \bar{\eta} + \eta. \tag{2.81}$$

By using this relation and Eq. (2.79), the effective dimension D (2.59) is able to be rewritten by the modified dimensional reduction [37]

$$D = d - 2 + \bar{\eta}(d) - \eta(d) = d - 2 + \eta(d) = d - 2 + \eta_0(D), \tag{2.82}$$

where $\eta_0(D)$ is the critical exponent of the D dimensional pure system.

Harris criterion

If a phase transition occurs at the fixed critical point in a random system, the important condition, the Harris criterion [42], must be satisfied:

$$d\nu \geq 2. \tag{2.83}$$

We briefly interpret this condition below. If we divide the system into clusters with volume ξ^d which can be count as independent subsystems, the standard deviation of the random-field inside the cluster is described as Eq. (2.64) and therefore fluctuation causes the fluctuation of the critical temperature of each subsystem,

$$\frac{\Delta T_c}{T_c} \propto \xi^{-d/2}. \tag{2.84}$$

The correlation length ξ cannot be larger than that corresponding to a temperature with Eq. (2.84), since if the growth of ξ causes larger fluctuation of T_c, T_c is scattered and T_c becomes ill-defined:

$$\xi \leq \left| \frac{\Delta T_c}{T_c} \right|^{-\nu} \propto \xi^{d\nu/2}. \tag{2.85}$$

This condition claims the criterion (2.83).

2.3.3 Spatially correlated random-field Ising model

If random fields are correlated with each other, it is predicted that the universality class becomes changed from the uncorrelated case. Consider the Gaussian random fields with algebraically long-range correlation,

$$P(h_i) = \frac{1}{\sqrt{2\pi}h_{\mathrm{R}}} \exp\left(-\frac{h_i^2}{2h_{\mathrm{R}}^2}\right), \quad [h_i h_j] = \begin{cases} h_{\mathrm{R}}^2 & (i=j) \\ \frac{a h_{\mathrm{R}}^2}{|\vec{r}_i - \vec{r}_j|^{d-\rho}} & (i \neq j). \end{cases} \tag{2.86}$$

Kardar et al. [13] predicted the universality class of the random-field Ising model with algebraically correlation as follows:

- If $\rho \leq 0$, the correlation does not affect the critical behavior, and therefore it corresponds to the uncorrelated random-field Ising model. Thus, in the following, we assume $\rho > 0$.
- The upper critical dimension of the correlated random-field Ising model d_{uCRF} becomes

  $$d_{uCRF} = d_{uRF} + \rho = 6 + \rho, \tag{2.87}$$

  which is obtained from the Landau-Ginzburg form.
- The lower critical dimension of the correlated random-field Ising model d_{lCRF} becomes

  $$d_{lCRF} = d_{lRF} + \rho = 2 + \rho, \tag{2.88}$$

  which is obtained from the extended domain-wall picture by Imry and Ma [7].

- A d-dimensional correlated random-field Ising model between upper and lower critical dimensions corresponds to the

$$D = d - 2 - \rho \tag{2.89}$$

dimensional pure Ising model, which is obtained from the first order renormalization group expansions. For $\rho \leq 0$, this prediction becomes same as a dimensional reduction prediction with $D = d - 2$ dimensional effective behavior, which has already confirmed on above Sec. 2.3.2 to lose its validity in lower dimensions. Kardar et al. [13] also confirmed the prediction fails at higher order expansion.

The phase diagram of the n-component spin model with correlated random-field is given in Fig. 2.1. To summarize, stronger correlation of the random fields makes the critical phenomena toward lower dimensional one.

Although this prediction seems to violate at least in the region between upper and lower critical dimensions and precise behavior is unclear. If we believe the prediction of the transition of the upper and lower critical dimensions which are deduced by comparatively reliable method at upper and lower critical dimensions, i.e., the Landau-Ginzbrug Hamiltonian and the domain-wall picture, respectively, it is natural and intuitive analogical inference that the effective dimension between upper and lower critical dimensions also decreases proportionally to ρ. The case we compare the effective dimensions of the d-dimensional correlated random-field Ising model with D'-dimensional uncorrelated one, this assertion is able to be reworded as

$$D' = d - \rho \tag{2.90}$$

for arbitrary dimensions. If we assume the modified dimensional reduction (2.82), the effective dimension D of the d-dimensional algebraically correlated random-field Ising model with exponent $-(d - \rho)$ is expressed as

$$D = D' - 2 + \eta(D') = d - \rho - 2 + \eta(d - \rho) = d - \rho - 2 + \eta_0(D), \tag{2.91}$$

where $\eta(D')$ and $\eta_0(D)$ are the critical exponents of the D'-dimensional uncorrelated random-field Ising model and the D-dimensional pure Ising model, respectively. For example, the universality class of the two-dimensional pure Ising model corresponds to $2 = d - 2 + 1/4 \to d = 3.75$ dimensional random-field Ising model. Therefore, four-dimensional correlated random field Ising model with $\rho = 1/4$ is predicted to correspond to the two-dimensional pure Ising model.

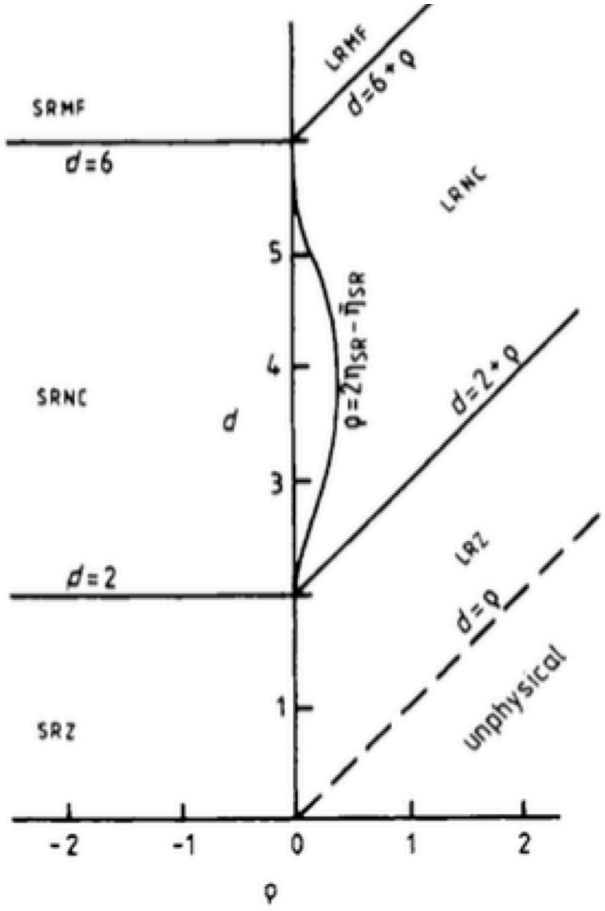

Figure 2.1: Phase diagram of the $O(n)$ spin model with correlated random-field in the d-ρ plane (taken from Ref. 4). SRMF is the mean-field region with short-range effective random-field correlations. LRMF is the mean-field region with long-range effective random-field correlations. SRNC and LRNC are short-range/long-range non-classical region, which has a behavior between upper and lower critical dimensions. SRZ and LRZ are below its lower critical dimension and hence do not have long-range order at finite temperature. The curve $\rho = 2\eta_{SR} - \bar{\eta}_{SR}$ is the boundary which has dominant short-range term behavior, i.e., the boundary between SRNC and LRNC. If the prediction (2.79) is correct, this curve lies on the d-axis. The random field correlation diverges and does not make sense at the unphysical region.

Chapter 3

Review of Numerical Simulation Algorithms

3.1 Markov chain Monte Carlo

3.1.1 What is Markov chain Monte Carlo method?

The Monte Carlo method is a statistical method to estimate expectation values by using pseudo random numbers [43]. One of the most simple examples is the expectation value of dice: The expectation value of hexahedral die, $\langle X \rangle$, is evaluated analytically as

$$\langle X \rangle = \sum_{i=1}^{6} P(i)X(i) = \sum_{i=1}^{6} (\frac{1}{6} \times i) = 3.5, \tag{3.1}$$

where $X(i)$ is the pip of a dice and $P(i)$ is its probability. On the other hand, $\langle X \rangle$ is also obtained by sufficient large number of trials, N, as

$$\langle X \rangle = \lim_{N \to \infty} \frac{1}{N} \sum_{i=1}^{N} X_i^r \approx \frac{1}{N} \sum_{i=1}^{N} X_i^r. \tag{3.2}$$

Here, X_i^r is the random number that returns an integer from one to six. Although Eq. (3.1) is superior for a simple model like a die as it is exact and it is easier to obtain the solution, the Monte Carlo method reveals its potential for the case where the analytic solution is hardly obtained.

The expectation value of a physical quantity X at thermal equilibrium is obtained by

$$\langle X \rangle = \sum_{c} \frac{\exp(-\beta \mathcal{H}_c)}{Z} X(c), \tag{3.3}$$

where $Z \equiv \sum_c \exp(-\beta \mathcal{H}_c)$ is the partition function, $\mathcal{H}_c$ is the Hamiltonian, and c denotes configuration of the system. As a simplest example, let us consider the three-dimensional Ising model of linear size $L = 5$. It has $5^3 = 125$ spins and the number of states is then $2^{125} \approx 10^{38}$. Even if one uses the K Computer, which peak performance is about 10^{16} flops, the brute-force

enumeration of Eq. (3.3) will take at least $10^{38}/10^{16} = 10^{22}$ sec $\approx$ 300 trillion years. That is, exact enumeration is impossible practically even for the present simple model. The Monte Carlo method with appropriate sampling scheme enables us far faster calculation with high precision.

Eq. (3.2) is an example of so-called simple sampling. As for the case of Eq. (3.3), the simple Monte Carlo sampling is expressed as follows:

$$\langle X \rangle \approx \frac{\sum_{s}^{N_{\rm MC}} \exp(-\beta \mathcal{H}_{c_s}) X(c_s)}{\sum_{s}^{N_{\rm MC}} \exp(-\beta \mathcal{H}_{c_s})} \quad \text{(simple sampling)}, \tag{3.4}$$

where $N_{\rm MC}$ is the number of Monte Carlo steps (samples) and c_s denotes the configuration of the s-th sample. In the Monte Carlo sampling, the way how to generate configurations affects greatly the final precision, i.e., the statistical error, of the average of physical quantities. The most simple way to generate samples is to get configurations uniformly at random [random sampling, Eq. (3.4)]. However, in many cases the random sampling does not work properly. Generating configurations uniformly at random corresponds to sample in the high temperature limit. For a system at low temperatures, almost all samples have exponentially small Boltzmann factor, $\exp(-\beta \mathcal{H}_{c_s})$, and only a few dominate the contribution to the partition function, and therefore the statistical error diverges as the temperature decreases. The importance sampling is a powerful technique to reduce the statistical error. In this method, configurations are not chosen uniformly at random, but generated according to some pre-defined probability density function, $P(c)$. Then, the statistical average of the physical quantity is estimated as

$$\langle X \rangle \approx \frac{\sum_{s}^{N_{\rm MC}} \exp(-\beta \mathcal{H}_{c_s}) X(c_s)/P(c_s)}{\sum_{s}^{N_{\rm MC}} \exp(-\beta \mathcal{H}_{c_s})/P(c_s)} \quad \text{(importance sampling)}. \tag{3.5}$$

The simple sampling (random sampling) corresponds to the case with $P(c) = \text{const}$. Ideally, if one can choose $P(c)$ so as to be proportional to the Boltzmann weight of the configuration, $\exp(-\beta \mathcal{H}_c)$, then the variance of the denominator of Eq. (3.5) can be eliminated and we get around to the following simple expression:

$$\langle X \rangle \approx \frac{1}{N_{\rm MC}} \sum_{s}^{N_{\rm MC}} X(c_s) \quad \text{(ideal sampling)}. \tag{3.6}$$

In practice, however, it is almost impossible to generate independent samples according to $P(c) = \exp(-\beta \mathcal{H}_c)/Z$. This is because that we can not know the normalization Z in advance. Even if one can calculate Z in some way, sample generation is still extremely difficult due to exponentially large number of configurations.

The Markov chain Monte Carlo (MCMC) method is one of the most powerful methods which realizes Monte Carlo simulations free from these difficulties [43, 44]. In the MCMC,

configuration of the system is changed by using the Markov chain, i.e., samples are generated from the previous one according to the transition matrix, $W^{(c_l)(c_k)}$, which defines the probability that a configuration changes from c_k to c_l. Note that transition matrix W has huge number of elements. The MCMC enables us to generate samples without using the whole transition matrix.

The transition matrix is not unique. Innumerable patterns of transition matrix can be used as long as it meets the requirements [45, 46]. The requirements for the transition matrix are as follows:

- Ergodicity: There exists an positive integer N, and for $n \geq N$,

$$(W^n)^{(c_l)(c_k)} > 0 \tag{3.7}$$

  is satisfied for any c_l and c_k. This condition guarantees that the all configurations with positive weights will be visited from any initial condition.

- Normalization: In order that $W^{(c_l)(c_k)}$ represents a probability,

$$0 \leq W^{(c_l)(c_k)} \leq 1 \tag{3.8}$$

  for any c_l and c_k, and

$$\sum_l W^{(c_l)(c_k)} = 1 \tag{3.9}$$

  for any c_k.

- Balance condition:

$$WP_{eq} = P_{eq}, \tag{3.10}$$

  or

$$\sum_k W^{(c_l)(c_k)} P_{eq}^{(c_k)} = P_{eq}^{(c_l)} \tag{3.11}$$

  for all c_l. This condition means that the equilibrium distribution $P_{\rm eq}$ is an eigenvector of W with eigenvalue unity, i.e., it is invariant before and after the transition, where $P_{\rm eq}$ is the target distribution, i.e., the Boltzmann distribution, $\exp(-\beta E^{(c_k)})/Z$ in the statistical physics problems.

  Instead of the balance condition (3.11), the transition matrix W is usually chosen so that it fulfills the detailed balance condition:

$$W^{(c_l)(c_k)} \exp(-\beta E^{(c_k)}) = W^{(c_k)(c_l)} \exp(-\beta E^{(c_l)}), \tag{3.12}$$

  which is a sufficient condition of the balance condition. Actually, by taking a summation over k on both sides of Eq. (3.12), the balance condition (3.11) is recovered since $\sum_k W^{(c_k)(c_l)} = 1$:

$$\begin{aligned} \sum_k W^{(c_l)(c_k)} \exp(-\beta E^{(c_k)}) &= (\sum_k W^{(c_k)(c_l)}) \exp(-\beta E^{(c_l)}) \\ &= 1 \times \exp(-\beta E^{(c_l)}). \end{aligned} \tag{3.13}$$

It can be shown that a Markov chain that satisfies the above conditions generates configurations according to the Boltzmann distribution in the long time limit, and thus the statistical average of the physical quantities can be evaluated via Eq. (3.4) by sampling long time enough from the Markov chain.

3.1.2 Single spin flip algorithm

The single spin flip algorithm is one of the most fundamental algorithms for the MCMC method. The single spin flip update for the Ising model is described as follows:

1. Choose a candidate spin uniformly at random or in series.

2. Flip a chosen spin according to

$$P_M = \min\{1, \exp(-\beta(\mathcal{H}(c_l) - \mathcal{H}(c_k)))\} \tag{3.14}$$

   (Metropolis method [47]), or

$$P_{HB} = \frac{\exp(-\beta\mathcal{H}(c_l))}{\exp(-\beta\mathcal{H}(c_k)) + \exp(-\beta\mathcal{H}(c_l))} \tag{3.15}$$

   (Heat bath method [48]), where c_k and c_l are the spin configurations before and after flipping the target spin, respectively.

By repeating this procedure, new configurations are generated in sequence. One can show that the above procedure fulfills the detailed balance condition (3.12) as seen below.

In the case where the transition from c_k to c_l increases the energy, the transition probability is expressed as

$$W^{(c_l)(c_k)} = \exp(-\beta(\mathcal{H}(c_l) - \mathcal{H}(c_k))) \tag{3.16}$$

$$W^{(c_k)(c_l)} = 1 \tag{3.17}$$

in the Metropolis method. By substituting it to Eq. (3.12), we obtain

$$\begin{aligned} \text{left-hand side} &= W^{(c_l)(c_k)} \exp(-\beta\mathcal{H}(c_k)) \\ &= \exp(-\beta(\mathcal{H}(c_l) - \mathcal{H}(c_k))) \times \exp(-\beta\mathcal{H}(c_k)) \\ &= \exp(-\beta\mathcal{H}(c_l)) \end{aligned} \tag{3.18}$$

$$\begin{aligned} \text{right-hand side} &= W^{(c_k)(c_l)} \exp(-\beta\mathcal{H}(c_l)) \\ &= 1 \times \exp(-\beta\mathcal{H}(c_l)). \end{aligned} \tag{3.19}$$

Thus, the Metropolis update satisfies the detailed balance. The same applies also for the heat bath method,

$$\begin{aligned} \text{left-hand side} &= W^{(c_l)(c_k)} \exp(-\beta\mathcal{H}(c_k)) \\ &= \frac{\exp(-\beta\mathcal{H}(c_l))\exp(-\beta\mathcal{H}(c_k))}{\exp(-\beta\mathcal{H}(c_k)) + \exp(-\beta\mathcal{H}(c_l))} \end{aligned} \tag{3.20}$$

$$\begin{aligned} \text{right-hand side} &= W^{(c_k)(c_l)} \exp(-\beta\mathcal{H}(c_l)) \\ &= \frac{\exp(-\beta\mathcal{H}(c_k))\exp(-\beta\mathcal{H}(c_l))}{\exp(-\beta\mathcal{H}(c_l)) + \exp(-\beta\mathcal{H}(c_k))}. \end{aligned} \tag{3.21}$$

In the single spin update algorithm, configurations before and after the transition are very similar with each other, since one Monte Carlo step updates only one spin. Therefore, the autocorrelation time between the succeeding configurations may become very long, and the relaxation may becomes very slow, especially near the phase transition point or at low temperatures, since correlation length diverges. In the next section, we introduce the cluster algorithm that can reduce the relaxation time drastically in many cases.

3.1.3 Cluster algorithm

Before we explain the cluster algorithm, we first review the Fortuin-Kasteleyn representation. In general, the energy of the system is expressed as a sum of local interactions (bonds), and thus the Boltzmann weight is written as a product of local weights:

$$Z = \sum_{\{c\}} \prod_{\{i,j\}} \exp(\beta J_{ij} S_i S_j) = \sum_{\{c\}} \prod_{l=0}^{N_b} \exp(\beta J_l \sigma_l), \tag{3.22}$$

where N_b is a number of bonds, $J_l = J_{ij}$ is the coupling constant of lth bond, $\sigma_l = S_i S_j$ is the product of the spin states of both ends of the bond l. In the Fortuin-Kasteleyn representation, the configuration space of the Ising model is extended from $\{c\}$ to $\{(c, g)\}$, where g is called a graph configuration.

The Swendsen-Wang algorithm is a cluster algorithm for the Ising model [49]. One Monte Carlo step of the Swendsen-Wang algorithm is described as follows:

1. For each bond l,
   - if spins on both sides have the same direction, activate bond l with probability P_l and let the spins into the same cluster, otherwise delete bond l and do nothing.
   - if spins on both sides are opposite with each other, delete bond l and do nothing.
2. Flip spins on each cluster simultaneously at random.

Using the Swendsen-Wang algorithm, configuration evolves much faster than the single spin flip method especially in the case where the correlation length at equilibrium becomes very large, because the length scale of generated clusters is proportional to the correlation length. The

Swendsen-Wang algorithm clearly satisfies the ergodicity; it is possible to reach an arbitrary configuration from any configuration only by one step, since constructing clusters that consist of single spins is always possible.

The Swendsen-Wang algorithm also satisfies the detailed balance. In the following, we prove the detailed balance by induction. Let us consider the partial Hamiltonian, $\mathcal{H}_n$, which contains only n bonds among N_b bonds in the original Hamiltonian. Clearly, $\mathcal{H}_{N_b}$ is equivalent to the original Hamiltonian, while $\mathcal{H}_0$ denotes non-interacting spins.

First, it is trivial that the Swendsen-Wang algorithm for $\mathcal{H}_0$ satisfies the detailed balance. In this case, the Swendsen-Wang algorithm generates independent clusters as there is no interaction in the system. As a result, all spins can be flipped freely and then configurations are sampled uniformly at random.

Next, let us assume that the Swendsen-Wang algorithm satisfies the detailed balance for $\mathcal{H}_{n-1}$ for some n $(0 < n \leq N_b)$, that is, the transition probability $T_{n-1}(c_k \to c_l)$ satisfies

$$\frac{T_{n-1}(c_k \to c_l)}{T_{n-1}(c_l \to c_k)} = \exp(-\beta[\mathcal{H}_{n-1}(c_l) - \mathcal{H}_{n-1}(c_k)]). \tag{3.23}$$

In the meantime, the transition probability for the Swendsen-Wang algorithm $\mathcal{H}_n$ can be expressed as

$$T_n(c_k \to c_l) = T_n^f(c_k \to c_l)P_n(c_k) + T_n^d(c_k \to c_l)[1 - P_n(c_k)], \tag{3.24}$$

where $T_n^d(c_k \to c_l)$ and $T_n^f(c_k \to c_l)$ are the conditional transition probabilities in the case where bond n is eliminated or activated, respectively. The former satisfies $T_n^d(c_k \to c_l) = T_{n-1}(c_k \to c_l)$, since n-th bond is always eliminated in T_{n-1}. On the other hand, $T_n^f = T_{n-1}$ if $\sigma_n = 1$ and $T_n^f = 0$ if $\sigma_n = -1$ in c_l, because two spins cannot be connected by n-th bond in the case where they have opposite directions with each other.

Let us consider the case where $\sigma_n = 1$ in both configurations, c_k and c_l. In this case, $P_n(c_k) = P_n(c_l) = 1 - \exp(-2\beta J_n)$. The ratio of transition probabilities is then written as

$$\begin{aligned}
\frac{T_n(c_k \to c_l)}{T_n(c_l \to c_k)} &= \frac{T_n^f(c_k \to c_l)[1 - \exp(-2\beta J_n)] + T_n^d(c_k \to c_l)\exp(-2\beta J_n)}{T_n^f(c_l \to c_k)[1 - \exp(-2\beta J_n)] + T_n^d(c_l \to c_k)\exp(-2\beta J_n)} \\
&= \frac{T_{n-1}(c_k \to c_l)[1 - \exp(-2\beta J_n)] + T_{n-1}(c_k \to c_l)\exp(-2\beta J_n)}{T_{n-1}(c_l \to c_k)[1 - \exp(-2\beta J_n)] + T_{n-1}(c_l \to c_k)\exp(-2\beta J_n)} \\
&= \frac{T_{n-1}(c_k \to c_l)}{T_{n-1}(c_l \to c_k)} = \exp(-\beta[\mathcal{H}_{n-1}(c_l) - \mathcal{H}_{n-1}(c_k)]) \\
&= \exp(-\beta[\mathcal{H}_n(c_l) - \mathcal{H}_n(c_k)])
\end{aligned} \tag{3.25}$$

as the local energy on bond n does not change between c_k and c_l. Similarly, in the case where $\sigma_n = -1$ in both configurations,

$$\begin{aligned}
\frac{T_n(c_k \to c_l)}{T_n(c_l \to c_k)} &= \frac{T_n^d(c_k \to c_l)}{T_n^d(c_l \to c_k)} = \exp(-\beta[\mathcal{H}_{n-1}(c_l) - \mathcal{H}_{n-1}(c_k)]) \\
&= \exp(-\beta[\mathcal{H}_n(c_l) - \mathcal{H}_n(c_k)]).
\end{aligned} \tag{3.26}$$

Finally, we consider the case where σ_n is different between c_k and c_l. If $\sigma_n = 1$ (-1) in c_k (c_l),

$$\begin{aligned}\frac{T_n(c_k \to c_l)}{T_n(c_l \to c_k)} &= \frac{T_{n-1}(c_k \to c_l)\exp(-2\beta J_n)}{T_{n-1}(c_l \to c_k)} \\ &= \exp(-\beta[\mathcal{H}_{n-1}(c_l) - \mathcal{H}_{n-1}(c_k)])\exp(-2\beta J_n) \\ &= \exp(-\beta[\mathcal{H}_n(c_l) - \mathcal{H}_n(c_k)]). \end{aligned} \tag{3.27}$$

Thus, if the Swendsen-Wang algorithm satisfies the detailed balance for $\mathcal{H}_{n-1}$, it also does for $\mathcal{H}_n$ $(0 < n \leq N_b)$. Since the detailed balance is satisfied for $n = 0$, it is proved for $n = N_b$ by induction.

3.2 Fukui-Todo method

The main difficulty in simulating the system with the long-range interaction is the large calculation cost. The number of pairs is $N(N-1)/2 \sim N^2$ for an N-spin system. A naive update in the Monte Carlo simulation will suffer from the $O(N^2)$ computational cost. To make matters worse, the system with the long-range interaction is known for the egregious finite-size and boundary effects compared to the short-range model. Much larger systems thus need to be calculated, for the estimation of critical exponents, than the case of the short-range interaction. In addition, it becomes important to take into account interactions from mirror-image cells across the periodic boundaries and the Ewald summation to further reduce the finite-size effect.

A first efficient algorithm for the Ising model with the long-range interaction was proposed by Luijten and Blöte [50], whose computational cost scales in $O(N \log N)$. We will adopt the Fukui-Todo cluster algorithm [11] that is a more powerful approach; it further reduces the computational cost down to $O(N)$ for generic (unfrustrated) long-range interacting spin models [11, 51, 52].

The Fukui-Todo cluster algorithm is based on the Swendsen-Wang cluster algorithm [49]. In the original Swendsen-Wang algorithm for inverse temperature β, we first activate each (interaction) bond with probability

$$P_{ij} = 1 - \exp(-2\beta J_{ij}), \tag{3.28}$$

when $S_i = S_j$. Then spin clusters, each of which consists of spins connected by activated bonds, are flipped independently to generate a next spin configuration.

In the Fukui-Todo cluster algorithm, first we introduce the extended Fortuin-Kasteleyn representation [53, 54]. The partition function of the Ising model (2.38) is rewritten into the extended Fortuin-Kasteleyn representation:

$$Z = \sum_{\{S_i\}} \sum_{\{k_{ij}\}} \prod_{i<j}^{N} \Delta(\sigma_{ij}, k_{ij}) V_{ij}(k_{ij}), \tag{3.29}$$

where $\sigma_{ij} = S_i S_j$ and k_{ij} is a non-negative integer assigned to each spin pair (i, j). The "compatibility function" $\Delta(\sigma_{ij}, k_{ij})$ and the "weight" $V_{ij}(k_{ij})$ in Eq. (3.29) are defined as

$$\Delta(\sigma_{ij}, k_{ij}) = \begin{cases} 1 & \text{if } \sigma_{ij} = 1 \text{ or } k_{ij} = 0 \\ 0 & \text{otherwise,} \end{cases} \tag{3.30}$$

and

$$V_{ij}(k_{ij}) = \frac{\exp(-2\beta J_{ij})(2\beta J_{ij})^{k_{ij}}}{k_{ij}!}, \tag{3.31}$$

respectively. Due to the property of the compatibility function, antiparallel spin configuration ($\sigma_{ij} = -1$) is prohibited when $k_{ij} \geq 1$. Then one can interpret a bond with $k_{ij} \geq 1$ and $k_{ij} = 0$ as an activated and deactivated bond, respectively, in a similar way to the original Swendsen-Wang algorithm. Note that $V_{ij}(k_{ij})$ is the probability mass function of the Poisson distribution with mean $2\beta J_{ij}$, and satisfies the normalization condition, $\sum_{k_{ij}=0}^{\infty} V_{ij}(k_{ij}) = 1$ for all (i, j).

Based on the generalized Fortuin-Kasteleyn representation (3.29), one Monte Carlo step of the Fukui-Todo cluster algorithm is performed as follows:

(i) Generate an integer k from the Poisson distribution $f(k; \lambda_{\text{tot}}) = \exp(-\lambda_{\text{tot}})\lambda_{\text{tot}}^k / k!$, where $\lambda_{\text{tot}} = 2\beta \sum_{i<j}^{N} J_{ij}$.

(ii) Choose a pair (i, j) according to the probability $\lambda_{ij}/\lambda_{\text{tot}}$, and increase $k_{i,j}$ by one if $\sigma_{ij} = 1$, where $\lambda_{ij} = 2\beta J_{ij}$.

(iii) Repeat (ii) k times in total.

(iv) Spins connected by bonds with $k_{ij} > 0$ are considered to belong to the same cluster. Flip clusters at random and generate a new spin configuration as in the original Swendsen-Wang method.

The probability that bond (i, j) is activated can be expressed as

$$P_{ij} = \sum_{k=1}^{\infty} f(k; \lambda_{\text{tot}}) \sum_{m=1}^{k} \frac{k!}{(k-m)!m!} \left(\frac{\lambda_{ij}}{\lambda_{\text{tot}}}\right)^m \left(1 - \frac{\lambda_{ij}}{\lambda_{\text{tot}}}\right)^{k-m}, \tag{3.32}$$

since it is the probability that bond (i, j) is chosen at least once. By using the normalization condition

$$\sum_{m=0}^{k} \frac{k!}{(k-m)!m!} \left(\frac{\lambda_{ij}}{\lambda_{\text{tot}}}\right)^m \left(1 - \frac{\lambda_{ij}}{\lambda_{\text{tot}}}\right)^{k-m} = 1 \tag{3.33}$$

of the binomial distribution, Eq. (3.32) can be rewritten as

$$\begin{aligned} P_{ij} &= 1 - \sum_{k=0}^{\infty} f(k; \lambda_{\text{tot}}) \left(1 - \frac{\lambda_{ij}}{\lambda_{\text{tot}}}\right)^k \\ &= 1 - \exp(-\lambda_{\text{tot}}) \sum_{k=0}^{\infty} \frac{1}{k!} (\lambda_{\text{tot}} - \lambda_{ij})^k \\ &= 1 - \exp(-2\beta J_{ij}). \end{aligned} \tag{3.34}$$

That is, the activation probability in the Fukui-Todo method is equal to the one in the original Swendsen-Wang algorithm (3.28). Thus the both stochastic processes are equivalent with each other, satisfying the detailed balance.

The computational cost of the Fukui-Todo method is proportional to the repeat count, k, of step (ii). The average of k is λ_{tot}, obeying the Poisson distribution, $f(k, \lambda_{\mathrm{tot}})$. For a system with N spins, λ_{tot} is expressed as

$$\begin{aligned} \lambda_{\mathrm{tot}} &= 2\beta \sum_{i<j}^{N} J_{ij} = \beta \sum_{i}^{N} \sum_{j\neq i}^{N} J_{ij} \\ &\approx \beta \sum_{i}^{N} \int_{1}^{N^{1/d}} \mathrm{d}r \; r^{d-1} J(r) \\ &= \beta N \int_{1}^{N^{1/d}} \mathrm{d}r \; r^{d-1} J(r). \end{aligned} \tag{3.35}$$

Here, we assume the translational invariance and that J_{ij} depends only on the distance between spins. If $J(r)$ decays faster than r^{-d}, which is equivalent to the condition of the convergence of energy density for the ferromagnetic ordered state, the integral in the last line of Eq. (3.35) converges to a finite value even in the thermodynamic limit. The convergence condition is unchanged even when the mirror-image cells are considered and the Ewald summation is taken (see Sec. 4.1). Thus, at a finite temperature, λ_{tot} increases in proportional to N instead of N^2 as long as $\sigma > 0$ and the energy density converges to a finite value. Because step (ii) is done in $O(1)$ computational cost thanks to the Walker's method of alias (see the appendices of Ref. 11), the total cost of the one Monte Carlo step of the Fukui-Todo cluster algorithm is $O(\lambda_{\mathrm{tot}}) \sim O(N)$.

Chapter 4

Ising Model with Long-Range Interaction

4.1 Generalized Ewald summation

4.1.1 Ewald method

In the simulation of systems with the long-range interaction under the periodic boundary conditions, we generally need to take into account interactions from mirror-image cells, which are imaginary systems across the periodic boundaries, in order to reduce strong finite-size corrections. The interaction between S_i and S_j is thus expressed as

$$\mathcal{H}_{ij} = -\sum_{\vec{\nu}} \frac{1}{|\vec{L}\cdot\vec{\nu} + \vec{r}_i - \vec{r}_j|^{d+\sigma}} S_i S_j, \tag{4.1}$$

where $\vec{L} = (L_1, L_2, \cdots, L_d)$ denotes the size of the hypercubic lattice, and $\vec{\nu} = (\nu_1, \nu_2, \cdots, \nu_d)$ with $\nu_\alpha = 0, \pm 1, \pm 2, \cdots$ $(\alpha = 1, 2, \cdots, d)$ represents the index of image cells. In the following we consider only the case where $\sigma > 0$. The summation in Eq. (4.1) is taken for all the image cells. The simplest way to get an approximate value of Eq. (4.1) is truncating the summation up to some threshold, $\nu_{\max}$, but this does not work well in practice because the summation of an algebraically decaying function converges very slowly. The Ewald summation technique [55, 56] is an efficient approach to calculate the contribution from image cells much faster [57, 58]; the summation is separated into two parts, the short-range term and the long-range term, and taken separately in the real space and the reciprocal space, respectively. Although the Ewald summation is usually formulated only for integer exponents, $\sigma = 0, 1, 2, \cdots$, such as the Coulomb interaction and the dipole interaction, here we generalize the Ewald summation for exponent of arbitrary positive real numbers.

Before we introduce the generalized Ewald summation in Sec. 4.1.3, first we briefly review the conventional Ewald summation technique for $d + \sigma = 1$, which describes the Coulomb potential, in Sec. 4.1.2.

4.1.2 Ewald summation for $d + \sigma = 1$

In this section, we consider the Ewald summation for $d + \sigma = 1$, i.e., the Coulomb potential expressed by

$$\phi(i,j) = \sum_{\vec{\nu}} \frac{1}{\left|\vec{L}_\nu + \vec{r}_i - \vec{r}_j\right|}. \tag{4.2}$$

In the Ewald method, each terms in Eq. (4.2) is separated into two parts by using the complementary error function:

$$\begin{aligned}
\phi(i,j) &= \sum_{\vec{\nu}} \frac{1}{\left|\vec{L}_\nu + \vec{r}_i - \vec{r}_j\right|} \\
&= \sum_{\vec{\nu}} \frac{1}{|\vec{r}_L|}\mathrm{erfc}(\kappa|\vec{r}_L|) + \sum_{\vec{\nu}} \frac{1}{|\vec{r}_L|}[1 - \mathrm{erfc}(\kappa|\vec{r}_L|)] \\
&= \sum_{\vec{\nu}} \frac{1}{|\vec{r}_L|}\mathrm{erfc}(\kappa|\vec{r}_L|) + \sum_{\vec{\nu}} \frac{1}{|\vec{r}_L|}\mathrm{erf}(\kappa|\vec{r}_L|) \\
&= \phi^{(1)}(i,j) + \phi^{(2)}(i,j),
\end{aligned} \tag{4.3}$$

where κ is the cutoff parameter, $|\vec{r}_L| = \left|\vec{L}_\nu + \vec{r}_i - \vec{r}_j\right|$, and $\mathrm{erf}(x)$ and $\mathrm{erfc}(x)$ are the error and the complementary error functions,

$$\mathrm{erf}(x) = \frac{2}{\sqrt{\pi}} \int_0^x \exp(-t^2)\,\mathrm{d}t \tag{4.4}$$

$$\mathrm{erfc}(x) = 1 - \mathrm{erf}(x) = \frac{2}{\sqrt{\pi}} \int_x^\infty \exp(-t^2)\,\mathrm{d}t, \tag{4.5}$$

respectively. The first and second term on the third line of Eq. (4.3) represent the short-range term $\phi^{(1)}(i,j)$ and the long-range term $\phi^{(2)}(i,j)$, respectively. In the short range term, the contribution of large $\vec{\nu}$ becomes exponentially small since $\mathrm{erfc}(x)$ diminishes for large x. On the other hand, in the long-range term, the contribution of small $\vec{\nu}$ is suppressed since $\mathrm{erf}(x)$ becomes exponentially small for small x. The cutoff parameter κ allocates the contribution of these terms; appropriate κ is required for faster convergence.

The long-range term converges very slow in the real space, while it converges very fast in the reciprocal space. Let us transform the summation of the long-range term from the real space to the reciprocal space. Changing the variable from u to $|\vec{r}_L|\rho$, the long-range term is rewritten as

$$\sum_{\vec{\nu}} \frac{1}{|\vec{r}_L|}\mathrm{erf}(\kappa|\vec{r}_L|) = \sum_{\vec{\nu}} \frac{2}{\sqrt{\pi}} \int_0^{\kappa|\vec{r}_L|} \frac{1}{|\vec{r}_L|} \exp(-u^2)\mathrm{d}u = \frac{2}{\sqrt{\pi}} \int_0^\kappa \sum_{\vec{\nu}} \exp(-|\vec{r}_L|^2\rho^2)\mathrm{d}\rho. \tag{4.6}$$

Next, we introduce the Fourier transform of $G(\vec{r}) = \sum_{\vec{\nu}} \exp(-|\vec{r}_L|^2\rho^2)$:

$$G(\vec{r}) = \sum_{\vec{h}} \frac{\pi^{d/2}}{\rho^d} \exp\left(-\frac{\pi^2}{\rho^2}|\vec{k}|^2 + 2\pi i \vec{k} \cdot (\vec{r}_i - \vec{r}_j)\right), \tag{4.7}$$

where

$$\vec{k} = \left(\frac{h_x}{L_x}, \frac{h_y}{L_y}\right) \tag{4.8}$$

$$|\vec{k}|^2 = \left(\frac{h_x^2}{L_x^2} + \frac{h_y^2}{L_y^2}\right) \tag{4.9}$$

$$\vec{k} \cdot (\vec{r}_i + \vec{r}_j) = \left(\frac{h_x}{L_x}(-r_{jx} + r_{ix}) + \frac{h_y}{L_y}(-r_{jy} + r_{iy})\right), \tag{4.10}$$

and $h_x, h_y = 0, \pm 1, \pm 2, \cdots$. In the three-dimensional case, by substituting Eq. (4.7) to Eq. (4.6) and using the quadrature formula

$$\int_0^\kappa \frac{1}{\rho^3} \exp\left(-\frac{a^2}{\rho^2}\right) \mathrm{d}\rho = \frac{1}{2a^2} \exp\left(-\frac{a^2}{\kappa^2}\right), \tag{4.11}$$

the long-range term can be expressed as

$$\phi^{(2)}(i,j) = \frac{1}{\pi} \sum_{\vec{h} \neq \vec{0}} \frac{1}{|\vec{k}|^2} \exp\left(-\frac{\pi^2 |\vec{k}|^2}{\kappa^2}\right) \cos\left(2\pi \vec{k} \cdot (\vec{r}_i - \vec{r}_j)\right). \tag{4.12}$$

The term with $\vec{h} = \vec{0}$, which represents the static charge of the whole system, must vanish because of the neutral condition. In other words, the non-neutral system with coulomb potential and periodic boundary conditions can not be well-defined, since the Hamiltonian of the system inevitably diverges to infinity.

In summary, the Ewald summation for the Coulomb potential is expressed as follows:

$$\phi(i,j) = \sum_{\vec{\nu}} \frac{1}{\left|\vec{L}_\nu + \vec{r}_i - \vec{r}_j\right|} = \phi^{(1)}(i,j) + \phi^{(2)}(i,j) \tag{4.13}$$

with the short-range term:

$$\phi^{(1)}(i,j) = \sum_{\vec{\nu}} \frac{1}{|\vec{r}_L|} \frac{2}{\sqrt{\pi}} \int_0^{\kappa |\vec{r}_L|} \exp(-t^2) \mathrm{d}t \tag{4.14}$$

and the long-range term:

$$\phi^{(2)}(i,j) = \frac{1}{\pi} \sum_{\vec{h} \neq \vec{0}} \frac{1}{|\vec{k}|^2} \exp\left(-\frac{\pi^2 |\vec{k}|^2}{\kappa^2}\right) \cos\left(2\pi \vec{k} \cdot (\vec{r}_i - \vec{r}_j)\right). \tag{4.15}$$

4.1.3 Generalized Ewald summation

Let us consider the potential with a exponent with an arbitrary real number:

$$\phi_m(i,j) = \sum_{\vec{\nu}} \frac{1}{|\vec{r}|^m}, \tag{4.16}$$

where $m = d + \sigma$ and $\vec{r} = \vec{r}(\vec{\nu}, \vec{r}_i, \vec{r}_j) \equiv \vec{L} \cdot \vec{\nu} + \vec{r}_i - \vec{r}_j$. We separate Eq. (4.16) into two terms by using the gamma function:

$$\begin{aligned}
\phi_m(i,j) &= \sum_{\vec{\nu}} \frac{1}{\Gamma(m/2)} \int_0^\infty \frac{1}{|\vec{r}|^m} t^{\frac{m}{2}-1} e^{-t} \mathrm{d}t \\
&= \sum_{\vec{\nu}} \left[\frac{1}{\Gamma(m/2)} \int_{(\kappa|\vec{r}|)^2}^\infty \frac{1}{|\vec{r}|^m} t^{\frac{m}{2}-1} e^{-t} \mathrm{d}t \right. \\
&\qquad \left. + \frac{2}{\Gamma(m/2)} \int_0^\kappa \rho^{m-1} e^{-|\vec{r}|^2\rho^2} \mathrm{d}\rho \right] \\
&= \phi_m^{(1)}(i,j) + \phi_m^{(2)}(i,j). \qquad (4.17)
\end{aligned}$$

Here, $\Gamma(x)$ denotes the gamma function:

$$\Gamma(x) = \int_0^\infty t^{x-1} \mathrm{e}^{-t} \mathrm{d}t, \qquad (4.18)$$

κ is an arbitrary positive real number,

$$\phi_m^{(1)}(i,j) = \sum_{\vec{\nu}} \frac{1}{\Gamma(m/2)} \frac{1}{|\vec{r}|^m} \int_{(\kappa|\vec{r}|)^2}^\infty t^{\frac{m}{2}-1} e^{-t} \mathrm{d}t \qquad (4.19)$$

represents the short-range term, and

$$\phi_m^{(2)}(i,j) = \sum_{\vec{\nu}} \frac{2}{\Gamma(m/2)} \int_0^\kappa \rho^{m-1} e^{-|\vec{r}|^2\rho^2} \mathrm{d}\rho \qquad (4.20)$$

does the long-range term. Note that in Eq. (4.20) we have replaced the integration variable, t, by $(|\vec{r}|\rho)^2$.

Next, we transform Eq. (4.20) from the integration in the real space into that in the reciprocal space. Let us consider the two-dimensional case, i.e., $d = 2$, $\vec{L} = (L_x, L_y)$, $\nu = (\nu_x, \nu_y)$, $\vec{r}_i = (r_{ix}, r_{iy})$, etc. We factor $\sum_{\vec{\nu}} e^{-|\vec{r}|^2\rho^2}$ in Eq. (4.20) into the two components for each coordinate axis as

$$G(\vec{r}_i, \vec{r}_j) = \sum_{\vec{\nu}} e^{-|\vec{r}|^2\rho^2} = G_x(r_{ix}, r_{jx}) G_y(r_{iy}, r_{jx}), \qquad (4.21)$$

where

$$G_x(r_{ix}, r_{jx}) = \sum_{\nu_x=-\infty}^{\infty} \exp[-(L_x\nu_x + r_{ix} - r_{jx})^2\rho^2] \qquad (4.22)$$

and

$$G_y(r_{iy}, r_{jy}) = \sum_{\nu_y=-\infty}^{\infty} \exp[-(L_y\nu_y + r_{iy} - r_{jy})^2\rho^2]. \qquad (4.23)$$

Then, Eq. (4.22) is rewritten by taking the Fourier transform on r_{ix} as

$$G_x(r_{ix}, r_{jx}) = \sum_{h_x=-\infty}^{\infty} \frac{1}{L_x} A_x(h_x, r_{jx}) \exp\left(i \frac{2\pi h_x}{L_x} r_{ix} \right), \qquad (4.24)$$

where

$$\begin{aligned} A_x(h_x, r_{jx}) &= \int_0^{L_x} G_x(r_{ix}, r_{jx}) \exp\left(-i\frac{2\pi h_x}{L_x} r_{ix}\right) \mathrm{d}r_{ix} \\ &= \sum_{\nu_x} \int_{L_x\nu_x - r_{jx}}^{L_x(\nu_x+1)-r_{jx}} \exp\Big[-\xi^2\rho^2 \\ &\qquad - i\frac{2\pi h_x}{L_x}\xi + i2\pi h_x\nu_x - i\frac{2\pi h_x}{L_x} r_{jx}\Big] \mathrm{d}\xi \\ &= \int_{-\infty}^{\infty} \exp\Big[-\xi^2\rho^2 - i\frac{2\pi h_x}{L_x}\xi - i\frac{2\pi h_x}{L_x} r_{jx}\Big] \mathrm{d}\xi \end{aligned} \tag{4.25}$$

with $\xi = L_x\nu_x + r_{ix} - r_{jx}$. Note that $\exp(i2\pi h_x\nu_x)$ vanishes because $h_x\nu_x$ takes integral values. Performing the Gaussian integration then yields

$$A_x(h_x, r_{jx}) = \frac{\sqrt{\pi}}{\rho} \exp\left(-\frac{\pi^2 h_x^2}{\rho^2 L_x^2} - i\frac{2\pi h_x}{L_x} r_{jx}\right). \tag{4.26}$$

Next, by using Eq. (4.24) with Eq. (4.26) and the similar expression for $G_y(r_{iy}, r_{jy})$, Eq. (4.21) is expressed as

$$\begin{aligned} G(\vec{r}_i, \vec{r}_j) \;&=\; \sum_{h_x,h_y} \frac{\pi}{L_x L_y \rho^2} \exp\Big[-\frac{\pi^2}{\rho^2}\left(\frac{h_x^2}{L_x^2} + \frac{h_y^2}{L_y^2}\right) \\ &\qquad + i2\pi\left(\frac{h_x}{L_x}(r_{ix} - r_{jx}) + \frac{h_y}{L_y}(r_{iy} - r_{jy})\right)\Big]. \end{aligned} \tag{4.27}$$

Introducing $\vec{k} = \left(\frac{h_x}{L_x}, \frac{h_y}{L_y}\right)$, Eq. (4.27) is further simplified as

$$\begin{aligned} G(\vec{r}_i, \vec{r}_j) \;&=\; \sum_{\vec{k}} \frac{\pi}{L_x L_y \rho^2} \exp[-\frac{\pi^2}{\rho^2}|\vec{k}|^2] \\ &\times\; \big(\cos[2\pi\vec{k}\cdot(\vec{r}_i - \vec{r}_j)] + i\sin[2\pi\vec{k}\cdot(\vec{r}_i - \vec{r}_j)]\big). \end{aligned} \tag{4.28}$$

Here, $\exp[-\frac{\pi^2}{\rho^2}|\vec{k}|^2]$ and $\cos[2\pi\vec{k}\cdot(\vec{r}_i - \vec{r}_j)]$ are even functions of $\vec{k}$. On the other hand, $\sin[2\pi\vec{k}\cdot(\vec{r}_i - \vec{r}_j)]$ is an odd function. Therefore, $\sin[2\pi\vec{k}\cdot(\vec{r}_i - \vec{r}_j)]$ and $\sin[2\pi(-\vec{k})\cdot(\vec{r}_i - \vec{r}_j)]$ are counterbalanced if summation is taken for all $\vec{k}$.

Extension of the above argument to arbitrary dimensions is straightforward. For the d-dimensional case, Eq(4.28) should be replace by

$$G(\vec{r}_i, \vec{r}_j) \;=\; \frac{\pi^{d/2}}{V\rho^d} \sum_{\vec{k}} \exp[-\frac{\pi^2}{\rho^2}|\vec{k}|^2] \cos[2\pi\vec{k}\cdot(\vec{r}_i - \vec{r}_j)], \tag{4.29}$$

where $V = \Pi_{\alpha=1}^{d} L_\alpha$ is the volume of the system. The long-range term (4.20) is finally expressed

as

$$\begin{aligned}\phi_m^{(2)}(i,j) &= \frac{2\pi^{d/2}}{\Gamma(m/2)V}\sum_{\vec{k}}\cos\left[2\pi\vec{k}\cdot(\vec{r}_i-\vec{r}_j)\right] \\ &\quad\times\int_0^{\kappa}\rho^{m-1-d}\exp\left[-\frac{\pi^2}{\rho^2}|\vec{k}|^2\right]\mathrm{d}\rho \\ &= \frac{2\pi^{d/2}}{\Gamma(m/2)V}\sum_{\vec{k}}\cos\left[2\pi\vec{k}\cdot(\vec{r}_i-\vec{r}_j)\right] \\ &\quad\times\frac{1}{2}(\pi|\vec{k}|)^{m-d}\int_{\frac{\pi^2|\vec{k}|^2}{\kappa^2}}^{\infty}t^{-\frac{1}{2}(m-d)-1}\mathrm{e}^{-t}\mathrm{d}t.\end{aligned} \tag{4.30}$$

In summary, the Ewald summation for generic exponent σ is expressed as Eq. (4.16) with the short-range term (4.19) and the long-range term (4.30). The terms in Eqs. (4.19) and (4.30) become small quite rapidly as $|\vec{\nu}|$ and $|\vec{k}|$ increase, respectively, due to the presence of the exponential functions. Note that the choice of the crossover parameter κ affects the speed of convergence of the summations over $\vec{\nu}$ and $\vec{k}$ (or $\vec{h}$). We find empirically that $\kappa = 2/L$ is a reasonable choice, by which both summations converge in double precision for $\max(|\nu_x|, |\nu_y|) \leq 4$ and $\max(|h_x|, |h_y|) \leq 4$.

The integrals in Eqs. (4.19) and (4.30) are calculated numerically. These integrals are known as the (upper) incomplete gamma function, which is defined as

$$\Gamma(s,x) = \int_x^{\infty}t^{s-1}\mathrm{e}^{-t}\mathrm{d}t. \tag{4.31}$$

Eqs. (4.19) and (4.30) are expressed by the incomplete gamma function as

$$\phi_m^{(1)}(i,j) = \sum_{\vec{\nu}}\frac{1}{\Gamma(m/2)}\frac{1}{|\vec{r}|^m}\Gamma\big(\frac{m}{2},(\kappa|\vec{r}|)^2\big) \tag{4.32}$$

$$\begin{aligned}\phi_m^{(2)}(i,j) &= \frac{2\pi^{d/2}}{\Gamma(m/2)V}\sum_{\vec{k}}\cos\left[2\pi\vec{k}\cdot(\vec{r}_i-\vec{r}_j)\right] \\ &\times\frac{1}{2}(\pi|\vec{k}|)^{m-d}\Gamma\big(-\frac{1}{2}(m-d),\frac{\pi^2|\vec{k}|^2}{\kappa^2}\big),\end{aligned} \tag{4.33}$$

respectively.

In the present simulation, we calculated the incomplete gamma function numerically by the Boost C++ library [59]. The function (4.31), however, is defined only for positive real s in the library. In the case for negative s, we used the following recursion formula obtained by the

integration by parts:

$$\begin{aligned}
\Gamma(s,x) &= \int_x^\infty t^{s-1}\mathrm{e}^{-t}\mathrm{d}t \\
&= \Big[\frac{1}{s}t^s\mathrm{e}^{-t}\Big]_x^\infty + \int_x^\infty \frac{1}{s}t^s\mathrm{e}^{-t}\mathrm{d}t \\
&= -\frac{1}{s}x^s\mathrm{e}^{-x} + \frac{1}{s}\Gamma(s+1,x) \\
&= -\frac{1}{s}x^s\mathrm{e}^{-x} - \frac{1}{s(s+1)}x^{s+1}\mathrm{e}^{-x} \\
&\quad + \frac{1}{s(s+1)}\Gamma(s+2,x) \\
&\vdots \\
&= -\sum_{i=1}^{n}\Big\{x^{s+i-1}\mathrm{e}^{-x}\prod_{j=1}^{i}\big(\frac{1}{s+j-1}\big)\Big\} \\
&\quad + \prod_{i=1}^{n}\big(\frac{1}{s+i-1}\big)\Gamma(s+n,x),
\end{aligned} \tag{4.34}$$

where $n = -\lfloor s \rfloor$. Note that this recursion formula breaks down when σ is an even (positive) integer since $-(m-d)/2 = -\sigma/2$ becomes a negative integer. The denominator in Eq. (4.34) then becomes zero during the recursion. For even σ, we stopped the recursion when the first argument of the incomplete gamma function becomes zero, and used

$$\Gamma(0,x) = \int_x^\infty t^{-1}\mathrm{e}^{-t}\mathrm{d}t = -\mathrm{Ei}(-x), \tag{4.35}$$

where $\mathrm{Ei}(-x)$ is the exponential integral.

4.2 Improved estimator

In the cluster algorithm Monte Carlo methods, so-called the improved estimators for physical quantities are available, which are defined in terms of the cluster configuration instead of the spin configuration. Some improved estimators can drastically reduce the asymptotic variance of physical quantities because they take the average of a number of spin configurations generated from a cluster configuration automatically. In the present work, we used the improved estimators for measuring the moments of magnetization, i.e., $\langle m^2 \rangle$, $\langle m^4 \rangle$, $\langle m^6 \rangle$, $\cdots$, to calculate the (combined) Binder ratios.

Let us consider a snapshot of graph configuration g composed of k clusters, and let n_1, n_2, $\cdots$, n_k be the number of spins included in each cluster. We define $m^\alpha(g)$ as an average of m^α over all possible 2^k different spin configurations that can be generated by flipping k clusters

independently:

$$\begin{aligned} m^{\alpha}(g) &= \frac{1}{2^k} \sum_{s_1,\cdots,s_k} \Big(\sum_i^k n_i s_i \Big)^{\alpha} \\ &= \frac{1}{2^k} \{ (+n_1 + n_2 + \cdots + n_k)^{\alpha} \\ &\quad + (-n_1 + n_2 + \cdots + n_k)^{\alpha} \\ &\quad + (+n_1 - n_2 + \cdots + n_k)^{\alpha} \\ &\quad \vdots \\ &\quad + (-n_1 - n_2 - \cdots - n_k)^{\alpha} \}, \end{aligned} \tag{4.36}$$

where $s_i = \pm 1$ denotes the spin direction of the i-th cluster. In Eq. (4.36), terms including an odd power of $n_1, n_2, \cdots, n_k$ are counterbalanced by other terms with the opposite sign. Hence we only have to consider the terms with even powers for all $\{n_i\}$. Thus, we can rewrite Eq. (4.36) as

$$\begin{aligned} m^{\alpha}(g) &= \frac{1}{2^k} 2^k \left(n_1 + n_2 + \cdots + n_k \right)^{\alpha}_{\text{even terms}} \\ &= \left(n_1 + n_2 + \cdots + n_k \right)^{\alpha}_{\text{even terms}} . \end{aligned} \tag{4.37}$$

Now we assume that $m^{\alpha}(g)$ can be expressed as

$$m^{\alpha}(g) = \sum_p a_p \prod_{j \in p} C_j, \tag{4.38}$$

with coefficients $\{a_p\}$ and

$$C_j = \sum_i^k n_i^j. \tag{4.39}$$

The summation $\sum_p$ in Eq. (4.38) is taken over all possible partitions of α into a set of even integers $\{j\}$. We do not need, nevertheless, to consider the combinations with odd j since they do not contribute after taking the average over the spin configurations as already mentioned. In the following, we introduce a simple way to obtain $\{a_p\}$ by expanding the right-hand side of Eqs. (4.37) and (4.38), and comparing their coefficients.

4.2.1 Second moment: $m^2(g)$

In order to determine the improved estimator for the second moment of magnetization, it is enough to consider a graph configuration composed of only one cluster. In this case, Eq. (4.37) becomes

$$m^2(g) = n_1^2. \tag{4.40}$$

On the other hand, Eq. (4.38) is expressed as

$$m^2(g) = a_1 \sum_i^k n_i^2 = a_1 n_1^2. \tag{4.41}$$

By comparing Eqs. (4.40) and (4.41), we obtain

$$a_1 = 1. \tag{4.42}$$

The improved estimator $m^2(g)$ is thus given by

$$m^2(g) = C_2. \tag{4.43}$$

4.2.2 Fourth moment: $m^4(g)$

Consider a graph configuration composed of two clusters. From Eq. (4.37), we obtain

$$\begin{aligned} m^4(g) &= (n_1 + n_2)^4_{\text{even terms}} \\ &= (n_1^4 + n_2^4) + 6n_1^2 n_2^2 \end{aligned} \tag{4.44}$$

On the other hand, Eq. (4.38) is expressed as

$$\begin{aligned} m^4(g) &= a_1 C_4 + a_2 C_2^2 \\ &= (a_1 + a_2)(n_1^4 + n_2^4) + 2a_2 n_1^2 n_2^2. \end{aligned} \tag{4.45}$$

By comparing Eqs. (4.44) and (4.45), we obtain

$$\begin{aligned} a_1 &= -2 \\ a_2 &= 3. \end{aligned} \tag{4.46}$$

The improved estimator $m^4(g)$ is thus given by

$$m^4(g) = -2C_4 + 3C_2^2. \tag{4.47}$$

4.2.3 Sixth moment: $m^6(g)$

Consider a graph configuration composed of three clusters. From Eq. (4.37), we obtain

$$\begin{aligned} m^6(g) &= (n_1 + n_2 + n_3)^6_{\text{even terms}} \\ &= (n_1^6 + n_2^6 + n_3^6) \\ &\quad + 15\{n_1^4(n_2^2 + n_3^2) + n_2^4(n_1^2 + n_3^2) + n_3^4(n_1^2 + n_2^2)\} \\ &\quad + 90 n_1^2 n_2^2 n_3^2 \end{aligned} \tag{4.48}$$

On the other hand, Eq. (4.38) is expanded as

$$\begin{aligned} m^6(g) &= a_1 C_6 + a_2 C_4 C_2 + a_3 C_2^3 \\ &= (a_1 + a_2 + a_3)(n_1^6 + n_2^6 + n_3^6) \\ &\quad + (a_2 + 3a_3)\{n_1^4(n_2^2 + n_3^2) + n_2^4(n_1^2 + n_3^2) \\ &\qquad + n_3^4(n_1^2 + n_2^2)\} \\ &\quad + 6a_3 n_1^2 n_2^2 n_3^2. \end{aligned} \tag{4.49}$$

By comparing Eqs. (4.48) and (4.49), we obtain

$$\begin{aligned} a_1 &= 16 \\ a_2 &= -30 \\ a_3 &= 15. \end{aligned} \tag{4.50}$$

The improved estimator $m^6(g)$ is thus given by

$$m^6(g) = 16C_6 - 30C_4C_2 + 15C_2^3. \tag{4.51}$$

4.2.4 Eighth moment: $m^8(g)$

Consider a graph configuration composed of four clusters. From Eq. (4.37), we obtain

$$\begin{aligned} m^8(g) &= (n_1+n_2+n_3+n_4)^8_{\text{even terms}} \\ &= \left(n_1^8+n_2^8+n_3^8+n_4^8\right) \\ &\quad + 28\sum_i n_i^6 \sum_{j\neq i} n_j^2 \\ &\quad + 420\sum_i n_i^4 \sum_{j\neq i} n_j^2 \sum_{\ell\neq j,\ell\neq i} n_\ell^2 \\ &\quad + 70\sum_i n_i^4 \sum_{j\neq i} n_j^4 \\ &\quad + 2520 n_1^2 n_2^2 n_3^2 n_4^2. \end{aligned} \tag{4.52}$$

On the other hand, Eq. (4.38) can be expanded as

$$\begin{aligned} m^8(g) &= a_1C_8 + a_2C_6C_2 + a_3C_4C_2^2 + a_4C_4^2 + a_5C_2^4 \\ &= (a_1+a_2+a_3+a_4+a_5)\sum_i n_i^8 \\ &\quad + (a_2+2a_3+4a_5)\sum_i n_i^6 \sum_{j\neq i} n_j^2 \\ &\quad + (2a_3+12a_5)\sum_i n_i^4 \sum_{j\neq i} n_j^2 \sum_{\ell\neq j,\ell\neq i} n_\ell^2 \\ &\quad + (2a_3+2a_4+6a_5)\sum_i n_i^4 \sum_{j\neq i} n_j^4 \\ &\quad + 24a_5 n_1^2 n_2^2 n_3^2 n_4^2. \end{aligned} \tag{4.53}$$

By comparing Eqs. (4.52) and (4.53), we obtain

$$\begin{aligned} a_1 &= -272 \\ a_2 &= 448 \\ a_3 &= -420 \\ a_4 &= 140 \\ a_5 &= 105. \end{aligned} \tag{4.54}$$

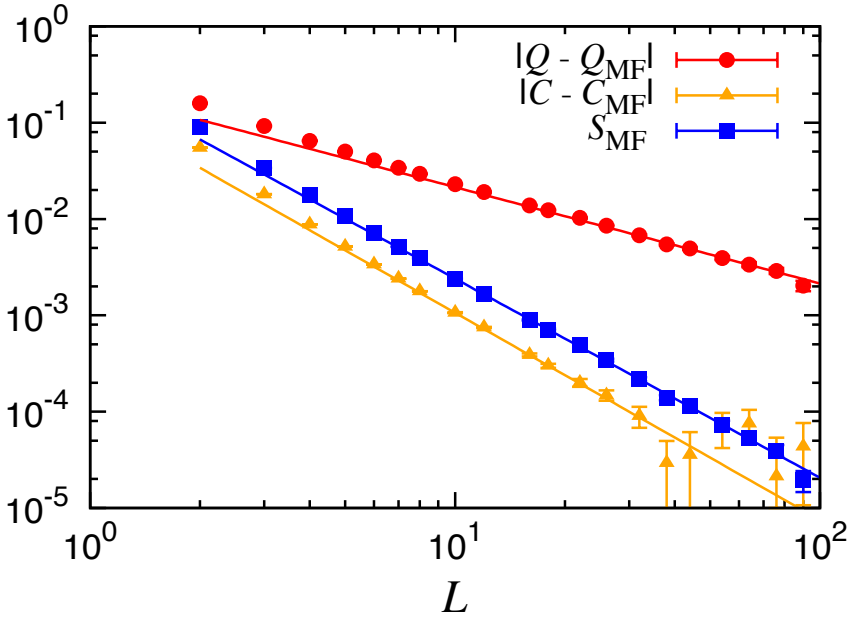

Figure 4.1: Convergence of the conventional Binder ratio (red circles), Q, the combined Binder ratio (orange triangles), C, and the self-combined Binder ratio (blue squares), S_{MF} at the critical point for the fully connected model. The conventional Binder ratio converges to Q_{MF} as $\sim L^{-1}$, while the combined Binder ratio and the self-combined Binder ratio converge as $\sim L^{-2}$ since the leading correction term is eliminated.

The improved estimator $m^8(g)$ is thus given by

$$m^8(g) = -272C_8 + 448C_6C_2 - 420C_4C_2^2 + 140C_4^2 + 105C_2^4. \tag{4.55}$$

4.3 Combined Binder ratio

4.3.1 Combined Binder ratio

In the next section, instead of the critical exponents, we use the value of the Binder ratio for investigating the universality class of the phase transition. The Binder ratio at the critical point, which is also referred to as the universal ratio, is constant and takes a universal value [44], since it is the ratio of two physical quantities that have the same anomalous dimension. It can be usually calculated more accurately than the critical exponents, which leads to a more reliable identification of the universality class [60]. The Binder ratio is defined as [44]

$$Q = \frac{\langle m^2 \rangle^2}{\langle m^4 \rangle}, \tag{4.56}$$

where $m = \sum_i S_i$ and $\langle \cdot \rangle$ denotes the Monte Carlo average.

In practice, the Binder ratio exhibits some system-size dependence that is called the correction-to-scaling. We write the Binder ratio at the critical temperature as follows:

$$Q(T_{\mathrm{c}}, L) = Q_{\infty} + f(L), \tag{4.57}$$

where Q_{∞} denotes the universal ratio and $f(L)$ does the finite-size correction. Note that the finite-size correction is not universal; i.e., it can be a different form even if the universality class is the same. Although it is generally difficult to know the explicit form of $f(L)$, the expression of the leading correction term is known for the fully connected Ising model [50]:

$$\begin{aligned} Q(T_{\mathrm{c}}, N) &= \frac{\langle m^2 \rangle^2}{\langle m^4 \rangle} \\ &= 4\frac{\Gamma(3/4)^2}{\Gamma(1/4)^2} + \frac{16\sqrt{3}\Gamma(3/4)^3}{5\Gamma(1/4)^3} N^{-\frac{1}{2}} + O(N^{-1}), \end{aligned} \tag{4.58}$$

where $\Gamma(x)$ is the gamma function. In the case of the two-dimensional fully connected Ising model ($N = L^2$), the leading correction is proportional to L^{-1}. One can consider different combinations of the moment of magnetization to build various "Binder ratios," whose universal ratio for the fully connected Ising model and its leading correction term at the critical point are also written explicitly as

$$\frac{\langle m^2 \rangle^3}{\langle m^6 \rangle} \simeq \frac{4\Gamma(3/4)^2}{3\Gamma(1/4)^2} + \left(\frac{4\sqrt{3}\Gamma(3/4)}{9\Gamma(1/4)} - \frac{16\sqrt{3}\Gamma(3/4)^3}{15\Gamma(1/4)^3} \right) N^{-\frac{1}{2}} \tag{4.59}$$

$$\frac{\langle m^2 \rangle \langle m^4 \rangle}{\langle m^6 \rangle} \simeq \frac{1}{3} + \left(\frac{\sqrt{3}\Gamma(1/4)}{9\Gamma(3/4)} - \frac{8\sqrt{3}\Gamma(3/4)}{15\Gamma(1/4)} \right) N^{-\frac{1}{2}} \tag{4.60}$$

$$\frac{\langle m^2 \rangle^4}{\langle m^8 \rangle} \simeq \frac{16\Gamma(3/4)^4}{5\Gamma(1/4)^4} + \frac{1536\sqrt{3}\Gamma(3/4)^5}{125\Gamma(1/4)^5} N^{-\frac{1}{2}}. \tag{4.61}$$

By using these Binder ratios, one can eliminate the lowest order of the correction-to-scaling. The simplest way is taking an appropriate linear combination, e.g.,

$$C(T_{\mathrm{c}}, N) = \frac{\langle m^2 \rangle^2}{\langle m^4 \rangle} - a\frac{\langle m^2 \rangle^3}{\langle m^6 \rangle} = C_{\mathrm{MF}} + O(N^{-1}), \tag{4.62}$$

where

$$a = \frac{\frac{16\sqrt{3}\Gamma(3/4)^3}{5\Gamma(1/4)^3}}{\left(\frac{4\sqrt{3}\Gamma(3/4)}{9\Gamma(1/4)} - \frac{16\sqrt{3}\Gamma(3/4)^3}{15\Gamma(1/4)^3} \right)} \tag{4.63}$$

and $C_{\mathrm{MF}} = 0.2843448$. Hereafter, we call $C(T, N)$ as the *combined Binder ratio*.

4.3.2 Self-combined Binder ratio

Unfortunately, the construction of the combined Binder ratio requires an explicit form of the leading correction term. The application to other universality classes rather than the mean-field

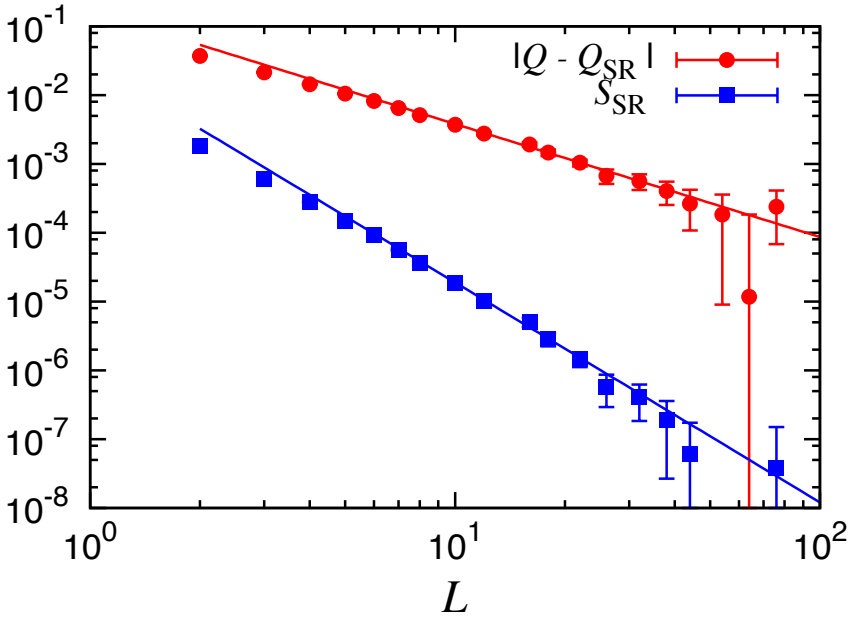

Figure 4.2: Convergence of the conventional Binder ratio (red circles), Q, and the self-combined Binder ratio (blue squares), $S_{\rm SR}$ at the critical point for the nearest neighbor model. The conventional Binder ratio converges to $Q_{\rm SR}$ as $\sim L^{-1.6}$, while the self-combined Binder ratio converges as $\sim L^{-3.2}$.

universality is not practical. We then introduce another quantity that also has smaller finite-size corrections, the "self-combined Binder ratio":

$$S(T,L) = \frac{1}{Q_\infty} Q(T,L) + Q_\infty \frac{1}{Q(T,L)} - 2. \tag{4.64}$$

This quantity is a linear combination of Q and Q^{-1}. It is easily seen that regardless of the form of $f(L)$, leading correction of the universal ratio is reduced from $O\left(f(L)\right)$ to $O\left(f(L)^2\right)$ if Q_∞ is chosen as the exact universal ratio:

$$\begin{aligned} S(T_{\rm c},L) &= \frac{1}{Q_\infty} Q(T_{\rm c},L) + Q_\infty \frac{1}{Q(T_{\rm c},L)} - 2 \\ &= \frac{Q_\infty + f(L)}{Q_\infty} + \frac{1}{1+\frac{1}{Q_\infty} f(L)} - 2 \\ &\simeq \frac{f(L)}{Q_\infty} - \frac{f(L)}{Q_\infty} + \left(\frac{1}{Q_\infty} f(L)\right)^2 \\ &= O\left(f(L)^2\right) \end{aligned} \tag{4.65}$$

In our analysis, we use the following self-combined Binder ratios:

$$S_{\rm MF}(T,L) = \frac{1}{Q_{\rm MF}} Q(T,L) + Q_{\rm MF} \frac{1}{Q(T,L)} - 2 \tag{4.66}$$

$$S_{\rm SR}(T,L) = \frac{1}{Q_{\rm SR}} Q(T,L) + Q_{\rm SR} \frac{1}{Q(T,L)} - 2, \tag{4.67}$$

where $Q_{\rm MF} = 0.456947$ and $Q_{\rm SR} = 0.856216$ are the universal ratio of the mean-field universality [50] and short-range universality [61], respectively. The former, $S_{\rm MF}(T, L)$, converges to zero at the critical point for the mean-field universality class, and the latter, $S_{\rm SR}(T, L)$, does for the short-range universality class. Both should exhibit faster convergence than the conventional Binder ratio, $Q(T, L)$, since the leading correction is eliminated.

In Figs. 4.1 and 4.2, we compare the convergence of the conventional Binder ratio, the combined Binder ratio, and the self-combined Binder ratio to the limiting values for the fully connected model and the nearest neighbor model in order to demonstrate the effectiveness of our new quantities. For both models, the (self-)combined Binder ratios converge much faster, in the double powers, than the conventional Binder ratio. Again note that the combined Binder ratio, $C(T, L)$ is available only for the mean-field universality class and not for the short-range case. We will apply these combined quantities to the phase transition of the Ising model with the algebraically decaying interaction.

4.4 Results

By means of the Fukui-Todo cluster method, the Monte Carlo simulation was performed on the two-dimensional $L \times L$ square lattice up to $L = 4096$ for $\sigma = 0.8, 0.9, 1.0, \cdots, 1.75, 1.9$, and 2.0. The periodic boundary conditions were imposed and the effect of the mirror images was taken into account by the generalized Ewald summation (Sec. 4.1.3). The thermal averages of the moments of the magnetization $\langle m^\alpha \rangle$ ($\alpha = 2, 4, \cdots$) were calculated by the improved estimator (Sec. 4.2). Measurement of physical quantities are performed for 16384 Monte Carlo steps, which is longer enough than the integrated autocorrelation time, e.g., $\tau_{\rm int} = 4.3$ and 4.0 for $\langle m^2 \rangle$ and $\langle m^4 \rangle$, respectively, at the critical temperature for $L = 4096$ and $\sigma = 1.75$. Before measurement, we discard 128 Monte Carlo steps. We also have confirmed that 128 Monte Carlo steps is longer enough than the exponential autocorrelation time, that is, there is no statistically significant difference between the measurement with 128 Monte Carlo thermalization steps and that with 256 Monte Carlo thermalization steps at the critical point for the largest system size.

4.4.1 Critical temperature

The critical temperature, $T_{\rm c}$, was estimated by the finite-size scaling of the Binder ratio. First, we estimated the critical temperature for each system size, $T_{\rm c}(L)$, as the crossing point of the conventional Binder ratios of system size L and $2L$ ($L = 64$, 128, 256, 512, 1024, 2048). The crossing point is estimated by the Bayesian scaling analysis [14, 15]. Then, we extrapolated the value in the thermodynamic limit by assuming the following form:

$$T_{\rm c}(L) = T_{\rm c} + aL^{-b}, \tag{4.68}$$

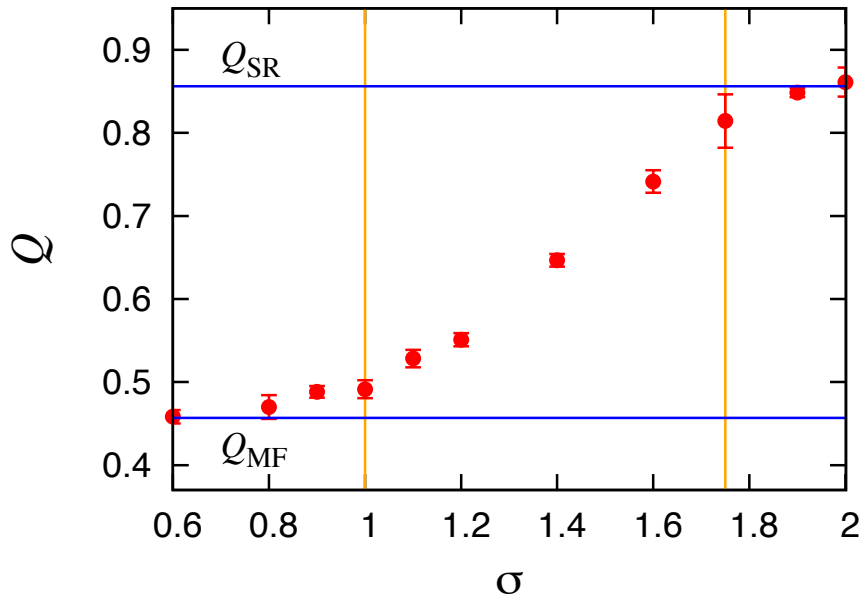

Figure 4.3: σ-dependence of the conventional Binder ratio at the critical point. The horizontal blue lines denote $Q_{\mathrm{MF}} = 0.456947$ [50] and $Q_{\mathrm{SR}} = 0.856216$ [61], respectively. The vertical orange lines denote the critical decay exponents $\sigma = 1$ and $7/4$ predicted by Sak [18].

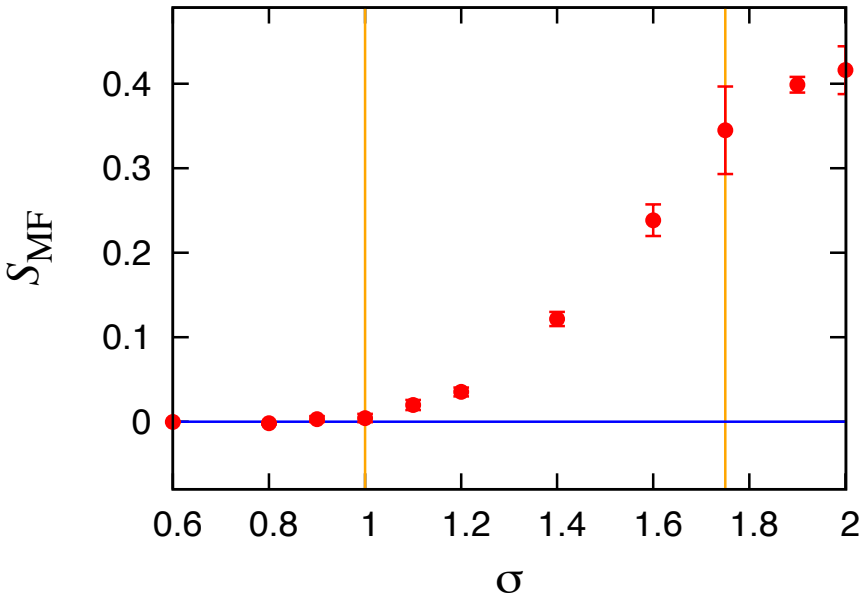

Figure 4.4: σ-dependence of the self-combined Binder ratio, S_{MF}, at the critical temperature. The vertical orange lines denote the critical decay exponents $\sigma = 1$ and $7/4$ predicted by Sak [18].

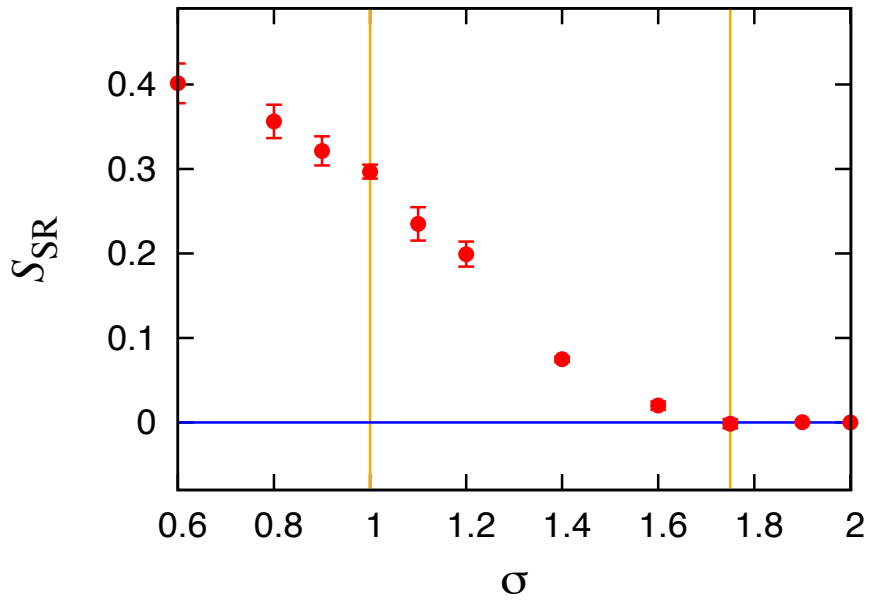

Figure 4.5: σ-dependence of the self-combined Binder ratio, S_{SR}, at the critical temperature. The vertical orange lines denote the critical decay exponents $\sigma = 1$ and $7/4$ predicted by Sak [18].

Table 4.1: σ-dependence of the critical temperature, T_{c}, and the normalized critical temperature, $\tilde{T}_{\mathrm{c}}$. The exact results for the fully connected model (FC) and the nearest neighbor model (NN) are also included.

σ	T_{c}	$\tilde{T}_{\mathrm{c}}$
0 (FC)	1	1
0.6	12.555(1)	0.954033(81)
0.8	9.76500(9)	0.923492(9)
0.9	8.80870(32)	0.906553(33)
1.0	8.03009(7)	0.888911(8)
1.1	7.38232(41)	0.870847(49)
1.2	6.83425(15)	0.852617(19)
1.4	5.95819(12)	0.816679(16)
1.6	5.29318(24)	0.782835(36)
1.75	4.89500(12)	0.759570(19)
1.9	4.56406(12)	0.738536(19)
2.0	4.37427(14)	0.725805(24)
∞ (NN)	2.269185	0.5672963

where the exponent b is related to the correction-to-scaling exponent, ω, as $1/\nu+\omega$. We observed that the value of b takes larger value in the intermediate regime as reported in Ref. 6. Its precise estimation, however, is quite difficult even with the precision of the present simulation.

The critical temperature obtained for each σ is summarized in Table 4.1. We confirmed that the extrapolation by assuming Eq. (4.68) produces estimates for the critical temperatures that agree with the values for the largest system size within the error bar. The estimation from the self-combined Binder ratio (crossing point) is also consistent with the result in Table 4.1. In the table, the normalized critical temperature is also listed, which is defined as $\tilde{T}_{\rm c} = T_{\rm c}/\tilde{J}$ with $\tilde{J} = \sum_{i\neq j} J_{ij}/N$, the sum of coupling constants connecting a single site to all the other sites. One can see that the normalized critical temperature, $\tilde{T}_{\rm c}$, increases slowly as σ decreases. This shift of $\tilde{T}_{\rm c}$ can be interpreted as the suppression of fluctuations due to the increase of the effective dimension.

4.4.2 Binder ratio at critical temperature

Next, let us discuss the universality class of the phase transition by using the Binder ratio at the critical temperature. As we have already discussed in Sec. 2.2, the three different regions are expected: the mean-field, the intermediate, and the short-range regimes. We will focus on the boundary, the critical decay exponent, separating the mean-field and the intermediate regimes, and the intermediate and the short-range regimes.

We calculated the Binder ratio at the critical temperature (Table 4.1) for each σ and L, and extrapolated the value of the thermodynamic limit by assuming the following form:

$$Q(T_{\rm c}, L) = Q_\infty + aL^{-b} \tag{4.69}$$

for each σ, where a and b are σ-dependent fitting parameters.

In Fig. 4.3, the universal ratio of the conventional Binder ratio, Q, is plotted as a function of σ. The extrapolated values of Q are consistent with $Q_{\rm MF}$ in the cases for $\sigma = 0.6$ and 0.8, and consistent with $Q_{\rm SR}$ for $\sigma = 1.9$ and 2. Meanwhile, the values deviate from $Q_{\rm MF}$ or $Q_{\rm SR}$ even outside the region, $1 < \sigma < 7/4$, which is similar to the Monte Carlo result by Picco [26] and in contradiction to the conclusion by Sak [18]. We will show below, however, that this deviation and the smooth change are artifacts due to strong corrections to scaling.

Next, we examine the behavior of the self-combined Binder ratio. In Fig. 4.4, $S_{\rm MF}$ [Eq. (4.66)] is plotted as a function of σ, which has smaller corrections if the transition belongs to the mean-field universality class. In contrast to the conventional Binder ratio, $S_{\rm MF}$ becomes zero within the error bar for $\sigma \leq 1$. Moreover, it is observed that $S_{\rm MF}$ grows as $\sim (\sigma - 1)^2$ for $\sigma > 1$. Thus, we conclude that the transition belongs to the mean-field universality for $\sigma \leq 1$ and the conventional Binder ratio changes linearly as $|Q - Q_{\rm MF}| \sim (\sigma - 1)$ for $\sigma > 1$; i.e., the critical decay exponent between the mean-field and the intermediate regimes is $\sigma = 1$ and Q (probably the critical exponents as well) is non-analytic at the boundary.

The boundary between the intermediate and the short-range regimes was investigated precisely by the use of the self-combined Binder ratio, $S_{\rm SR}$ [Eq. (4.67)], as shown in Fig. 4.5. In a similar way to the previous case, $S_{\rm SR}$ decreases as $\sim (7/4-\sigma)^2$ for $\sigma < 7/4$ and becomes zero for $\sigma \geq 7/4$. Thus, we conclude that the critical decay exponent is $\sigma = 7/4$.

The apparent deviation of the conventional Binder ratio from the mean-field and short-range values at $\sigma = 1$ and $7/4$, respectively, is due to the existence of strong (likely logarithmic [6, 17, 62]) corrections at the critical decay exponents. Indeed the nearest neighbor model exhibits the logarithmic correction-to-scaling in the upper critical dimension ($d = 4$) [63]. In Figs. 4.6 and 4.7, we compare the system-size dependence of the conventional Binder ratio, the combined Binder ratio (only for $\sigma = 1$), and the self-combined Binder ratio for $\sigma = 1$ and $7/4$, respectively. We observe that in both cases the combined or the self-combined Binder ratio converges to zero smoothly. On the other hand, the conventional Binder ratio has the stronger size dependence than the combined Binder ratios, which yields large error bars in the extrapolated values (open symbols). This observation indicates that the conventional Binder ratio presumably suffers from logarithmic-type corrections, while the (self-)combined Binder ratio is free from the strong corrections. In other words, we successfully remove the leading corrections of the conventional Binder ratio by considering the appropriate combination. Note that the combined and the self-combined Binder ratios have smaller error bars than the conventional Binder ratio. It is expected that the statistical fluctuations of the terms of the combined quantities cancel with each other in the linear combination.

At last, it is quite interesting to see, in Fig. 4.6, that the combined Binder ratio [Eq. (4.62)] has even smaller corrections than the self-combined Binder ratio at $\sigma = 1$. The behavior of the conventional Binder ratio (red circles in Fig. 4.6) indicates that the leading correction term might have a different exponent (smaller than $1/2$) and have a quite different form from Eq. (4.58). In such a case, Eq. (4.62) with coefficient (4.63) usually cannot eliminate the leading correction. The reason for this accidental cancellation is not clear at the moment. It remains a future problem.

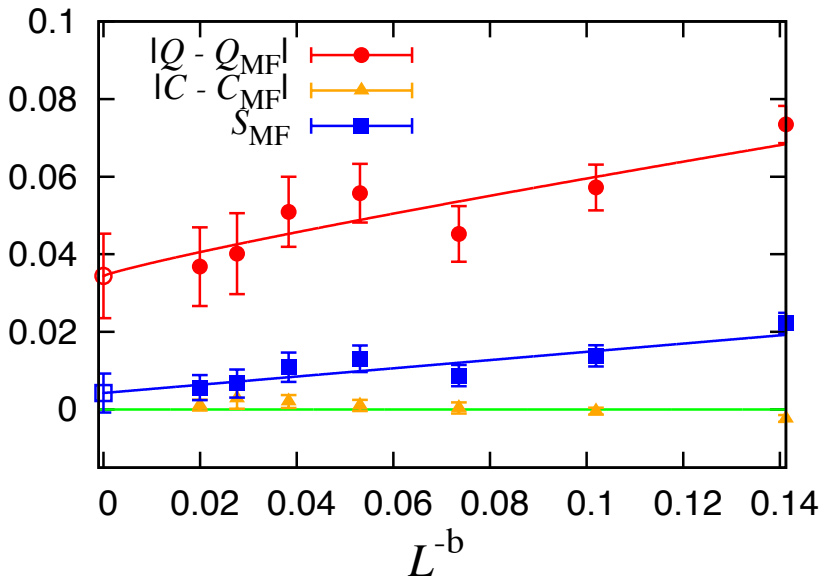

Figure 4.6: System-size dependence of the conventional Binder ratio (Q with red circles), the combined Binder ratio (C with orange triangles), and the self-combined Binder ratio ($S_{\rm MF}$ with blue squares) at $\sigma = 1$. Open symbols denote the extrapolated values to the thermodynamic limit by the fit to a function, $A + aL^{-b}$, where A, a, and b are fitting parameters. The least-squares fitting yields $b \simeq 0.41$ and 0.47 for Q and $S_{\rm MF}$, respectively. The x-axis is taken as L^{-b} with $b = 0.41$.

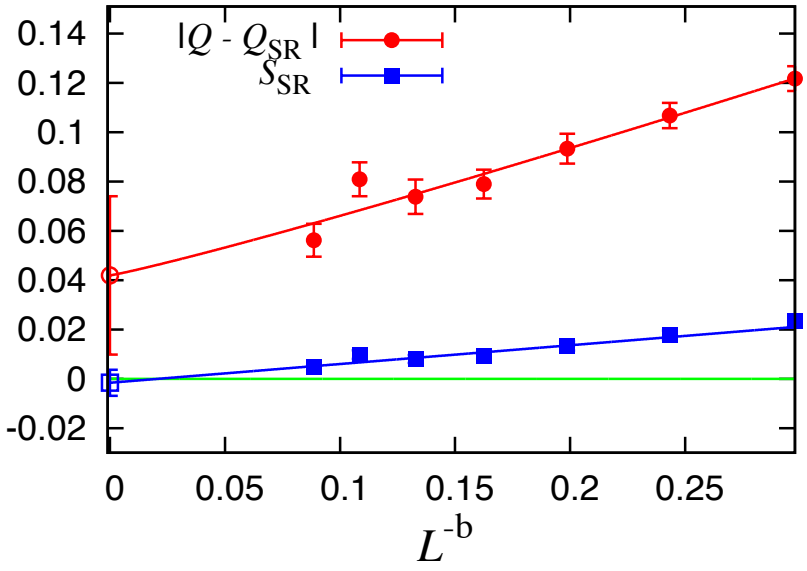

Figure 4.7: System-size dependence of the conventional Binder ratio (Q with red circles) and the self-combined Binder ratio ($S_{\rm SR}$ with blue squares) at $\sigma = 7/4$. Open symbols denote the extrapolated values to the thermodynamic limit by the fit to a function, $A + aL^{-b}$, where A, a, and b are fitting parameters. The least-squares fitting yields $b \simeq 0.32$ and 0.29 for Q and $S_{\rm SR}$, respectively. The x-axis is taken as L^{-b} with $b = 0.32$.

Chapter 5

Spatially Correlated Random-Field Ising Model

5.1 Correlated random field generation

To conduct Monte Carlo simulations of the spatially correlated random-field Ising model (RFIM), generating correlated random numbers described by Eq. (2.86) is needed. In other words, random fields should have a correlation matrix C described by

$$C = \begin{pmatrix} 1 & \frac{a}{|\vec{r}_1 - \vec{r}_2|^{d-\rho}} & \cdots & \frac{a}{|\vec{r}_1 - \vec{r}_N|^{d-\rho}} \\ \frac{a}{|\vec{r}_2 - \vec{r}_1|^{d-\rho}} & 1 & \cdots & \frac{a}{|\vec{r}_2 - \vec{r}_N|^{d-\rho}} \\ \vdots & \vdots & \ddots & \vdots \\ \frac{a}{|\vec{r}_N - \vec{r}_1|^{d-\rho}} & \frac{a}{|\vec{r}_N - \vec{r}_2|^{d-\rho}} & \cdots & 1 \end{pmatrix}, \tag{5.1}$$

where a is an arbitrary constant.

This random-field generation is accomplished with uncorrelated Gaussian random numbers and the decomposition of the correlation matrix. Consider the decomposition of the correlation matrix into matrices M and its transpose M^T,

$$C = MM^T. \tag{5.2}$$

This decomposition is able to be done by the Cholesky decomposition or the diagonalization. The decomposition by the diagonalization is done by

$$C = U\lambda U^{-1} = U\lambda U^T = U\sqrt{\lambda}\sqrt{\lambda}U^T := MM^T, \tag{5.3}$$

where U a unitary matrix of eigenvectors of the correlation matrix, λ is a diagonal matrix with eigenvalues, and $\sqrt{\lambda}$ is a diagonal matrix with the square root of eigenvalues. By multiplying the matrix M and a vector of uncorrelated Gaussian random numbers, X, we obtain the Gaussian random vector Y with correlation C,

$$Y = MX. \tag{5.4}$$

This is easily verified as follows. Consider the covariance matrix of the random vector Y, which corresponds to the correlation matrix if random variables are normalized. The covariance matrix is described as the expectation value of the multiplication of the random vector Y and its transpose Y^T as

$$\begin{aligned} E\left[YY^T\right] &= E\left[(MX)(MX)^T\right] = E\left[MXX^TM^T\right] && (5.5)\\ &= ME\left[XX^T\right]M^T = MIM^T = MM^T = C, && (5.6)\end{aligned}$$

where the matrix M commutes with the expectation $E[\cdot]$, since the multiplication is a linear operation. Thus, the correlation matrix of the random vector Y can give exactly the arbitrary correlation matrix C. This transformation also does not distort the marginal distribution of the Gaussian distributed vector. The joint distribution function of the k-dimensional multivariate Gaussian distribution with zero mean and identity covariance I is expressed as

$$f(X) = \frac{1}{\sqrt{(2\pi)^k}} \exp\left(-\frac{1}{2}X^TI^{-1}X\right). \tag{5.7}$$

By using the transformation (5.4), since $X = M^{-1}Y$ and $(M^T)^{-1}(M)^{-1} = (MM^T)^{-1}$, the distribution becomes

$$\begin{aligned} f(Y) &= \frac{1}{\sqrt{(2\pi)^k}} \exp\left(-\frac{1}{2}Y^T(M^T)^{-1}I^{-1}(M)^{-1}Y\right)\\ &= \frac{1}{\sqrt{(2\pi)^k}} \exp\left(-\frac{1}{2}Y^T\left(MM^T\right)^{-1}Y\right)\\ &= \frac{1}{\sqrt{(2\pi)^k}} \exp\left(-\frac{1}{2}Y^TC^{-1}Y\right). && (5.8)\end{aligned}$$

Thus the transformation makes the distribution into the one with correlation matrix C, still the Gaussian distribution.

Note that too large coefficient a in Eq. (5.1) is unphysical and it causes a fail in the transformation since the diagonalization (5.3) returns some negative eigenvalues and thus $\sqrt{\lambda}$ becomes imaginary. On the other hand, if a is too small, the effect of correlation also becomes small and thus hardly observed especially for finite-size lattices. In brief, we have to use sufficiently large but not too large coefficient a. In this work, we have used $a = 0.2$ to generate random fields from empirical insight.

Although the correlated random-field generation may become a bottleneck of the Monte Carlo simulation for larger system sizes since the computational cost of diagonalization proportional to $O(N^3)$, it does not reach the bottleneck yet for the condition used in this work, i.e., system size $N = 2^{15}$ and 2^{10} random samples.

5.2 Path in the phase diagram

A schematic phase diagram of the RFIM is presented in Fig. 5.1. To detect a phase transition,

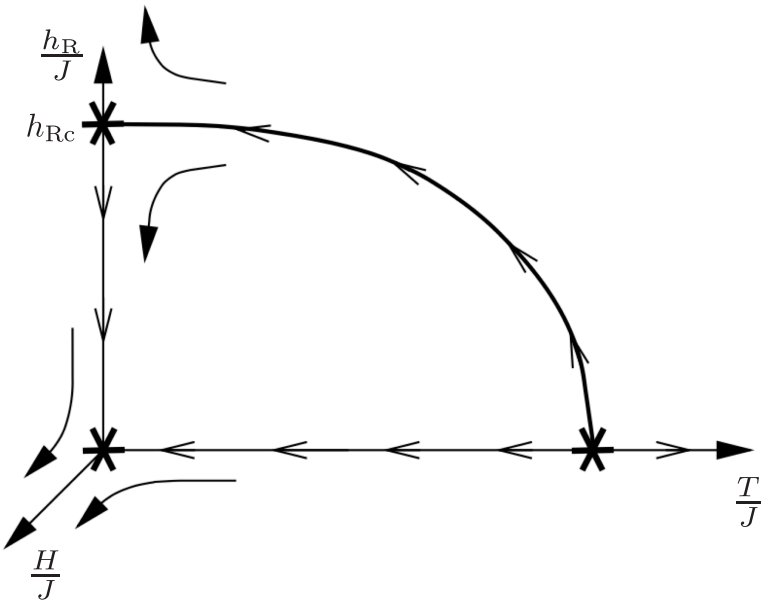

Figure 5.1: Schematic phase diagram of the RFIM in the T-h_{R}-H space (taken from Ref. 64), where T is the temperature, h_{R} is the standard deviation of the random fields, and H is the uniform external field.

one can consider arbitrary paths with crossing the phase boundary on the $H = 0$ plane. In this work, paths are slightly tuned for the efficient computation as follows.

- We use the path with h_{R}/T fixed, in other words, an intensity of the random field h_{R} is set to be proportional to temperature T. In this work, the critical random-field intensity h_{Rc} is possibly changed from the uncorrelated case, and its value is not known in advance. Generally, by introducing correlations between random fields, the critical random-field intensity becomes smaller, since the correlation makes the effect of the random field stronger, as shown in the results below. It is expected that the random-field intensity becomes zero if correlation exponent ρ becomes large enough so that the effective dimension reaches to the lower critical dimension, and our work indeed includes the simulation around the lower critical dimension. The path to $T = h_{\mathrm{R}} = 0$ guarantees the crossing with the phase boundary even for a sufficient small but finite critical random-field intensity h_{Rc}. This path also makes the effect of random fields moderate since it avoids spins from freezing completely by too strong random field at low temperatures, and also makes it easier to distinguish the system from the ferromagnetic one without magnetic field by large enough random fields at high temperatures.

- Although the mean value of the Gaussian random field is zero, the average of random fields in each random sample has some deviation proportional to $\sqrt{N}$ from the central limit theorem. This deviation affects as an effective uniform field and causes some bias in

the order parameter distribution. To eliminate this bias, a uniform field $H = -\sum_i h_i/N$ is introduced to each sample so that to counterbalance the deviation of the random fields, which is expected to work the same as the equal-weight path [65].

Note that the introduction of the uniform field $H = -\sum_i h_i/N$ slightly alters the correlation between the random fields as described below. Let us consider the effective external field $h'(\vec{r}) = h(\vec{r}) + H$ and its correlation function $C'(\vec{r}_1, \vec{r}_2) = [h'(\vec{r}_1)h'(\vec{r}_2)]$. The correlation function of the random field without a uniform field, $C(\vec{r}_1, \vec{r}_2)$, is described as

$$C(\vec{r}_1, \vec{r}_2) = [h(\vec{r}_1)h(\vec{r}_2)] = \begin{cases} h_{\mathrm{R}}^2 & (\vec{r}_1 = \vec{r}_2) \\ \frac{a h_{\mathrm{R}}^2}{|\vec{r}_1 - \vec{r}_2|^{d-\rho}} & (\vec{r}_1 \neq \vec{r}_2). \end{cases} \tag{5.9}$$

By using $C(\vec{r}_1, \vec{r}_2)$, the modified correlation function, $C'(\vec{r}_1, \vec{r}_2)$, is decomposed into

$$\begin{aligned} C'(\vec{r}_1, \vec{r}_2) &= [(h(\vec{r}_1) + H)\,(h(\vec{r}_2) + H)] \\ &= \left[h(\vec{r}_1)h(\vec{r}_2) + h(\vec{r}_1)H + h(\vec{r}_2)H + H^2\right] \\ &= C(\vec{r}_1, \vec{r}_2) + 2\,[h(\vec{r})H] + [H^2], \end{aligned} \tag{5.10}$$

where we have assumed $[h(\vec{r}_1)H] = [h(\vec{r}_2)H] = [h(\vec{r})H]$ by the translational symmetry. The second term in the last line of Eq. (5.10) can be evaluated as

$$[h(\vec{r})H] = \left[h(\vec{r}) \sum_j \frac{-h(\vec{r}_j)}{N}\right] = -\frac{1}{N}\left(\left[h(\vec{r})^2\right] + \sum_{\vec{r}_j \neq \vec{r}} [h(\vec{r})h(\vec{r}_j)]\right). \tag{5.11}$$

The first term in the right hand side of Eq. (5.11) is the variance of the marginal distribution h_{R}^2. As for the second term, by taking the continuous limit and replacing the summation by the integration, we obtain

$$\begin{aligned} \sum_{\vec{r}_j \neq \vec{r}} [h(\vec{r})h(\vec{r}_j)] &\simeq \int_0^L \mathrm{d}r_j^d\, [h(\vec{r})h(\vec{r}_j)] \\ &= \int_0^L \mathrm{d}r_j^d \frac{a}{|\vec{r} - \vec{r}_j|^{d-\rho}} \\ &\simeq \int_0^{L/2} \mathrm{d}r'_j \frac{a}{r_j'^{d-\rho}} S_{d-1} r_j'^{d-1} \\ &= \frac{a S_{d-1}}{2^\rho \rho} L^\rho, \end{aligned} \tag{5.12}$$

where r'_j is $|\vec{r} - \vec{r}_j|$, and S_{d-1} is the surface area of the d-dimensional unit sphere, and we have assumed the spherical symmetry of the system. Thus, Eq. (5.11) becomes

$$[h(\vec{r})H] \simeq -h_{\mathrm{R}}^2 N^{-1} - \frac{a S_{d-1}}{2^\rho \rho} N^{-(1-\rho/d)}. \tag{5.13}$$

The third term in the last line of the Eq. (5.10) can be evaluated similarly as

$$\begin{aligned}
[H^2] &= \left[\sum_j \frac{h(\vec{r}_j)}{N} \sum_k \frac{h(\vec{r}_k)}{N}\right] \\
&\simeq \frac{1}{N^2}\left(N\left[h(\vec{r}_j)^2\right] + \int_0^L \int_0^L \mathrm{d}r_j^d \mathrm{d}r_k^d \frac{a}{|\vec{r}_j - \vec{r}_k|^{d-\rho}}\right) \\
&\simeq \frac{1}{N^2}\left(Nh_{\mathrm{R}}^2 + \int_0^L \mathrm{d}r_k^d \int_0^{L/2} \mathrm{d}r'_j \frac{a}{r_j'^{d-\rho}} S_{d-1} r_j'^{d-1}\right) \\
&= \frac{1}{N^2}\left(Nh_{\mathrm{R}}^2 + N\frac{aS_{d-1}}{2^\rho \rho} L^\rho\right) \\
&= h_{\mathrm{R}}^2 N^{-1} + \frac{aS_{d-1}}{2^\rho \rho} N^{-(1-\rho/d)}. \qquad (5.14)
\end{aligned}$$

By using Eqs. (5.13) and (5.14), we finally obtained the asymptotic form of the effective correlation function (5.10) as

$$C'(\vec{r}_1, \vec{r}_2) \simeq C(\vec{r}_1, \vec{r}_2) - h_{\mathrm{R}}^2 N^{-1} - \frac{aS_{d-1}}{2^\rho \rho} N^{-(1-\rho/d)} \qquad (5.15)$$

The effect of negative correlation decreases as the system size increases since $\rho/d < 1$ to ensure the physical requirement that the random-field correlation must decay for long distance.

To summarize, the above conditions modify the Hamiltonian as

$$\mathcal{H} = -J \sum_{\langle i,j \rangle} S_i S_j - \sum_i h_i S_i - H \sum_i S_i, \qquad (5.16)$$

where $h_{\mathrm{R}}/T = \text{const.} \to h_{\mathrm{R}} \propto T$ and $H = -\sum_i h_i/N$. In this work, we have used the condition $h_{\mathrm{R}}/T = 0.35$ for the uncorrelated random-field case and $h_{\mathrm{R}}/T = 0.2$ for the correlated one, to keep the moderate critical temperature.

5.3 Results

As described in Chap. 2, correlation between random fields is believed to change the critical behavior toward lower dimensional one. In this work, we have studied the three-dimensional and the four-dimensional spatially correlated RFIMs. Previous analytical studies predict the three-dimensional and the four-dimensional RFIMs reach to the lower critical dimension at $\rho \geq 1.0$ and $\rho \geq 2.0$, respectively, from Eq. (2.88).

We have used the Metropolis algorithm with 8192 Monte Carlo steps for sampling, after the 1024 steps for thermalization, and performed 1024 random average for correlated/uncorrelated random-field configurations. For the three-dimensional system, we have studied the uncorrelated, $\rho = 0.0$, $\rho = 0.5$, $\rho = 1.0$, and $\rho = 2.0$, and for the four-dimensional system, we have studied the uncorrelated, $\rho = 0.0$, $\rho = 0.5$, $\rho = 1.0$ and $\rho = 1.5$. In this section, we especially

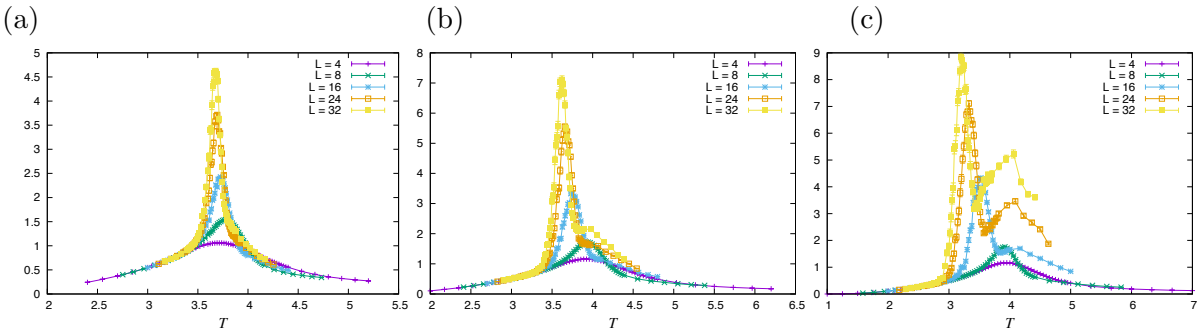

Figure 5.2: Temperature dependence of the specific heat of the three-dimensional RFIM with (a) $\rho = -\infty$, (b) $\rho = 0.5$, and (c) $\rho = 2.0$. Growth of a double-peak structure is clearly observed for larger ρ.

focus on how spatially correlated random fields affect the critical phenomena, and the identity of the critical phenomena between systems in different dimensions, i.e., the identity of the effective dimension.

5.3.1 Specific heat

Does Harris criterion restrict α to negative?

It is generally argued that the Harris criterion (2.83) conducts the restriction on the critical exponent, $\alpha \leq 0$, by using the hyperscaling relation (2.31), and thus the specific heat of a random system should remain finite even at the critical point [42]. For the RFIM, however, since the modified hyperscaling relation (2.58) should be satisfied instead of the hyperscaling relation (2.31), $\alpha = 2 - \nu(d - \theta) \neq 2 - d\nu$, $\alpha \leq \nu\theta$ is concluded instead of $\alpha \leq 0$.

In the case of the correlated RFIM, the Harris criterion should be further modified by replacing the dimension from d to $D' = d - \rho$ [12] as

$$(d - \rho)\nu \geq 2. \tag{5.17}$$

As a result, the critical exponent α should satisfy

$$\alpha \leq \nu(\theta - \rho). \tag{5.18}$$

in the spatially correlated RFIM.

Weird double-peaked behavior at large ρ

In general, the specific heat has a peaked singular behavior near the critical temperature if the exponent α is positive. For the present RFIM, we observe that for larger ρ an extra peak appears at higher temperature in addition to the peak near the critical point as shown in Fig. 5.2. Although we cannot conclude the solid reason for this weird double-peak behavior for the moment, it possibly suggests manifestation of another type of critical behavior [66].

5.3.2 Disconnected Binder ratio

The Binder ratio, which is used to detect the critical point, also can be applied to random systems. For a random system, one can define the connected and disconnected Binder ratios, as described in Sec. 2.3.2. The connected and disconnected Binder ratios are defined respectively as follows

$$Q_{\rm con} = \frac{\left[\langle m^2\rangle^2\right]}{[\langle m^4\rangle]} \tag{5.19}$$

$$Q_{\rm dis} = \frac{\left[\langle m^2\rangle\right]^2}{\left[\langle m^2\rangle^2\right]}, \tag{5.20}$$

where $\langle\cdot\rangle$ denotes the thermal average and $[\cdot]$ does the random average. Both of the Binder ratios are known to converge to the constant value at the critical point, but the connected one does not show a crossing behavior since it converges to the some value for $N \to \infty$ also in the ordered phase [34], while the disconnected Binder ratio still shows the crossing behavior and it is thus more useful for the random case.

We investigate the critical behavior of the disconnected Binder ratio for various ρ. The disconnected Binder ratio of the three-dimensional RFIM is shown in Figs. 5.3, 5.4, 5.5, 5.6, and 5.7. The four-dimensional one is also shown in Figs. 5.8, 5.9, 5.10, 5.11, and 5.12. Note that in these figures we plot $1 - Q_{\rm dis}$ in logarithmic scale since the critical behavior of RFIM are close to the first-order phase transition and thus the value of the disconnected Binder ratio at the crossing point is found to be very close to unity. The disconnected Binder ratio of the uncorrelated or weakly correlated systems, presented in Figs. 5.3, 5.4, 5.8, and 5.9, exhibits the constant crossing point near the critical temperature. On the other hand, the systems with stronger correlations, or larger ρ, shows a gradual shift of the crossing point toward lower temperatures as the system size increases, which seems to suggest the stronger finite-size effect or the absence of finite-temperature phase transitions. If we consent to the prediction Eq. (2.88), three-dimensional RFIM with $\rho \geq 1.0$ reaches or exceeds the lower critical dimension, and thus the extrapolation of the crossing points in Figs. 5.6 and 5.7 would be the zero temperature in the thermodynamic limit.

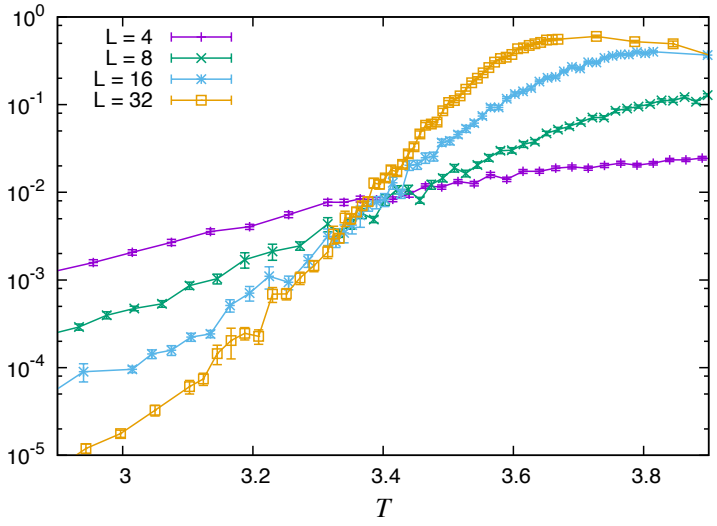

Figure 5.3: Disconnected Binder ratio $(1 - Q_{\mathrm{dis}})$ of the three-dimensional uncorrelated RFIM.

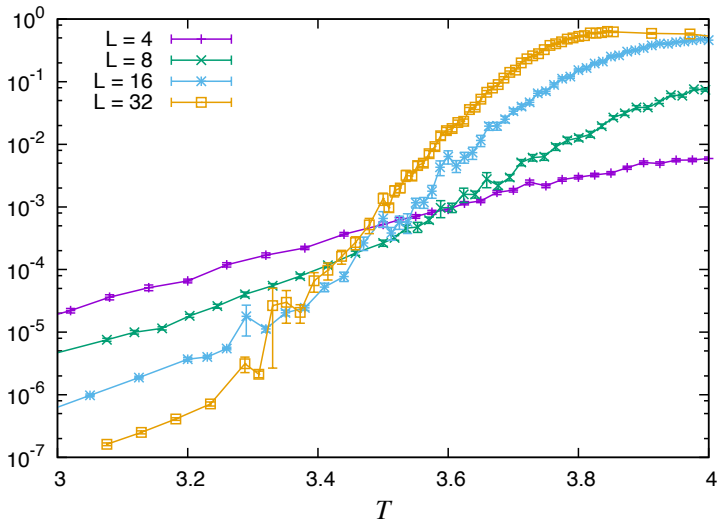

Figure 5.4: Disconnected Binder ratio $(1 - Q_{\mathrm{dis}})$ of the three-dimensional RFIM with $\rho = 0.0$.

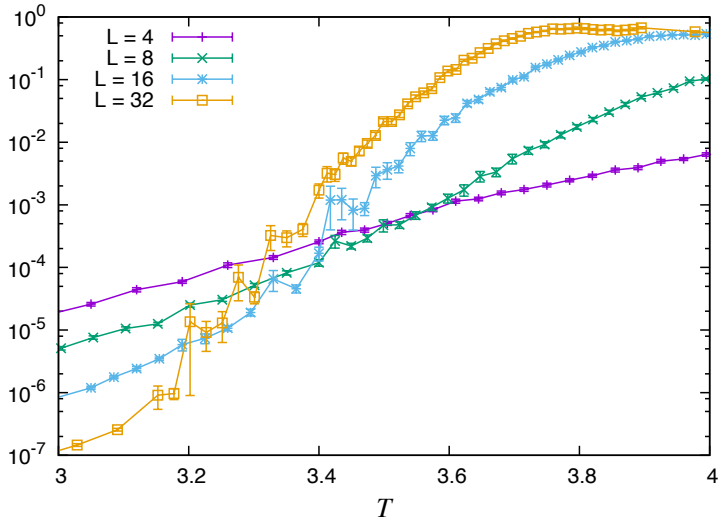

Figure 5.5: Disconnected Binder ratio $(1 - Q_{\mathrm{dis}})$ of the three-dimensional RFIM with $\rho = 0.5$.

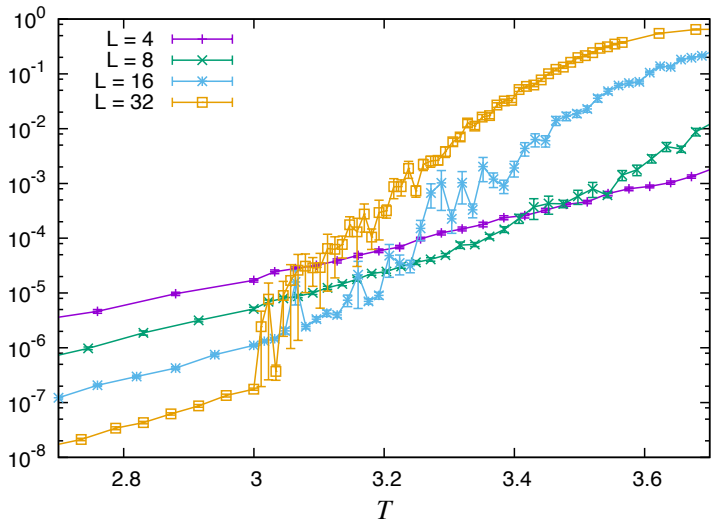

Figure 5.6: Disconnected Binder ratio $(1 - Q_{\mathrm{dis}})$ of the three-dimensional RFIM with $\rho = 1.0$.

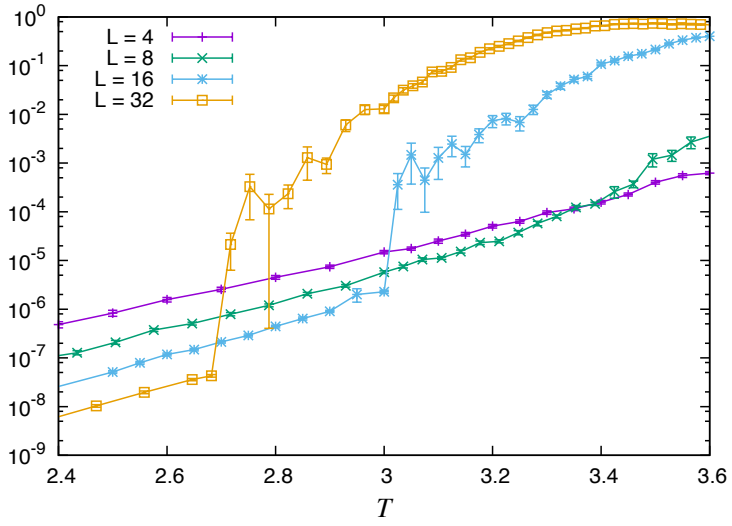

Figure 5.7: Disconnected Binder ratio $(1 - Q_{\mathrm{dis}})$ of the three-dimensional RFIM with $\rho = 2.0$.

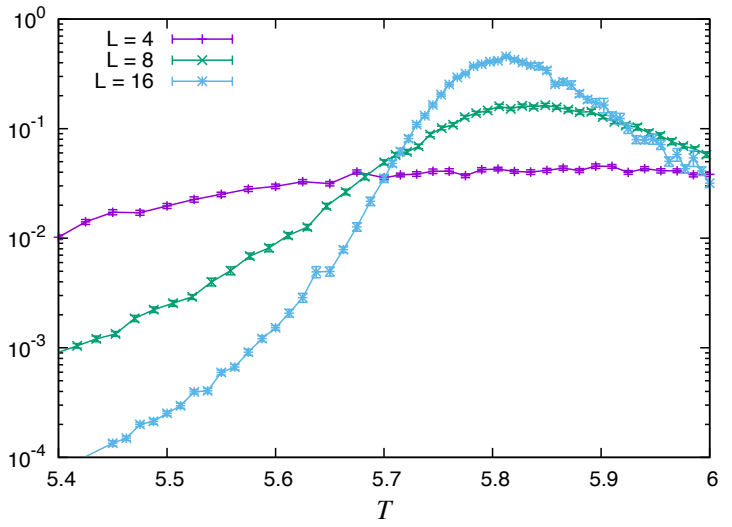

Figure 5.8: Disconnected Binder ratio $(1 - Q_{\mathrm{dis}})$ of the four-dimensional uncorrelated RFIM.

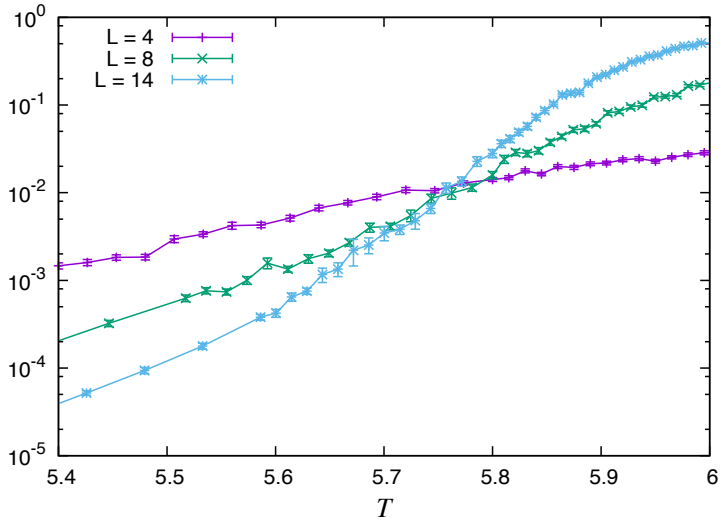

Figure 5.9: Disconnected Binder ratio of the four-dimensional RFIM with $\rho = 0.0$.

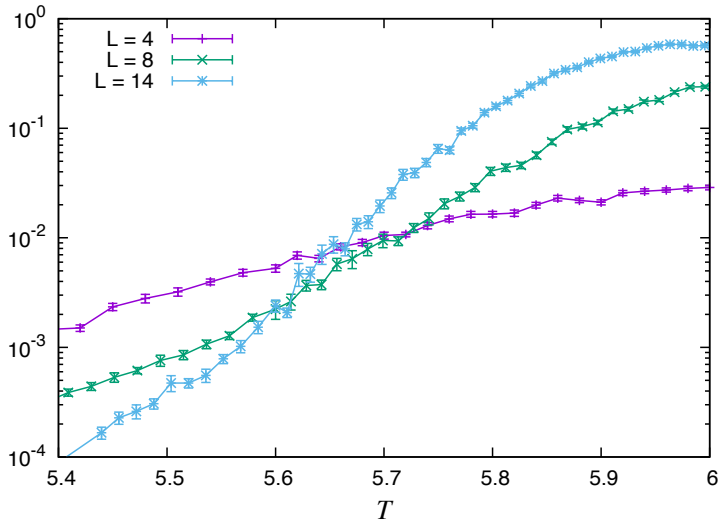

Figure 5.10: Disconnected Binder ratio $(1 - Q_{\mathrm{dis}})$ of the four-dimensional RFIM with $\rho = 0.5$.

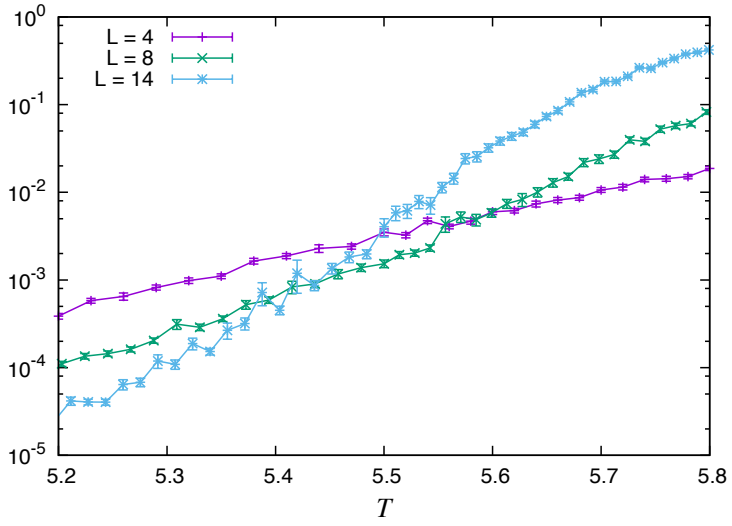

Figure 5.11: Disconnected Binder ratio $(1 - Q_{\mathrm{dis}})$ of the four-dimensional RFIM with $\rho = 1.0$.

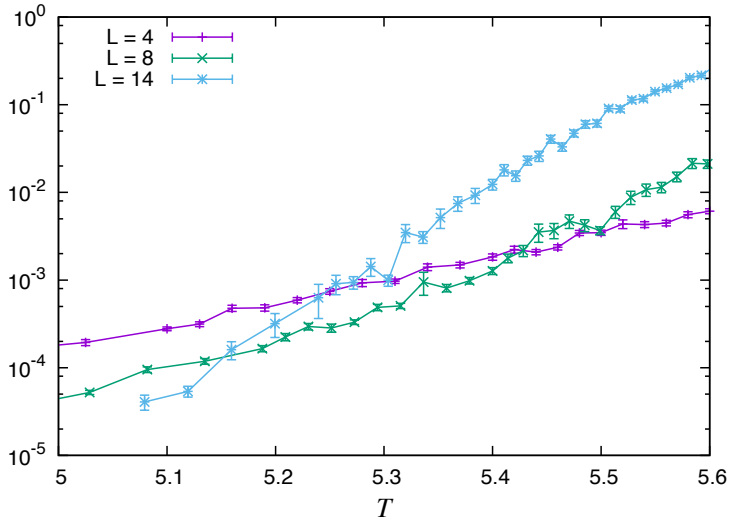

Figure 5.12: Disconnected Binder ratio $(1 - Q_{\mathrm{dis}})$ of the four-dimensional RFIM with $\rho = 1.5$.

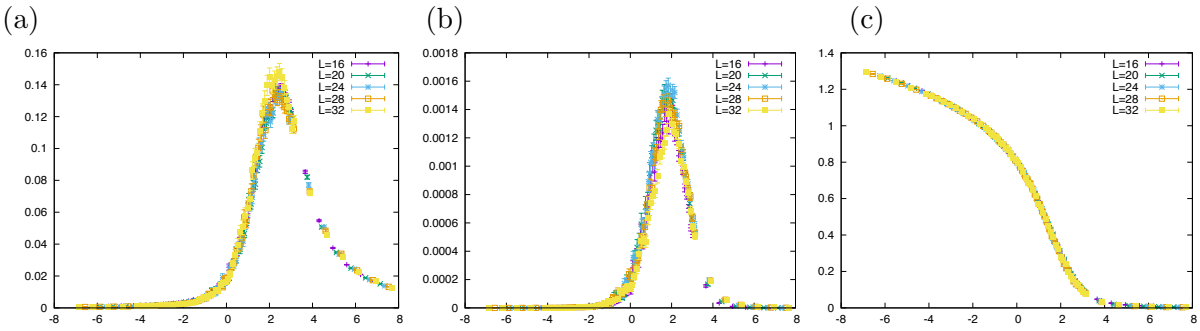

Figure 5.13: Scaling plot of the three-dimensional uncorrelated RFIM. (a) Connected magnetic susceptibility χ_{con}. (b) Disconnected magnetic susceptibility χ_{dis}. (c) Square of the magnetization $\langle m^2 \rangle$.

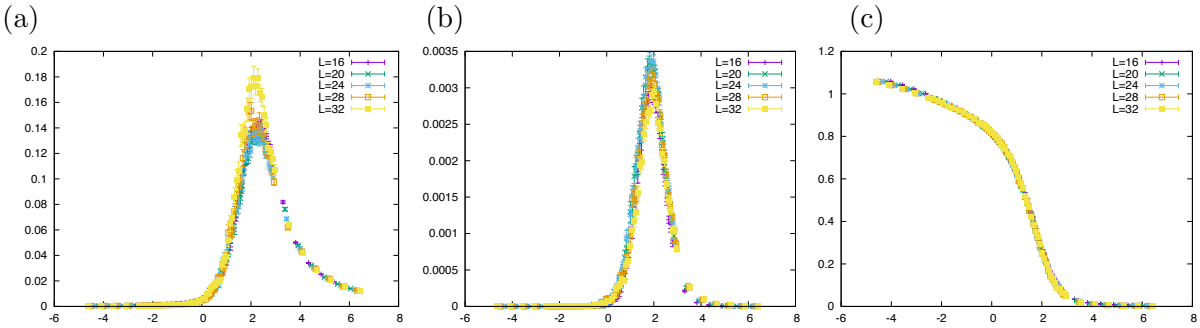

Figure 5.14: Scaling plot of the three-dimensional RFIM with $\rho = 0.0$. (a) Connected magnetic susceptibility χ_{con}. (b) Disconnected magnetic susceptibility χ_{dis}. (c) Square of the magnetization $\langle m^2 \rangle$.

5.3.3 Finite-size scaling

Next, we perform the finite-size scaling analysis for the connected magnetic susceptibility (2.75), the disconnected magnetic susceptibility (2.76), and the square of the magnetization $\left[\langle m^2 \rangle\right]$ simultaneously with assuming the critical temperature T_c and the critical exponent ν as sharing parameters of these quantities, by using the Bayesian scaling analysis [14,15]. We avoided to use the specific heat because of its difficulty and the weird behavior described in subsection 5.3.1.

For three-dimensional systems, $L = 16, 18, 20, 22, 24, 28, 30$, and 32 was used. For uncorrelated four-dimensional systems, $L = 10, 12, 14$, and 16 was used, while $L = 8, 10, 12$, and 14 for the correlated cases. The result of finite-size scaling for the three-dimensional system with uncorrelated, $\rho = 0.0$, $\rho = 0.5$, and $\rho = 1.0$, are shown in Figs. 5.13, 5.14, 5.15, and 5.16, respectively. For $\rho = 2.0$, we can not obtain a reasonable finite-size scaling plot, which suggests the effective dimension becomes smaller than the lower critical dimension in this case. The four-dimensional system with uncorrelated, $\rho = 0.0$, $\rho = 0.5$, $\rho = 1.0$, and $\rho = 1.5$ are shown in Figs. 5.17, 5.18, 5.19, 5.20, and 5.21, respectively. The scaling plots also suggest stronger finite-size effect for larger correlation, i.e., larger ρ makes larger deviation in the scaling plot.

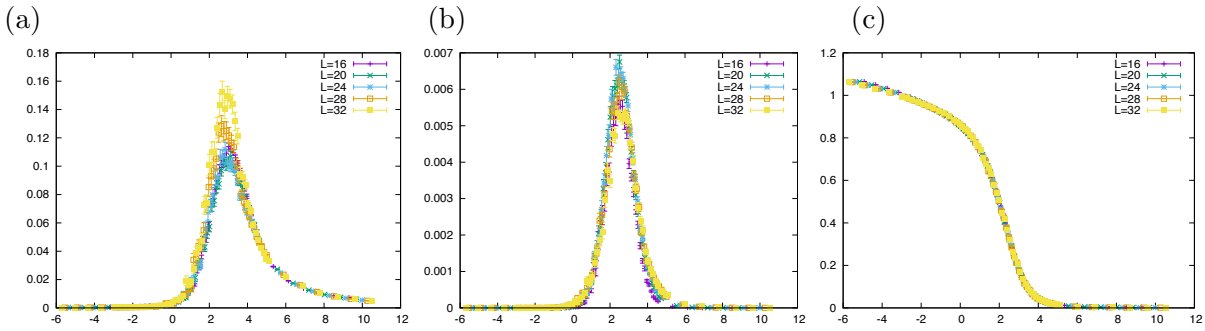

Figure 5.15: Scaling plot of the three-dimensional RFIM with $\rho = 0.5$. (a) Connected magnetic susceptibility $\chi_{\rm con}$. (b) Disconnected magnetic susceptibility $\chi_{\rm dis}$. (c) Square of the magnetization $\langle m^2 \rangle$.

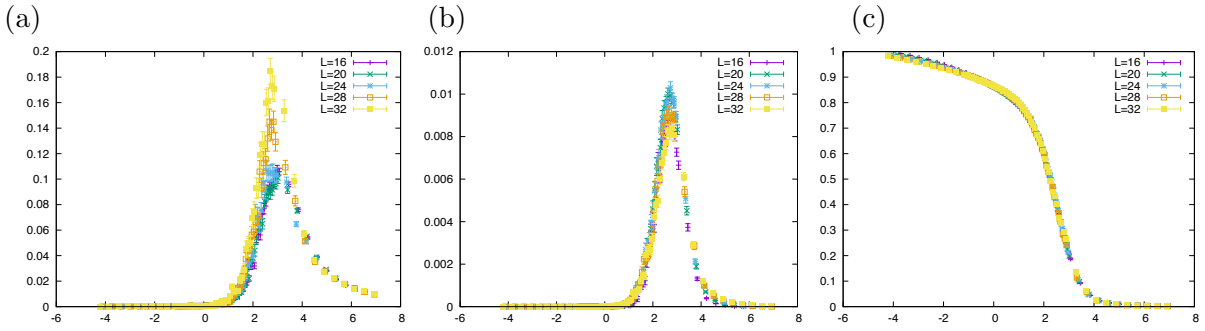

Figure 5.16: Scaling plot of the three-dimensional RFIM with $\rho = 1.0$. (a) Connected magnetic susceptibility $\chi_{\rm con}$. (b) Disconnected magnetic susceptibility $\chi_{\rm dis}$. (c) Square of the magnetization $\langle m^2 \rangle$.

5.3.4 Critical exponents

We have estimated the critical exponents from the finite-size scaling plot of the connected magnetic susceptibility $\chi_{\rm con}$, the disconnected magnetic susceptibility $\chi_{\rm dis}$, and square of the magnetization m^2, as explained in Sec. 5.3.3. The estimates for the critical exponents are summarized in Table 5.1, in which $\rho = -\infty$ means the uncorrelated case. The critical exponents, α, η, and $\bar{\eta}$, and the effective dimension D are obtained from Eqs. (2.19), (2.33), (2.77), and (2.91), respectively. The confidence intervals, which are denoted by the figures in parenthesis, are estimated by the largest deviation of the finite-size scaling results with subsets of Ls. The subsets are chosen for all possible combination of the nearest four system sizes. For three-dimensional system, the subsets are $\{16, 18, 20, 22\}$, $\{18, 20, 22, 24\}$, $\cdots$, and $\{26, 28, 30, 32\}$. For four-dimensional system, the subsets are $\{6, 8, 10, 12\}$ and $\{8, 10, 12, 14\}$. For three-dimensional system with $\rho = 1.0$, the Bayesian scaling analysis fails to converge for more than half of the subsets, which probably suggests the effective dimension becomes smaller than the lower critical dimension.

Here, we note that the direct comparison of the critical temperatures T_c between the uncorrelated and correlated models is meaningless since the variance of random fields is different, as

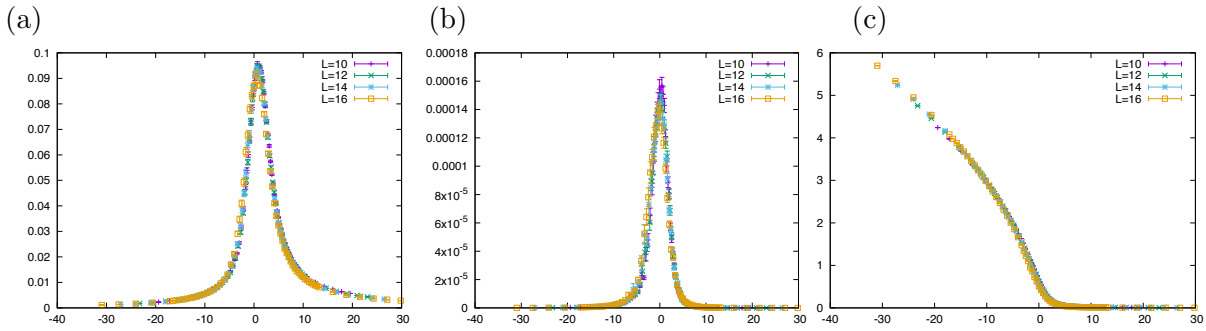

Figure 5.17: Scaling plot of the four-dimensional uncorrelated RFIM. (a) Connected magnetic susceptibility $\chi_{\rm con}$. (b) Disconnected magnetic susceptibility $\chi_{\rm dis}$. (c) Square of the magnetization $\langle m^2 \rangle$.

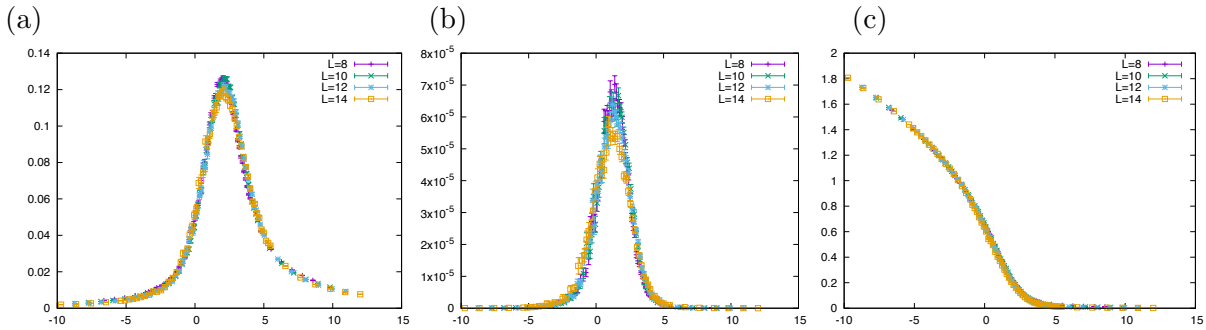

Figure 5.18: Scaling plot of the four-dimensional RFIM with $\rho = 0.0$. (a) Connected magnetic susceptibility $\chi_{\rm con}$. (b) Disconnected magnetic susceptibility $\chi_{\rm dis}$. (c) Square of the magnetization $\langle m^2 \rangle$.

explained in Sec. 5.2. If the same variance is used for both cases, the critical temperature T_c of the correlated RFIM should be significantly smaller than the uncorrelated RFIM, since the introduction of correlation between random fields decreases the critical intensity $h_{\rm Rc}$.

We found that γ gradually increases with increasing ρ. This behavior is consistent with the larger ρ makes the effective dimension lower since lower dimensional Ising model has larger γ (cf. in the pure case, γ of the mean-field model, three-dimensional Ising model, and 2D Ising model are 1, 1.2372, and $7/4 = 1.75$, respectively). Eq. (2.90) predicts the identities of the critical behavior between different dimensional systems. For example, the four-dimensional system with $\rho = 1.0$ is identical to the three-dimensional system with $\rho < 0.0$, and this identification seems valid at these points, $1.3 \simeq 1.4$, and therefore the effective dimension of the three-dimensional uncorrelated RFIM and four-dimensional RFIM with $\rho = 1.0$ are estimated from $D \simeq 1.3$ to $D \simeq 1.4$.

On the other hand, quantitative estimation of the critical exponents seems to fail for larger ρ, especially for the disconnected critical exponents $\bar{\gamma}$ and $\bar{\eta}$. The relation (2.80) expects the $\bar{\gamma}/\gamma = 2$, but it seems to be broken for larger ρ as well. Although Eq. (2.80) is merely a prediction, in addition to the violation of the $\bar{\gamma}/\gamma = 2$, the exact relation (2.78) is also broken,

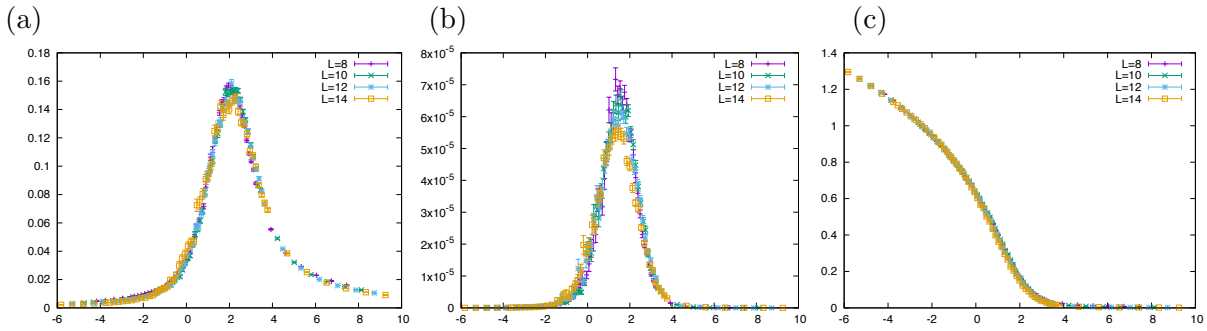

Figure 5.19: Scaling plot of the four-dimensional RFIM with $\rho = 0.5$. (a) Connected magnetic susceptibility $\chi_{\rm con}$. (b) Disconnected magnetic susceptibility $\chi_{\rm dis}$. (c) Square of the magnetization $\langle m^2 \rangle$.

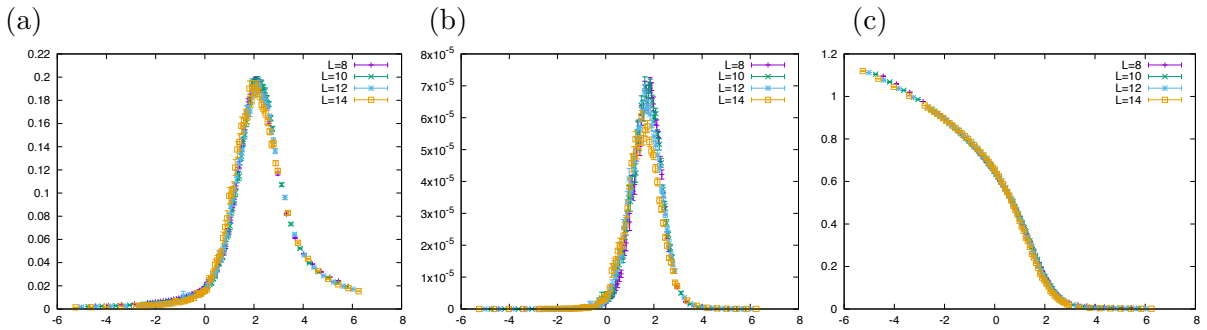

Figure 5.20: Scaling plot of the four-dimensional RFIM with $\rho = 1.0$. (a) Connected magnetic susceptibility $\chi_{\rm con}$. (b) Disconnected magnetic susceptibility $\chi_{\rm dis}$. (c) Square of the magnetization $\langle m^2 \rangle$.

$0.8 > 2 \times 0.3 = 0.6$ at $\rho = 0.5$. We have no other choices but to interpret as the failure of estimation of the correct disconnected critical exponents for larger ρ. The effective dimension D of the three-dimensional system with $\rho = 0.5$ is also invalid since $D = 0.8$ is smaller than the lower critical dimension despite $\rho < 1.0$. In the region with effective dimension $D' = d - \rho < 3$, where D' is the effective dimension from the aspect of the uncorrelated RFIM, there seems be strong finite-size effect and we conclude that the precise estimation of the critical exponents is extremely difficult by the present scale of the simulations.

The origin of stronger finite-size corrections for the larger correlation is qualitatively explained as follows: Strongly correlated random fields tend to align toward the same direction, and each aligned region behaves like a bulk of external field. This implies that the number of effective spins decreases compared with the uncorrelated case, and hence the correlated RFIM behaves as a effectively smaller system.

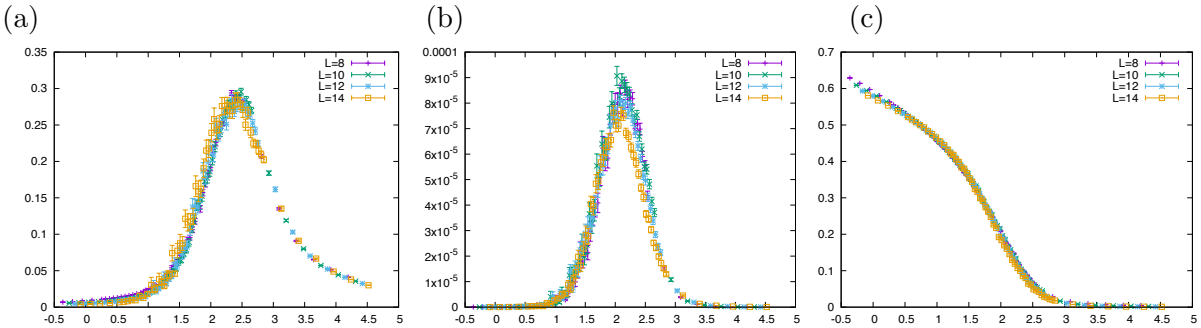

Figure 5.21: Scaling plot of the four-dimensional RFIM with $\rho = 1.5$. (a) Connected magnetic susceptibility χ_{con}. (b) Disconnected magnetic susceptibility χ_{dis}. (c) Square of the magnetization $\langle m^2 \rangle$.

Table 5.1: Critical temperature and critical exponents of the spatially correlated RFIM.

d	ρ	T_c	ν	γ	$\bar{\gamma}$	β	$\bar{\gamma}/\gamma$	α	η	$\bar{\eta}$	D
3	$-\infty$	3.42(4)	1.4(2)	2.3(2)	4.8(8)	0.09(14)	2.1(4)	-0.5(2)	0.3(1)	0.5(4)	1.3(1)
3	0.0	3.55(6)	1.5(4)	2.5(7)	5.1(7)	0.05(2)	2.0(4)	-0.6(3)	0.4(2)	0.6(5)	1.4(2)
3	0.5	3.43(5)	1.5(3)	2.5(4)	4.7(8)	0.04(1)	1.9(3)	-0.6(4)	0.3(3)	0.8(5)	0.8(3)
3	1.0	3.17(9)	1.8(4)	3.0(2)	5.5(6)	0.01(2)	1.9(2)	-1.0(1)	0.3(3)	0.9(3)	0.3(3)
4	$-\infty$	5.74(3)	0.8(1)	1.5(2)	3.4(5)	0.28(3)	2.2(1)	-0.1(1)	-0.04(6)	-0.6(2)	2.0(2)
4	0.0	5.82(6)	1.1(2)	2.1(3)	5.6(6)	0.19(3)	2.67(2)	-0.5(2)	0.1(2)	-1.0(5)	2.1(2)
4	0.5	5.68(9)	1.3(3)	2.3(3)	6.7(8)	0.14(5)	2.87(3)	-0.6(2)	0.2(2)	-1.1(5)	1.7(2)
4	1.0	5.45(15)	1.6(3)	2.6(4)	8(1)	0.07(6)	3.15(6)	-0.7(3)	0.3(2)	-1.2(6)	1.3(2)
4	1.5	4.92(30)	2.3(6)	3.4(7)	11(1)	-0.1(1)	3.56(6)	-1.2(4)	0.5(1)	-1.3(5)	1.0(1)

Chapter 6

Summary

In the present thesis, we have studied the critical phenomena of the Ising model with various effective dimensionality, includes the non-integer effective dimensions. In higher dimensions, spins interact with more and more spins, and that makes easier to develop the long-range order. This difference also makes the critical behavior different. Conversely, the difference of the universality class is qualitatively explained as the difference in the difficulty of the development of the long-range order. By introducing the interaction which increases or disturbs the growth of the long-range order, we expect that the system exhibits different universality class in effectively different dimensions. In this work, we have studied the Ising model with long-range interaction (LRI) and the spatially correlated random-field Ising model (RFIM), both of which are expected to change the critical behavior continuously.

In Chap. 2, we introduced the theory and the previous studies of the general critical phenomena, the Ising model with LRI, and the spatially correlated RFIM. The Ising model with LRI changes its universality class with respect to the decay exponent σ. For a sufficiently small σ (strong LRI), the universality corresponds to the mean-field one since the strong LRI is qualitatively the same as the fully connected model. On the other hand, for a sufficiently large σ (weak LRI), the universality corresponds to the short-range interaction since the LRI is no longer effective. The boundary of these regions, that is, the critical decay exponents, were not known well in spite of the simple form of the Hamiltonian.

The RFIM, on the other hand, is believed to change the critical behavior from pure Ising model toward lower dimensional one since random fields scatter the ordered clusters toward random directions and the development of the long-range order becomes more difficult. The scaling relation of the random-field Ising model is different from the pure system and there are various predictions, but the exact scaling relations are not established yet and under the controversy. The case where random fields have spatial correlations with each other, the critical behavior becomes different further. Correlated random fields tend to align toward the same direction and each aligned region behaves like a bulk of external field. The scattering effect of these aligned bulks is stronger than independent one since a spin is excited not only by a

random field acting on that site but also nearby random fields via exited spins aligned toward the same direction as the bulk random fields. Since both of the parameters, the long-range interaction σ and the correlation of the random-field ρ, are believed to change the effective dimension continuous, these models are expected to have the continuous dimensions, i.e., non-integer effective dimensions.

In Chap. 3, we introduced the various Markov chain Monte Carlo methods. The single spin flip algorithm and the cluster algorithm, the most fundamental Monte Carlo algorithms, are introduced. In addition to these fundamental algorithms, we introduced the Fukui-Todo method, which drastically decreases the computational cost for the system with LRI from $O(N^2)$ to $O(N)$.

In Chap. 4, we presented the results for the two-dimensional Ising model with LRI. In this chapter, we especially focused on the quantitative classification of the universality class by decay exponent σ. Concretely, we estimated the boundaries between the mean-field and the intermediate, and between the intermediate and the short-range. The main difficulty of the Monte Carlo study of the LRI is divided into two parts, the huge computation cost and the extremely slow (possibly log-like) convergence of the physical quantities. The former was solved by the Fukui-Todo method, which was introduced in Chap. 3. In addition to the Fukui-Todo method, we developed the generalized Ewald summation and the improved estimator. Although the Ewald summation is known to improve the convergence of the summation of the periodic potential far faster than the brute-force summation, it was available only for the algebraic potential with integral exponents. We generalized the exponent of the Ewald summation from integral numbers into real numbers. We used the improved estimator, which is a more efficient method used in the cluster algorithm to obtain the expectation value of the magnetization. To derive the equation of the improved estimator, we introduced the simple method to obtain the equation of the improved estimator for the power of the magnetization with an arbitrary even number. To overcome the extremely slow convergence of the physical quantities occurring in the LRI, we used the Binder ratio instead of the critical exponents and introduced the combined Binder ratio, which converges far faster than the conventional Binder ratio at the critical point. The results of the current work, Monte Carlo simulations of the two-dimensional Ising model with LRI and its analysis, concluded the boundary of the mean-field and the short-range are $\sigma = 1.0$ and $\sigma = 1.75$, respectively. Our results agree with one of the renormalization group predictions [18, 30].

In Chap. 5, we introduced the research of the spatially correlated RFIM. To accomplish the Monte Carlo simulation with the correlated random-field, we generated correlated Gaussian random variables by the diagonalization of the correlation matrix. We analyzed the behavior of the three-dimensional and the four-dimensional correlated RFIMs. The disconnected Binder ratio [34], which is used to estimate the critical point of the RFIM, revealed the universal crossing point for the uncorrelated or weakly correlated system, but the shift of the crossing point was

observed for the strongly correlated RFIM. The finite-size scaling of the RFIM also exhibited larger deviation in the strongly correlated region. These behaviors imply that the stronger correlation of random fields causes the larger finite-size effect. The critical exponents are estimated by the finite-size scaling technique. The critical exponents suggest that the larger correlation shifts the effective critical behavior toward lower dimensional one, but unfortunately quantitative estimation seems to be quite difficult especially for the system with strongly correlated random fields by the present scale of the simulations.

Bibliography

[1] Bauer, B. & *et al.* The ALPS project release 2.0: open source software for strongly correlated systems. *J. Stat Mech.* P05001 (2011). [One citation in p. iii.]

[2] http://alps.comp-phys.org/. [One citation in p. iii.]

[3] Nishimori, H. & Ortiz, G. *Elements of Phase Transition and Critical Phenomena* (Oxford University Press, 2011). [5 citations in pp. 1, 2, 5, 12, and 15.]

[4] Bray, A. J. Long-range random-field models: Scaling theory and 1/n expansion. *J. Phys. C* **19**, 6225 (1986). [4 citations in pp. 1, 2, 14, and 23.]

[5] Fisher, D. S. Scaling and critical slowing down in random-field ising systems. *Phys. Rev. Lett.* **56**, 416 (1986). [5 citations in pp. 1, 3, 18, 19, and 20.]

[6] Angelini, M. C., Parisi, G. & Ricci-Tersenghi, F. Relations between short-range and long-range ising models. *Phys. Rev. E* **89**, 062120 (2014). [5 citations in pp. 1, 11, 13, 51, and 52.]

[7] Imry, Y. & Ma, S. K. Random-field instability of the ordered state of continuous symmetry. *Phys. Rev. Lett.* **35**, 1399 (1975). [4 citations in pp. 2, 14, 17, and 21.]

[8] Aharony, A., Imry, Y. & Ma, S. K. Lowering of dimensionality in phase transitions with random fields. *Phys. Rev. Lett.* **37**, 1364 (1976). [2 citations in pp. 2 and 17.]

[9] Young, A. P. On the lowering of dimensionality in phase transitions with random fields. *J. Phys. C* **10**, L257 (1977). [2 citations in pp. 2 and 17.]

[10] Parisi, G. & Sourlas, N. Random magnetic fields, supersymmetry, and negative dimensions. *Phys. Rev. Lett.* **43**, 744 (1979). [One citation in p. 2.]

[11] Fukui, K. & Todo, S. Order-N cluster Monte Carlo method for spin systems with long-range interactions. *J. Comp. Phys.* **228**, 2629 (2009). [3 citations in pp. 2, 31, and 33.]

[12] Weinrib, H. & Halperin, B. I. Critical phenomena in systems with long-range-correlated quenched disorder. *Phys. Rev. B* **27**, 413 (1983). [2 citations in pp. 2 and 60.]

[13] Kardar, M., McClain, B. & Taylor, C. Dimensional reduction with correlated random fields. a superspace renormalization-group calculation. *Phys. Rev. B* **27**, 5875 (1983). [4 citations in pp. 2, 14, 21, and 22.]

[14] Harada, K. Byesian inference in the scaling analysis of critical phenomena. *Phys. Rev. E* **84**, 056704 (2011). [3 citations in pp. 10, 48, and 67.]

[15] http://kenjiharada.github.io/BSA/. [3 citations in pp. 10, 48, and 67.]

[16] Dyson, F. J. Existence of a phase-transition in a one-dimensional Ising ferromagnet. *Commun. Math. Phys.* **12**, 91 (1969). [One citation in p. 10.]

[17] Fisher, M. E., Ma, S.-K. & Nickel, B. G. Critical exponents for long-range interactions. *Phys. Rev. Lett.* **29**, 917 (1972). [4 citations in pp. 10, 11, 12, and 52.]

[18] Sak, J. Recursion relations and fixed points for ferromagnets with long-range interactions. *Phys. Rev. B* **8**, 281 (1973). [8 citations in pp. 10, 11, 12, 13, 49, 50, 51, and 74.]

[19] Kraemer, C. *et al.* Dipolar antiferromagnetism and quantum criticality in $LiErF_4$. *Science* **336**, 1416–1419 (2012). [One citation in p. 10.]

[20] Prüser, H. *et al.* Interplay between the Kondo effect and the Ruderman-Kittel-Kasuya-Yosida interaction. *Nat. Commun.* **5**, 6417 (2014). [One citation in p. 10.]

[21] Landig, R. *et al.* Quantum phases from competing short- and long-range interactions in an optical lattice. *Nature* **532**, 476–479 (2016). [One citation in p. 10.]

[22] Husimi, K. *Proc. Int. Conf. Theor. Phys.* 531 (1953). [One citation in p. 11.]

[23] Temperley, H. N. V. *Proc. Phys. Soc.* **67**, 233 (1954). [One citation in p. 11.]

[24] van Enter, A. C. D. Instability of phase diagrams for a class of "irrelevant" perturbations. *Phys. Rev. B* **26**, 1336 (1982). [3 citations in pp. 11, 12, and 13.]

[25] Luijten, E. & Blöte, H. W. J. Boundary between long-range and short-range critical behavior in systems with algebraic interactions. *Phys. Rev. Lett.* **89**, 025703 (2002). [2 citations in pp. 11 and 13.]

[26] Picco, M. Critical behavior of the Ising model with long range interactions `arXiv:1207.1018`. [3 citations in pp. 11, 13, and 51.]

[27] Blanchard, T., Picco, M. & Rajabpour, M. A. Influence of long-range interactions on the critical behavior of the Ising model. *Europhys. Lett.* **101**, 56003 (2013). [2 citations in pp. 11 and 13.]

[28] Katzgraber, H. G., Larson, D. & Young, A. P. Study of the de Almedia-Thouless line using power-law diluted one-dimensional Ising spin glasses. *Phys. Lev. Lett* **102**, 177205 (2009). [One citation in p. 11.]

[29] Banos, R. A., Fernandez, L. A., Martin-Mayor, V. & Young, A. P. Correspondence between long-range and short-range spin glasses. *Phys. Rev. B* **86**, 134416 (2012). [One citation in p. 11.]

[30] Defenu, N., Trombettoni, A. & Codello, A. Fixed-point structure and effective fractional dimensionality for o(n) models with long-range interacitons. *Phys. Rev. E* **92**, 052113 (2015). [3 citations in pp. 11, 13, and 74.]

[31] Aharony, A. Tricritical points in system with random fields. *Phys. Rev. B* **18**, 3318 (1978). [2 citations in pp. 14 and 17.]

[32] Binder, K. Random-field induced interface widths in ising systems. *Z. Phys. B* **50**, 343 (1983). [One citation in p. 15.]

[33] Grinstein, G. Ferromagnetic phase transitions in random fields: The breakdown of scaling laws. *Phys. Rev. Lett.* **37**, 944 (1976). [One citation in p. 17.]

[34] Vink, R. L. C., Fischer, T. & Binder, K. Finite-size scaling in Ising-like systems with quenched random fields: Evidence of hyperscaling violation. *Phys. Rev. E* **82**, 051134 (2010). [4 citations in pp. 17, 18, 61, and 74.]

[35] Villain, J. Equilibrium critical properties of random field systems : new conjectures. *J. Physique* **46**, 1843 (1985). [3 citations in pp. 18, 19, and 20.]

[36] Schwatrz, M. & Soffer, A. Exact inequality for random systems: Application to random fields. *Phys. Rev. Lett.* **55**, 2499 (1985). [2 citations in pp. 18 and 20.]

[37] Schwatrz, M. The random-field puzzle. i. solution by equivalent annealing. *J. Phys. C* **18**, 135 (1985). [2 citations in pp. 18 and 20.]

[38] Schwatrz, M., Gofman, M. & Natterman, T. On the missing scaling relation in random field systems. *Physica A* **178**, 6 (1991). [One citation in p. 18.]

[39] Gofman, M., Adler, J., Aharony, A., Harris, A. B. & Schwartz, M. Evidence for two exponent scaling in the random field Ising model. *Phys. Rev. Lett.* **71**, 1569 (1993). [2 citations in pp. 18 and 20.]

[40] Hohenberg, P. C. & Halperin, B. I. Theory of dynamic critical phenomena. *Rev. Mod. Phys.* **49**, 435 (1977). [One citation in p. 19.]

[41] Bray, A. J. & Moore, M. A. Scaling theory of the random-field Ising model. *J. Phys. C* **18**, L927 (1985). [One citation in p. 20.]

[42] Harris, A. B. Effect of random defects on the critical behaviour of Ising models. *J. Phys. C* **7**, 1671 (1974). [2 citations in pp. 21 and 60.]

[43] Robert, C. P. & Casella, G. *Monte Carlo Statistical Methods* (Springer, New York, 2004), 2nd edn. [2 citations in pp. 25 and 26.]

[44] Landau, D. P. & Binder, K. *A Guide to Monte Carlo Simulations in Statistical Physics* (Cambridge University Press, Cambridge, 2005), 2nd edn. [2 citations in pp. 26 and 45.]

[45] Tierney, L. Markov chain for exploring posterior distributions. *Ann. Stat.* **22**, 1701 (1994). [One citation in p. 27.]

[46] Meyn, S. P. & Tweedie, R. L. *Markov Chains and Stochastic Stability* (Springer, New York, 1993). [One citation in p. 27.]

[47] Metropolis, N., Rosenbluth, A. W., Rosenbluth, M. N., Teller, A. H. & Teller, E. Equation of state calculations by fast computing machines. *J. Chem. Phys.* **21**, 1087 (1953). [One citation in p. 28.]

[48] Creutz, M. Monte Carlo study of quantized SU(2) gauge theory. *Phys. Rev. D* **21**, 2308 (1980). [One citation in p. 28.]

[49] Swendsen, R. H. & Wang, J. S. Nonuniversal critical dynamics in Monte Carlo simulations. *Phys. Rev. Lett.* **58**, 86 (1987). [2 citations in pp. 29 and 31.]

[50] Luijten, E. & Blöte, H. W. J. Monte Carlo method for spin models with long-range interactions. *Int. J. Mod. Phys. C* **6**, 359 (1995). [4 citations in pp. 31, 46, 48, and 49.]

[51] Tomita, Y. *J. Phys. Soc. Jpn.* **78**, 014002 (2009). [One citation in p. 31.]

[52] Todo, S. & Suwa, H. Geometric allocation approaches in Markov chain Monte Carlo. *J. Phys.: Conf. Ser.* **473**, 012013 (2013). [One citation in p. 31.]

[53] Fortuin, C. M. & Kasteleyn, P. W. On the random-cluster model I. introduction and relation to other models. *Physica* **57**, 536 (1972). [One citation in p. 31.]

[54] Kawashima, N. & Gubernatis, J. E. Generalization of the Fortuin-Kasteleyn transformation and its application to quantum spin simulations. *J. Stat. Phys.* **80**, 169 (1995). [One citation in p. 31.]

[55] Ewald, P. P. Die berechnung optischer und elektrostatischer gitterpotentiale. *Ann. Phys* **64**, 253 (1921). [One citation in p. 35.]

[56] Karasawa, N. & Goddard, W. A. Acceleration of convergence for lattice sums. *J. Chem. Phys.* **93**, 7320 (1989). [One citation in p. 35.]

[57] Kretschmer, R. & Binder, K. Ordering and phase transitions in Ising systems with competing short range and dipolar interactions. *Z. Phys. B* **34**, 375 (1979). [One citation in p. 35.]

[58] Ueda, A. *Computer Simulation (in Japanese)* (Asakura, Tokyo, 1990). [One citation in p. 35.]

[59] http://www.boost.org/. [One citation in p. 40.]

[60] Yasuda, S. & Todo, S. Monte Carlo simulation with aspect-ratio optimization: Anomalous anisotropic scaling in dimerized antiferromagnets. *Phys. Rev. E* **88**, 061301(R) (2013). [One citation in p. 45.]

[61] Kamieniarz, G. & Blöte, H. W. J. Universal ratio of magnetization moments in two-dimensional Ising models. *J. Phys. A: Math. Gen.* **26**, 201 (1993). [2 citations in pp. 48 and 49.]

[62] Brézin, E., Parisi, G. & Ricci-Tersenghi, F. the crossover region between long-range and short-range interactions for the critical exponents. *J. Stat. Phys.* **157**, 855 (2014). [One citation in p. 52.]

[63] Brézin, E. An investigation of finite size scaling. *J. Phys. (France)* **43**, 15 (1982). [One citation in p. 52.]

[64] Nattermann, T. Theory of the random field Ising model `arXiv:970529`. [One citation in p. 57.]

[65] Borgs, C. & Kappler, S. Equal weight versus equal height: a numerical study of an asymmetric first-order transition. *Phys. Lett. A* **171**, 37 (1992). [One citation in p. 58.]

[66] Sacconi, R. Numerical study of the transition of the four-dimensional random field Ising model. *J. Phys. A: Math. Gen.* **31**, 3751 (1997). [One citation in p. 60.]